UNIVERSITY OF CALIFORNIA
RIVERSIDE

Air-Stable Metal Nanowire Networks for Flexible Transparent Electrodes

A Dissertation submitted in partial satisfaction
of the requirements for the degree of

Doctor of Philosophy

in

Chemical and Environmental Engineering

by

Yangzhi Zhu

June 2019

Dissertation Committee:
Dr. Ruoxue Yan, Chairperson
Dr. Juchen Guo
Dr. Bryan Wong

The Dissertation of Yangzhi Zhu is approved:

Committee Chairperson

University of California, Riverside

ACKNOWLEDGEMENTS

It has been a great honor and pleasure to have been cultured in the Yan Research Group, where I not only had a chance to take part in the pioneering research in the field of nanomaterial synthesis and flexible transparent electrodes, but also learned how to tackle tough problems systematically from my advisors and lab mates with multidisciplinary backgrounds.

First and foremost, I would like to thank my advisor Professor Ruoxue Yan for providing me a precious opportunity and a great platform to do research in the fascinating field of nanowire synthesis and flexible transparent electrode fabrication. As a mentor, she was always very supportive, friendly, thoughtful and encouraging. She was always available and glad to discuss the experimental results with me, followed by valuable guidance. As a scientist, she was extremely diligent, knowledgeable, talented and insightful. She was able to give analysis and explanation of research results from the perspective of chemistry, physics, material science and engineering. Without his mentoring and help, I would not have been able to bring this dissertation into existence.

Also, I want to express my sincere thanks to Prof. Ming Liu for his continuous help and support since I joined lab. Especially he gave me many helpful suggestions for my research and shared his own valuable research experience with me when I was down, which encourage me to move forward. Many thanks to Prof. Juchen Guo to give me valuable advices on my LIB project. And Much appreciate to Prof. Guo for recommending me the possible postdoctoral position in peer lab.

Special thanks to Dr. Bozhilov and Dr. llkeun Lee for teaching me many skills in SEM and TEM instrument operation and sample preparation, Dr. Sanggon Kim for helpful support and precious advices, Ning Yu for helping me take HRTEM image for my samples. I would also like to extend my thanks to those in Prof. Ming Liu's lab and Prof. Juchen Guo's lab whom we often work with: Xuezhi Ma, Qiushi Liu, Da Xu; Zheng Yan, Jian Zhang, Jiayan Shi. I will miss the time spent together with everyone and I also wish the best of luck for them and their research.

Last but not least, I want to express my deepest gratitude to my parents, Mr. Yanjun Zhu and Mrs. Mei Yang, my brother Mr. Yangli Zhu, my girlfriend Peipei Liu for their permanent support and unconditional love. Without their constant love, support, and personal sacrifices, I would not be in such a position to succeed. Never before did they doubt my abilities to succeed academically despite not showing it early on. It was through them that I awakened a love for learning, and I am deeply grateful for it. Thank you all!

ABSTRACT OF THE DISSERTATION

Air-Stable Metal Nanowire Networks for Flexible Transparent Electrodes

by

Yangzhi Zhu

Doctor of Philosophy, Graduate Program in Chemical and Environmental Engineering
University of California, Riverside, June 2019
Dr. Ruoxue Yan, Chairperson

Transparent conductive electrodes are essential components in many optoelectronic devices such as solar cells, touch panels, and organic light-emitting diodes (OLEDs), all of which are growing in demand. Traditionally, this role has been well served by doped metal oxides, the most common of which is indium tin oxide, or ITO, which alone accounts for 93% of the entire market of the transparent conductor. However, there are several attributes of ITO that are undesirable. (1), ITO is a ceramic material that is brittle and prone to cracking. (2), The abundance of indium in the earth's crust is low (0.05 ppm), and its cost is correspondingly high, approximately \$700 kg^{-1}. (3), ITO is produced by a slow vapor phase sputtering process, leading to high fabrication cost that dominates the cost of ITO (Indium costs only ~2% for 100 nm thick ITO). In addition, the rate of film throughput decreases with increasing film thickness, making thicker, high-conductivity ITO (~\$26/m^2 for 10 Ω sq^{-1}) more expensive than thinner, low-conductivity ITO (~\$5.5/m^2 for 150 Ω sq^{-1}), which is especially problematic for OLEDs and solar cells due to their need to carry

higher currents, and thus use relatively expensive ITO with a low sheet resistance. In these devices, ITO can account for over 50% of the material cost.

This proposal will focus on developing scalable and cost-efficient methods to fabricate air-stable metal nanowire networks for transparent flexible electronics, targeting at a sheet resistance (Rs) of <60 Ωsq^{-1} at 90% transmittance (T) and low cost. This overall objective will be realized through two thrusts: (1), developing air-stable, highly-oriented epitaxial Ag@Au core-shell nanowire networks, aiming for large-scale roll-to-roll solution-phase fabrication of high-performance transparent conducting films for flexible optoelectronics; (2), developing air-stable super-stretchable Cu@rGO core-shell nanowire networks, aiming at cost-efficient foldable and wearable electronics.

Contents

List of Tables.

List of Figures

Chapter 1. Introduction

Transparent conductive films (TCFs) are essential components in many optoelectronic devices such as solar cells[1-4], touch panels[5-7], and organic light-emitting diodes (OLEDs)[8-10], all of which are growing in demand. Traditionally, this role has been well served by doped metal oxides, the most common of which is indium tin oxide, or ITO, which alone accounts for 93% of the entire market of the transparent conductor[11]. However, there are several attributes of ITO that are undesirable. (1), ITO is a ceramic material that is brittle and prone to cracking. (2), The abundance of indium in the earth's crust is low (0.05 ppm), and its cost is correspondingly high, approximately \$700 /kg[12]. (3), ITO is produced by a slow vapor phase sputtering process, leading to high fabrication cost that dominates the final cost of ITO (Indium costs only ~2% for 100 nm thick ITO[13]). In addition, the rate of film throughput decreases with increasing film thickness, making thicker, high-conductivity ITO (~\$26/m^2 for 10 Ω sq^{-1}) more expensive than thinner, low-conductivity ITO (~\$5.5/m^2 for 150 Ω sq^{-1})[13],which is especially problematic for OLEDs and solar cells due to their need to carry higher currents, and thus use relatively expensive ITO with a low sheet resistance. In these devices, ITO can account for over 50% of the material cost[14].

Therefore, there is an on-going drive to replace ITO with a material that gives comparable performance but can be fabricated through fast and large-scale solution-phase coating processes that have much lower fabrication and equipment maintenance costs[14-15]. Over

the last decade, different ITO alternatives, including conducting polymers[16-17], carbon nanotubes[18-19], graphene[20-21], metal thin films[22-23], metal grids[24-25], nanofibers[26-27], and metal nanowires[28-29] were extensively studied. Although each material has its unique strengths and targeted applications, metal nanowires are the only materials that can be processed with low-cost, scalable solution-phase coating techniques while providing ITO-level performance[13]. And the comparison of TCFs in terms of their compatibility with solution-processed techniques and performance relative to ITO is concluded in Table 1

Table 1. Comparison of transparent conducting materials in terms of their compatibility with solution processed techniques and performance relative to ITO

TCF Materials	Solution Processed	Flexibility	Color	ITO-level Performance	Examples
Metal Nanowires	Yes	Yes	No	Yes	Ag[30], Cu[31]
Graphene	Yes	Yes	No	No	[32-33]
Carbon Nanotubes	Yes	Yes	No	No	[34-35]
Conductive Polymers	Yes	Yes	Yes	No	PEDOT: PSS[36-37]
Metal Thin Films	No	Yes	No	No	Au[38], Ag[39], Ni[40], Cr[41]
Doped-Metal Oxides	No	No	Yes	Yes	Al: ZnO[42], Ga: ZnO[43]
Nanofibers	No	Yes	Yes	Yes	Cu[44]

Ag and Cu nanowires are known as one of the best metal materials for flexible TCFs, because Both Ag and Cu nanowires have excellent intrinsic chemical, optic and electrical properties because of their high crystallinity, high surface-to-volume ratio, low defect level and atomically flat surface[45]. Thus, highly transparent Ag nanowire (or Cu nanowire) based conductive films with low sheet resistance have been confirmed. For example, Li, et al optimized the synthesis, purification and coating of Ag nanowires to achieve films with a sheet resistance of 130 Ω/sq at a transparency of 99.1%[46]. Guo, et al fabricated transparent

electrodes with high-aspect-ratio Cu nanowire ink and a sheet resistance of 51.5 Ω/sq at a high transparency of 93.1% could be achieved as well[47].

However, the biggest issue that limits the commercial application of metal (e.g. Ag and Cu) nanowire networks is their long-term stability under operating conditions. Atmospheric sulfides will react with Ag, converting it into Ag_2S[48-49], which are much less conductive and has a greater absorption cross-section. Similar with Ag, Cu can easily react with oxygen even at ambient conditions, followed by quickly oxidize and finally nanowire becomes non-conductive more quickly. Therefore, Cu and Ag nanowires both require protection from atmospheric corrosion, preferably through a low-cost, scalable solution-phase technique and without sacrificing film performance.

In this review, we summarize the current advances being made in the understanding of the synthesis, mechanistic comprehension of 1D metal nanowires with enhanced stability, and the properties, applications of metal nanowires based flexible TCFs. We start with a comprehensive introduction to the two kinds of typical metal nanowires (Ag and Cu) used for flexible TCFs in section 2. Section 3 provides an overview of the different routes to grow on the Ag or Cu nanowire a layer of conductive yet chemically stable shell to form core-shell nanowires with enhanced stability, as well as the current mechanistic understanding of the formation process. Section 4 reviews the characteristics of flexible TCFs including the optical, electrical, flexibility properties and fabrication process of flexible TCFs. In section 5, we highlight how the unique structure-property relationships of 1D core-shell nanowires have enabled the performance of flexible TCFs. Varieties of applications for core-shell nanowire based flexible TCFs are covered in section 6.

1.1 Nuclei synthesis of 1D core nanowires

There has been a strong drive to replace ITO with a material that gives comparable performance, but is highly flexible, has low near-IR absorption and can be coated from the solution at speeds orders of magnitude faster than the sputtering processes used to deposit ITO. Metal nanowires especially for Ag nanowire and Cu nanowire can be an ideal alternative to ITO that meets thes requirements. Moreover, it is well established through theoretical simulations and experiments that the performance (Transparency V.S. Sheet resistance) of metal nanowire based transparent conductive film is largely determined by the aspect ratio (L/D) of nanowires[50]. Here, we provide a brief account of the common practice in syntheising Ag nanowire and Cu nanowire especially for high aspect ratio nanowire.

1.1.1 Silver Nanowires

So far, the polyol-mediated reduction approach developed by Xia group represents the state-of-the-art synthesis technique suitable for solution-phase scalable production of commercial Ag nanowires[51-57]. This recipe involves the reduction of silver precursors (usually $AgNO_3$) by ethylene glycol (EG) in the presence of polyvinylpyrrolidone (PVP) used as capping reagent. Typically, the reductant EG is preheated to the specific temperature such as 180°C before dropping reaction solutions containing the silver precursor such as $AgNO_3$ and capping reagent such as PVP. The addition of a trace amount

of metal salt such as $CuCl_2$[58], NaCl[59], KBr[57] and $Fe(NO_3)_3$[60] have also been confirmed to modify the morphology of the final products. Reductant/solvent EG firstly react slowly with the Ag^+ to produce Ag (0). The Ag atoms then agglomerate to form nuclei, the nucleation favors multiply twinned decahedral particles (MTPs) by the more closely packed {111} facets and these MTPs are the seeds for the later formation of Ag nanowires. Since the twin defect represents the highest energy site on the surface of MTP, silver atoms will preferentially crystallize on these sites, resulting in an elongation of the decahedron into a pentagonal rod with sides bounded by {100} facets. Once the pentagonal rod has formed, PVP will preferentially binds with {100} over {111} facets. Loosely packed {100} facets tend to offer more space for the attachment of surfactants PVP while the more closely packed {111} facets serve as low surface energy sites for the deposition of Ag atoms. Therefore, the nanorod can readily grow into long nanowires[61]. The size of nanowires can be modified by changing reducing agent amount, silver precursor concentration and the trace amount of metal salt.

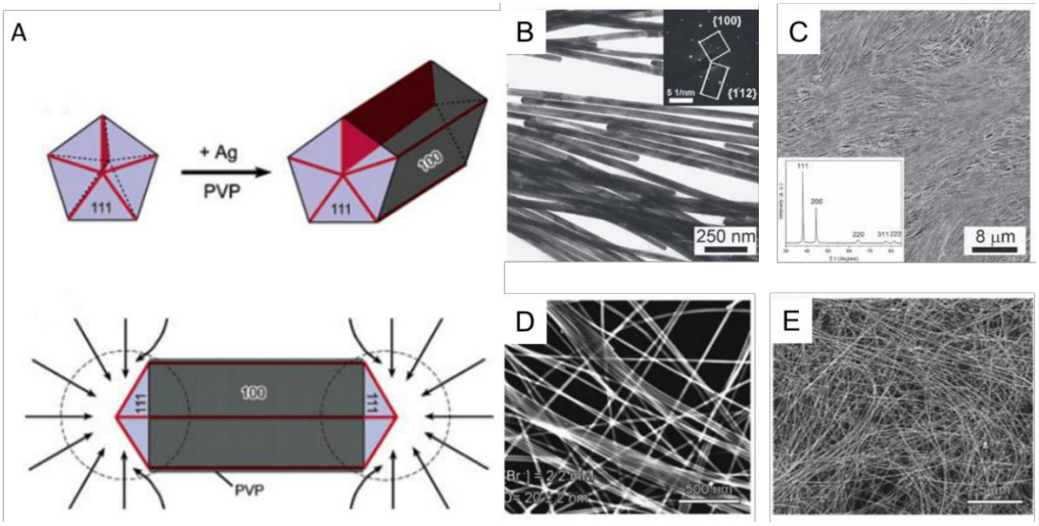

Figure 1.1. Polyol-mediated synthesis of Ag nanowires. (A) Schematic illustration of the mechanism proposed to account for the growth of Ag nanowires[52]. (B) TEM image of the Ag nanowires and the corresponding selected area electron diffraction (SAED) pattern of a single Ag nanowire[62]. (C) Low magnification SEM image of dense Ag nanowire sample[62]. (D) SEM images of Ag nanowires with 20 nm of diameter[46]. (E) Low magnification SEM images of purified Ag nanowire sample[46]. (A) Reprinted with permission from ref 52. Copyright 2007 Elsevier. (B, C) Reprinted with permission from ref 62. Copyright 2002 Elsevier. (D, E) Reprinted with permission from ref 46. Copyright 2009 Elsevier.

Prof.Xia has demonstrated the used of polyol synthesis for the production of Ag nanowires with diameters controlled in the range of 20-150 nm, together with lengths up to 100 μm[54-55, 57]. Benjamin modified this approach by mixing the Ag precursor ($AgNO_3$) with NaCl or NaBr, followed by heating the mixture under inert atmosphere. They demonstrated the production of Ag nanowires with diameters below 30 nm and lengths of 50 μm[46]. More recently, Prof.Xia et al, synthesized Ag nanowires with diameters below 20 nm and aspect ratio more than 1000 in high morphology purity through a protocol involved with NaBr under atmospheric pressure at 160°C (Figure 2)[57]. Kim suggested a high pressure (~3 atm) polyol synthesis technique that the Ag nanowires whose diameters could be controlled in

the range of 15-30 nm and lengths up to ~20 μm by introducing a mixture of KBr and NaCl into a polyol synthesis[63]. Except for the one-pot synthesis, Ko et al, developed a successive multistep growth method using the as-prepared nanowires as seeds for growing longer nanowires, which was repeated several times on the same nanowires leads to the final nanowires with lengths of 500 μm and average diameters of 160 nm[64]. Even though the aspect ratio of these nanowires is relatively high, the successive growth method is not practical for large scale production of Ag nanowires.

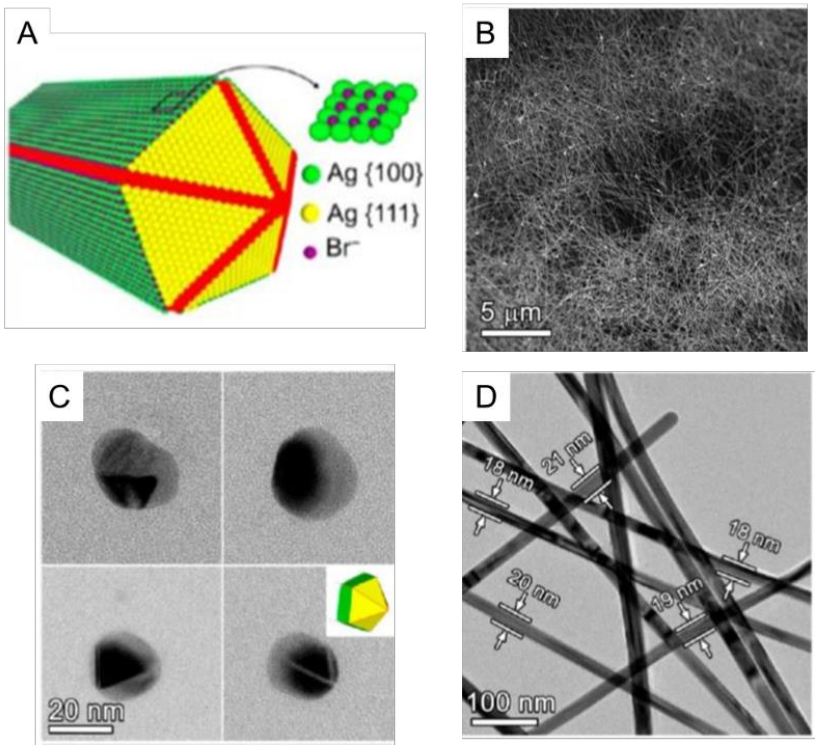

Figure 1.2. Facile synthesis of sub-20 nm Ag nanowires via bromide-mediated polyol method. (A) Schematic illustration displaying the function of Br^- ions in the synthesis of sub-20 nm Ag nanowires. (B) Low magnification of as-prepared Ag nanowire sample. (C) shows the typical seeds formed in the nucleation stage during a synthesis. The nanoseeds clearly suggest facets with twin boundaries, which finally evolve to Ag nanowires in a reaction. (D) SEM images of Ag nanowires to display the sub-20 nm of diameters.[57] Reprinted with permission from ref 57. Copyright 2016 American Chemical Society.

1.1.2 Copper nanowires

Cu is known as 1000 times more abundant than Ag or 22000 times abundant than Au. And Cu has the second-best intrinsic conductivity and only 6% less conductive than Ag while 30% more conductive than Au. Meanwhile, Cu is much cheaper than Ag, Au or Indium by 100 times[11]. And Cu nanowire based transparent conductive films could provide comparable ITO levels of electrode performance at a lower cost which was demonstrated in the recent work[31, 47, 65]. So, motivated by the low cost of solution phase processing and the low cost of Cu, Cu nanowires become an attractive replacement to Ag nanowires for flexible TCF fabrication. Large amount of Cu nanowire syntheses has been reported over the decades. Generally, the production of Cu nanowires can be concluded into three methods: (1) one-pot; (2) seed-mediated synthesis; (3) template-directed.

In a one-pot synthesis, Cu atoms are first formed via chemical reeducation, followed via chemical reduction, followed by their aggregation into nuclei and then further growth into seeds and the corresponding nanostructures. Surface capping agents are typically involved in the growth process. Based on the different reducing agent used, it can be divided into two major protocols: (1) ethylenediamine (EDA)-mediated synthesis, and (2) alkylamine-mediated synthesis.

In ethylenediamine-mediated synthesis, Cu (II) ions are reduced by hydrazine (N_2H_4) in basic system including ethylenediamine as the capping agent. Zeng synthesized Cu nanowires with one of the first scalable solution phase techniques in 2005[66]. And the final Cu nanowires were 90-120 nm in diameter and 40-50 μm in length (Aspect Ratio: 350-

450). Without ethylenediamine used as a capping agent, only copper nanoparticles with large diameter distribution were found in this synthesis. Ye et al. increased the aspect ratio up to 2280 (80 μm long and 35 nm wide) by modifying the ethylenediamine-mediated synthesis[29]. And they also claimed that the size and shape of the resulted Cu nanowire samples could be controlled by tuning the molar ratio of copper precursor, hydrazine, and ethylenediamine.

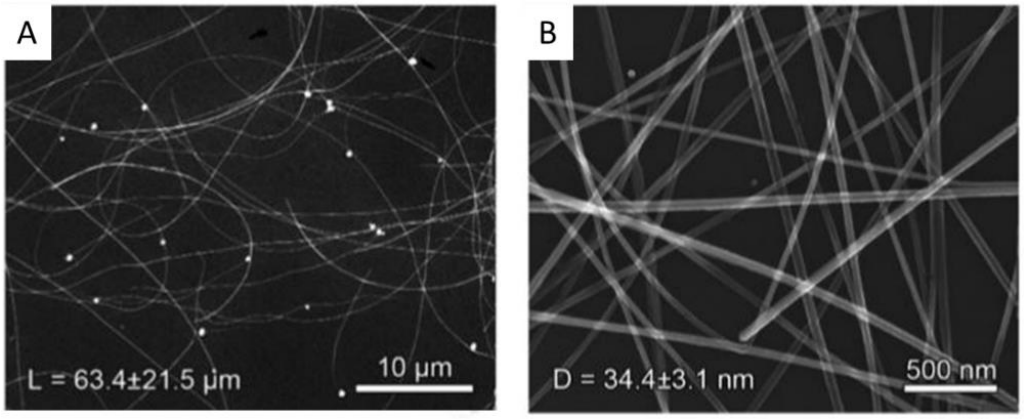

Figure 1.3. A rapid synthesis of high aspect ratio Cu nanowires. (A, B). SEM images to show the Cu nanowires with 63.4 μm in length and 34.4 nm in diameter[67]. Reprinted with permission from ref [67]. Copyright 2014 Wiley.

In alkylamine-mediated synthesis, it generally requires a higher temperature compared than ethylenediamine-mediated synthesis. Peng et al. reported a solution-phase processed protocol to prepare Cu nanowires by reducing $CuCl_2$ in oleylamine solution at 80-175°C[47]. In this recipe, oleylamine was served as a capping agent and Ni (II) was introduced as a catalyst for reduction of Cu (II). This recipe increased the average length to 40μm, and the mean diameter were reduced to below 16 nm (aspect ratio: ~2500). Xia introduced glucose

as a reductant and replaced oleylamine with hexadecylamine to produce Cu nanowires with a mean diameter of 25 nm and a length ranging from tens to hundreds of micrometers[68]. Recently, Yang and co-workers used an additional reducing agent, tris(trimethylsilyl)silane to reduce the diameter of Cu nanowires to 17 nm and the length are 17 μm in long (aspect ratio: 1000)[31].

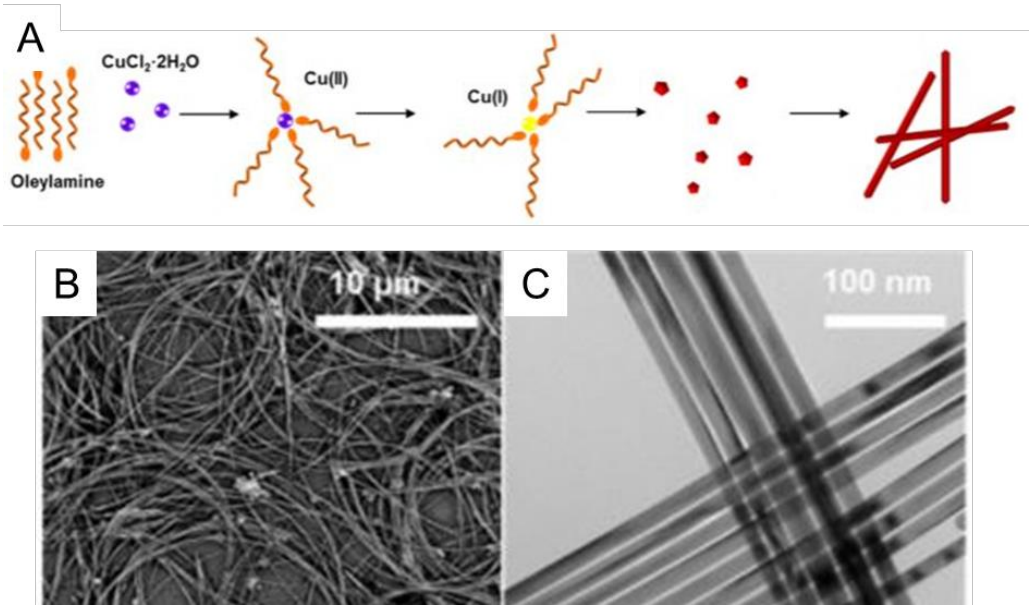

Figure 1.4. Synthesis of ultrathin Cu nanowires using tris(trimethylsilyl)silane as a reductant. (A). Schematic illustration of copper source reduction, five twinned seeds nucleation, and nanowire evolution. (B, C) SEM and TEM images of as-grown Cu nanowires with a mean diameter of 17 nm[31]. Reprinted with permission with ref 31. Copyright 2015 American Chemical Society.

In addition to ethylenediamine-mediated and alkylamine-mediated synthesis, hydrothermal approach was also explored to produce Cu nanowires in one pot synthesis. For example, Cu nanowires with uniform diameter (64±8 nm) and lengths ranging from several hundreds of micrometers to several micrometers have been successfully produced with simple hydrothermal method by Zoltan et al[69].

Both the ethylenediamine-mediated and alkylamine-mediated synthesis can prepare long, thin copper nanowires that have comparable or even higher ITO-level performance when processed to fabricate transparent electrodes. And both methods can be performed under atmospheric pressures which make it more practical for scalable production.

Not only for the one pot synthesis; various types of templates have also been used to direct the growth of Cu nanowires. CTAB was believed to act as a soft template to guide the growth of Cu nanowires. For example, Lu and his co-workers reported that Cu nanowires could be produced in a medium with a tubular liquid-crystalline provided by CTAB, with $Cu(acac)_2$ serving as a copper precursor, and hexadecylamine as a reducing agent[70]. The result shows that the average diameter of the Cu nanowires was about 78 nm while the length of the Cu nanowires varied form tens to hundreds of micrometers. Except for this, DNA was also employed to act as template for the formation of Cu nanowires and the formed Cu nanowires which has less than 10 nm in thick[71]. However, this method is not scalable, and the aspect ratio of the resulted Cu nanowires is too small to achieve a good performance of nanowire based flexible TCFs.

1.2 Different techniques to form 1D metal core-shell nanostructures

A core-shell nanostructure consists of an inner core coated with a shell made of another metal (or non-metal). The introduction of core-shell nanostructures can bring up several advantages, including enhancement in performance of flexible TCFs, due to the

improvement in thermal and chemical stability and tuning of optical property. In the past decades, a variety of synthetic methods have been developed for producing core-shell nanostructures, such as chemical reduction, electroplating, chemical vapor deposition (CVD), electrochemical deposition. Typically, the conformal deposition of another metal can lead to the formation of core-shell structures with a shape or morphology like that of the core that serves as a physical template for the coating process. By tuning the amount of metal precursor added, one could be able to precisely control the shell thickness if the deposition follows a layered growth mode. In the following discussion, we will mainly focus on the solution-processed coating techniques.

1.2.1 Chemical reduction

The chemical reduction method can produce metal-based core-shell nanostructures in solution phase. The principle of this technique is to grow a metal shell or nanocrystal on a metal core (i.e. Ag or Cu as core), through the chemical reduction of metal precursors with a reducing agent in the presence of surfactants. The growth rate, the reduction potential between metal precursor and core metal, and even the lattice mismatch are the key factors for achieving uniform and conformal deposition of metal on another core metal to form core-shell nanostructures and even the epitaxial growth.

Initially, this method was used to deposit a metal shell onto another metal nanocrystal to form core-shell nanostructures, especially noble metal core-shell nanowires. However, when the ions of one metal with a higher reduction potential are added to a solution

containing a reduced metal with a lower reduction potential, the metal with the lower reduction potential will be oxidized and replaced by atoms of the metal with a higher reduction potential through galvanic replacement reaction. In this case, voids can be formed, and a hollow, alloy nanostructure can be obtained. To avoid the damage or even removal of the core due to galvanic replacement, several methods can be applied, such as adding a reducing agent to serve as an alternative source of electrons, modifying the reduction potential of the metal ions, and the use of protective layers. For example, Ag@Au core-shell nanowires could be produced via the reduction of Au^{3+} by ascorbic acid (AA) in the presence of Ag nanowires under an alkaline condition. Because of the higher reduction potential of Au^{3+}/Au (1.52V versus SHE) compared to Ag^{+}/Ag pairs (0.8V versus SHE), galvanic replacement reaction between Ag and Au can be happened, making it challenge to generate a core-shell nanostructure with Ag nanowire. In this study, a much stronger reductant AA under pH=10 was used to enable electrons from AA oxidation to replace those from Ag oxidation. In addition, the Cl^{-} in $AuCl^{4-}$ can be replaced by OH^{-} to form Au $(OH)^{4-}$, thereby reducing the reduction potential of Au (III) precursor in an alkaline condition, thus the galvanic replacement between Ag and Au was suppressed to some extent and Ag@Au core-shell nanowires were prepared. With the production from the Au shell, the core-shell nanowire based transparent electrode improved its stability against oxidative etching.

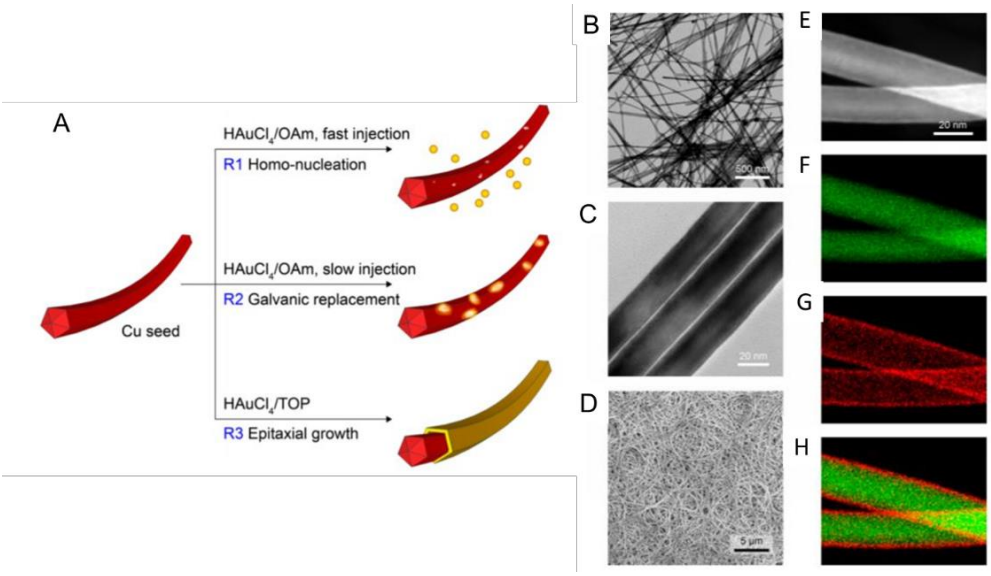

Figure 1.5. Ultrathin epitaxial growth of Cu@Au core-shell nanowires. (A) Chemical reduction of $HAuCl_4$ precursor with Cu nanowires as coating seeds under different ligand environments such as Oleylamine and trioctylphosphine. TEM (B, C) and SEM (D) images with different magnifications of Cu@Au nanowires, HAADF-STEM image (E), and the corresponding EDS mapping images (F-H) of as-grown Cu@Au nanowires[72]. Note: red color represents Au and green color represents Cu. Reprinted with permission from ref [72]. Copyright 2017 American Chemical Society.

In another example on the synthesis of Cu@Au core shell nanowires (Figure 1.5)[72], trioctylphosphine (TOP) was used as a strong binding ligand to avoid galvanic replacement reaction. Based on the hard and soft acids and bases theory, Au(III) ion is a soft Lewis acid, therefore, the introduction of a soft Lewis base such phosphine would strongly bind to the Au (III) ions and lead to a decrease in the reduction potential, when Au (III) precursor was added in the presence of TOP, the reduction rate of Au(III) was suppressed, and thus a core-shell nanostructure was generated. When oleylamine (OLA) was used instead of TOP, OLA was a hard Lewis base and could not bind strongly to Au (III). In this case, galvanic replacement dominated the reaction and voids, or pores could be found in the final

nanowire products. Furthermore, the core-shell nanowire based transparent conductors displayed supreme stability in the air or even in the high temperature/ high humidity (80℃/80%).

Not only for Au deposition, Ni, Sn, Pt, and Zn can also be used as protective shell deposited on Cu nanowire surface. For example, Cu@Ni core-shell nanowires were synthesized by adding Cu nanowires to a solution containing PVP (dispersing agent), ethylene glycol (solvent), Ni $(NO_3)_2$ (Nickel source), and N_2H_4 (reducing agent) at 120℃[73]. As the Ni was reduced onto the Cu nanowires that was confirmed by EDS mapping image. The shell thickness was controlled by the initial molar ratio of Cu to Ni ions. Another research showed that Pt, Ag can both be reduced onto Copper nanowire surface by introducing a stronger ascorbic acid (AA) to the solution[74]. It is thought that the reduction potential of AA (-0.35V) is strong enough that it can reduce the copper oxide on nanowire surface and prevent the oxidation of nanowires but not so strong that it reduces the noble metal ions in solution and self-formed nanoparticles. And the Cu@Ni core-shell nanowires and the Cu@Ag nanowires based transparent conductive films showed an improved stability in high temperature (85℃ or 160℃) while the copper nanowire based transparent conductive films showed a quickly and dramatically increase in sheet resistance in such harsh environment.

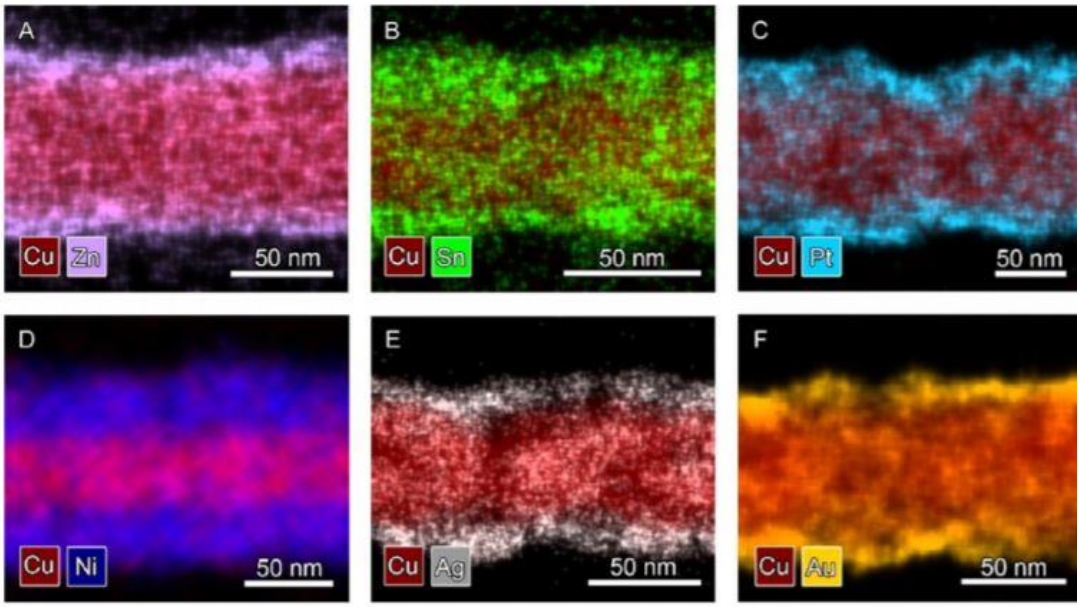

Figure 1.6. Synthesis of different types of core-shell nanowires (CuNW as core nanowire). EDS mapping images of (A) Cu-Zn, (B) Cu-Sn, (C) Cu-Pt, (D) Cu-Ni, (E) Cu-Ag, and (F) Cu-Au core-shell nanowire by (A-C) electroplating and (D-F) electroless plating.[74] Reprinted with permission from ref [74]. Copyright 2016 American Chemical Society.

1.2.2 Electroplating

Another method to prepare core-shell nanostructure is electroplating, and it starts with the production of Cu nanowire film to serve as working electrodes. The basic plating process involves depositing the desired metal ions onto the Cu nanowire surface by holding the Cu nanowire film electrode at a negative potential. For example, nickel can be continuously deposited onto Cu nanowires by applying a potential of -0.75v VS NHE for various times[75]. This Ni coating can be confirmed by the color of the resulted sample, SEM and TEM image.

In addition, Zn can also be easily plated onto Cu nanowires to create a 15 nm thick of shell after electroplating at -1.15V for 10 min. However, for Sn, the constant-potential electroplating at -0.65V resulted in an uneven coating consisting of nanoparticles with diameters in the tens to hundreds of nanometers[76]. To fix this problem, the electroplating of Sn (II) to Sn (0) was carried out by alternating the reduction and oxidation of Sn at -0.7 and -0.2V, respectively, with successive cyclic voltammetry scans. As a result, a smooth Sun shell with an average thickness of 3-5 nm was achieved after 250 cycles of successive cyclic voltammetry scans.

For metals more noble than Cu, such as Pt, how to avoid galvanic replacement was the first priority, or the film will become nonconductive. And in this study[77], galvanic etching by Pt can be prevented by holding the film at -0.3V prior to the addition of K_2PtCl_6 to the plating solution, with a pre-applied negative potential, 7 nm thickness of Pt shell was formed within 10 min.

1.2.3 Chemical vapor deposition

Chemical vapor deposition (CVD) has proved to be a powerful method to grow nanomaterials, including 2D materials, and is also one of the most widely used methods for the construction of core-shell nanowires to improve the stability of Ag or Cu nanowire based transparent conductive films. In CVD, a substrate containing metal nanowires is typically placed in a furnace chamber and then exposed to one or more gas and/ or vapor precursors, which react and/ or decompose on the substrate to obtain the desired materials.

For example, Jinsub Park demonstrated that graphene coated Cu core-shell nanowires was synthesized via thermal CVD at a low temperature (600℃) with optimized conditions, and this graphene layer could prevent Cu nanowires from oxidation which was confirmed by the thermo-hygrostat test (85℃/85% RH) for two weeks[78]. It is thought that with hydrogen and argon as carrier gases, methane as precursor was flowed into the chamber and diffused through the boundary layer from the mainstream and reaches the surface of Cu nanowires. And then, CH_4 undergoes adsorption on Cu nanowire surfaces and catalytic dehydrogenation to form active carbon species. Therefore, a graphene layer was formed on the nanowires surface. Moreover, the transparent conducting film of Cu@Graphene core-shell nanowires showed high performance in optical and electrical properties (~37 Ω/sq at 89% of transmittance) that has a comparable level of ITO.

Another example shows that graphene coated copper core-shell nanowires was synthesized using a low temperature plasma-enhanced chemical vapor deposition process at temperature as low as 400℃ for the first time[79]. It is hypothesized that a hydrogen plasma was applied to remove an oxide layer and other organic contaminants on the surface of the Cu nanowire and a reaction gas mixture composed of methane and hydrogen was introduced into the chamber, then a vacuum plasma enhanced chemical vapor deposition was performed to grow a thin graphene layer on Cu nanowire surfaces. The transparent conductive electrode-based graphene coated Cu core shell nanowire exhibited excellent optical and electrical properties comparable to those of conventional ITO. Not only for this, because of the protection of graphene layer, it displayed remarkable thermal oxidation and chemical stability. This plasma-enhanced CVD process has several advantages such as

low-temperature processing, fast deposition rate, composition controllability and good uniformity compared with other CVD coating method.

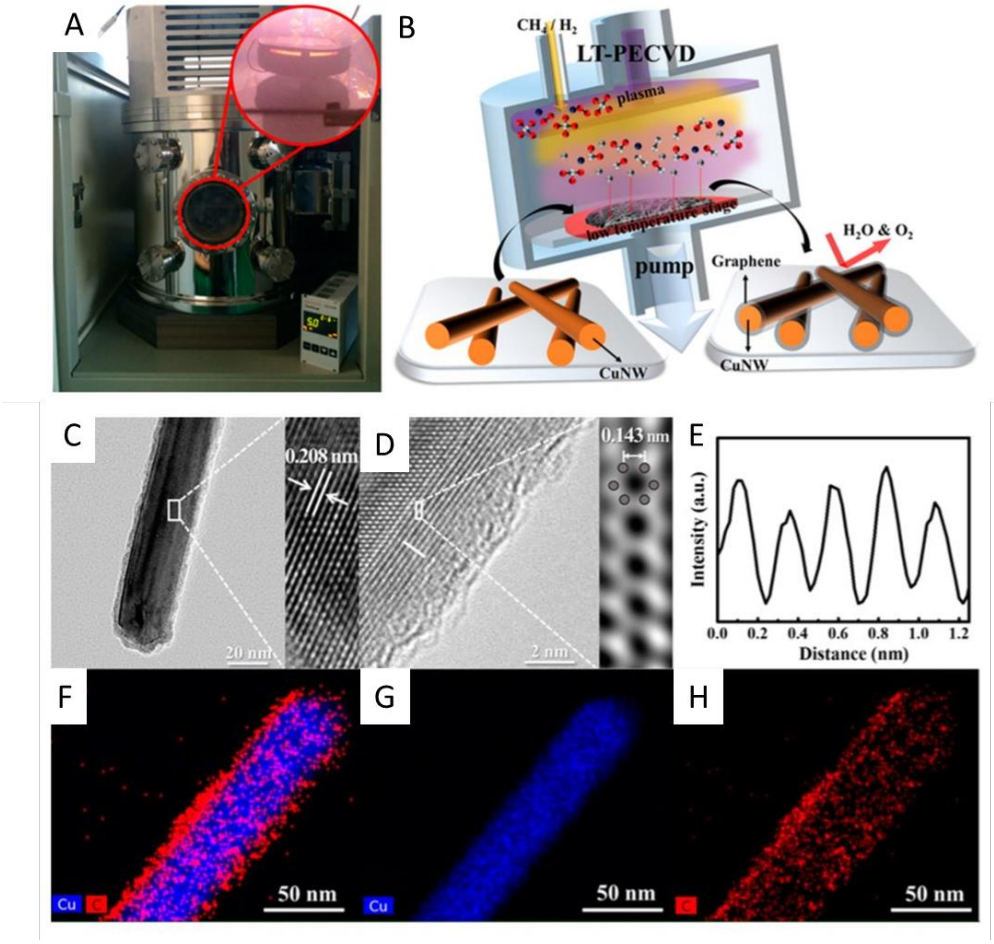

Figure 1.7. Synthesis of Cu-Graphene core-shell nanowire with low temperature plasmon enhanced chemical vapor deposition (LT-PECVD). (A) Digital photo of the LT-PECVD reaction system for the synthesis of Cu-Graphene core-shell nanowires. (B) Schematic illustration for the synthesis of the Cu -Graphene Core-Shell nanowires by the LT-PECVD protocol. (C) TEM image of Cu-Graphene Core-Shell nanostructure. (D) High resolution TEM image of Cu-Graphene Core-Shell nanowire. (E) Line scanning along the selected line of the Cu-Graphene core-shell nanowire. (F) EDS mapping measurement of Cu-Graphene core-shell nanowire. (G) Cu element and (H) carbon elemental mapping of the single Cu-Graphene core-shell nanowire[79]. Reprinted with permission from ref [79]. Copyright 2015 American Chemical Society.

1.2.4 Solution-process coating technique

Except for the chemical reduction and CVD coating method to improve the Cu nanowire that is applied for transparent conductive film, a new solution method-based approach was reported to wrap graphene nanosheets on the surface of Cu nanowires. And then graphene oxide can be reduced, and highly conductive reduced graphene oxide coated Cu core shell nanowires were final produced[80].

It is hypothesized that the thin native oxide layer with an average thickness of 1-3 nm on Cu nanowire surface would have strong interactions with the hydroxyl and carboxyl groups. Since GO is highly oxidized, it serves as a multidentate ligand and interacts with much stronger with oxide surface. This provides large driving force for the ligand replacement and then the graphene oxide layer could be wrapped onto Cu nanowire surface.

Moreover, the transparent conductive films were fabricated with these core-shell nanowires have comparable performance to ITO or Ag nanowire films (sheet resistance ~28 Ω/sq, haze ~2% at transmittance of ~90%). and furthermore, this protection from reduced graphene oxide greatly improved the stability of the core-shell nanowires based transparent conductive film in the air environment even in the high temperature condition.

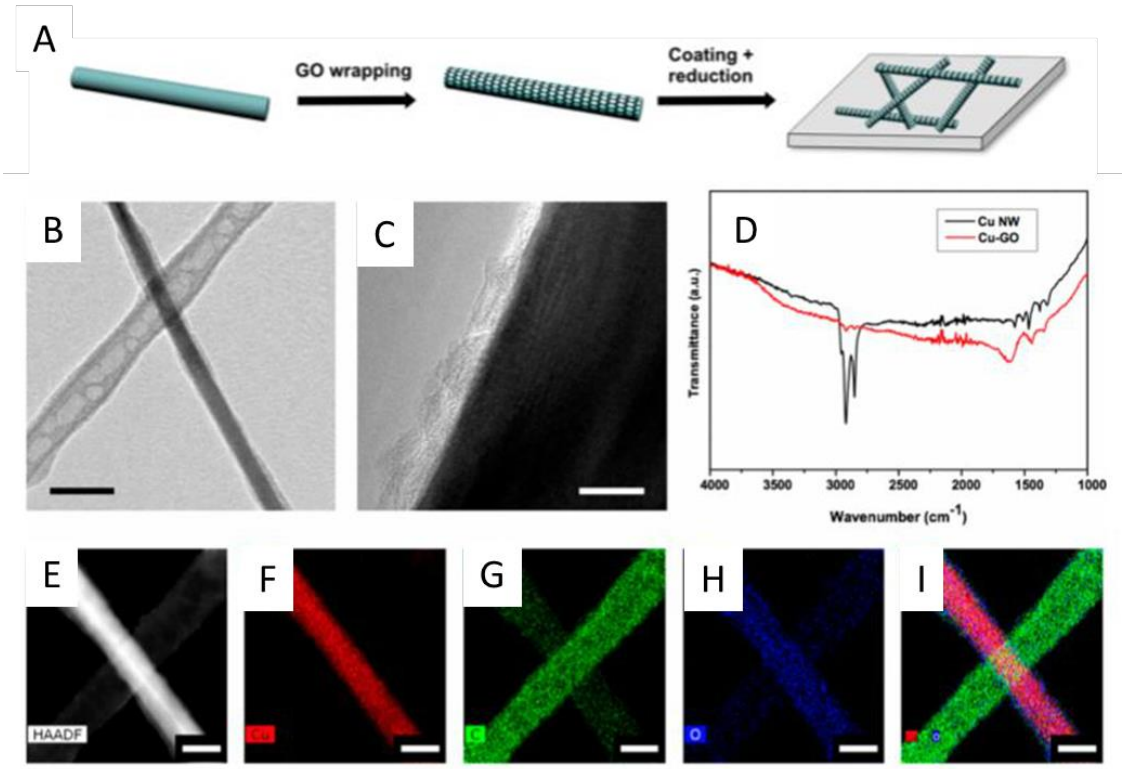

Figure 1.8. Solution-processed Cu-Reduced Graphene Oxide core-shell nanowires. (A) Schematic illustration of the graphene oxide wrapping on nanowire surface film deposition, and thermal reduction process to fabricate the transparent nanowire transparent electrodes. (B) TEM image of the Cu-GO core-shell nanowire. (C) High resolution TEM image of the GO coated Cu nanowire. (D) FTIR spectra of the Cu nanowire before and after GO coating. (E-I) EDS mapping of a core-shell nanowire displaying the elemental distribution of copper, carbon, oxygen, and the combination of the three elements. Scale bar: 40nm[80]. Reprinted with permission from ref [80]. Copyright 2016 American Chemical Society.

1.3 Characteristic of flexible transparent conductive film

Flexible transparent electrodes are those flexible electrodes can not only have high transmission at a low sheet resistance. The function relationship between the dimensions of nanowires and the properties of the film would be very helpful in guiding how to optimize the comprehensive performance of flexible transparent conductive film. (1) the

dependence of optical performance on the area fraction and dimensions of nanowires. (2) the dependence of film conductivity on nanowire size and area density. (3) the dependence of flexibility property on the dimensions of metal nanowires and nanowire materials. In this section, we review current progress in the optical performance, electrical property, and flexibility characterization of flexible TCFs.

1.3.1 Optical Properties of the Networks

Generally, researchers would like to create a nanowire network that is as transparent as possible. The transmittance, %T, of a nanowire network can be described by equation 1:

$$\%\mathrm{T} = e^{-AF \times Q_{ext}} \qquad (1)$$

Where AF is the area of the film covered by the nanowires and Q_{ext} is the extinction efficiency of the nanowires[11].

And the area fraction AF can be described as $\mathrm{AF} = N \times L \times D$, where N is the number density of the nanowires, L is the length of the nanowires, D is the diameter of the nanowires. Q_{ext} is the ratio of the amount of light scattered and absorbed by a nanowire relative to its geometric cross-section. And it can be approximated from Mie theory[81]. Figure displays that the extinction efficiency decreased with diameter. Because nanowires with large diameters are more efficient at blocking light than nanowires with smaller

diameters due to their larger extinction cross-sections. So, the optical properties could be enhanced by producing thinner nanowires.

Haze is another unique optical property of nanowire based FTCFs, and it is defined as the percentage of transmitted light which in passing through the film deviates more than 2.5° from the incident light by forward scattering[11].

$$H = \frac{(I_s)_{2.5°-90°}}{I_d + (I_s)_f} \quad (2)$$

Where I_d is the light flux transmitted directly, and $(I_s)_f$ is the flux undergoing forward scattering.

Haze is therefore especially important in display applications, where scattering will reduce the sharpness of images. Generally, haze should be below 1% for an ideal display. Large value in haze become a big challenge for nanowire based flexible TCFs, because nanowires are strong scattering centers. And the haze increases exponentially with increasing nanowire diameter. So, in order to reduce the haze, lower diameter nanowires should be desired.

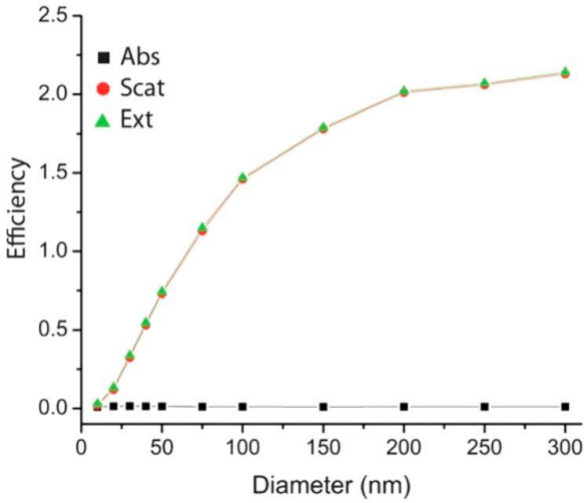

Figure 1.9. Efficiency of absorption, scattering, and extinction of Ag nanowires as a function of their diameters[50]. Reprinted with permission from ref [50]. Copyright 2012 Royal Society of Chemistry.

1.3.2 Electrical properties of flexible TCFs

To understand how the electrical conductivity of a random nanowire network changes with the number of nanowires, it is necessary to start with the simple case of a square grid of nanowires with diameter D and length L[81]. Based on Kirchhoff's laws, the sheet resistance Rs for a square network with N multiply N nanowires is

$$R_s = \frac{N}{N+1} R_{nanowire} \quad (3)$$

For the case of nanowires, $R_{nanowire} = \frac{4\rho L}{\pi D^2}$, where ρ is the resistivity of the nanowires. If the amount of nanowires is far more than 1, then

$$R_s = \frac{4\rho L}{\pi D^2} \quad (4)$$

Thus, the sheet resistance of a large square network of nanowires is just equal to the resistance of an individual nanowire, this equation can be rewritten in terms of the area fraction of the nanowires with AF= (1- D/L) ≈ 2D/L. For a nanowire network (L>D).

$$R_s = \frac{8\rho}{\pi DAF} \qquad (5)$$

This equation indicates that Rs will increase linearly with nanowire diameter and area fraction AF.

All in all, longer and thinner nanowires are desired to improve the performance of nanowire based transparent electrodes.

1.3.3 Flexibility properties of flexible TCFs

One clear advantage of a metal nanowire-based transparent conductor compared to ITO is its mechanical flexibility and stretch ability. Several research groups have demonstrated that metal nanowire-based films can retain their conductivity after hundreds of bending cycles, whereas ITO is not conductive after a few cycles of bending[82-85]. In terms of stretch ability, films made of metal nanowires can retain their conductivity up to strains of ~50%, and this can be increased to several hundred percent if the films start in a pre-strained, buckled states and consist of nanowires hundreds of micrometers in length. In comparison, individual nanowires fracture at strains <5%. It is thought that the stretch ability of a nanowire network is accommodated by a mixture of network deformation and sliding.

Reversible sliding was observed at low nanowire densities for a Cu nanowire-based dielectric elastomer actuator that achieved area strains of 200%. Higher nanowire densities led to nanowire entanglement and fracture. Pretraining the substrate before stretching leads to out of plane bending of the nanowires, allowing them to accommodate greater strains before fracture.

One can also create wavy nanostructures by bending them in-plane. One way to accomplish this is by compressing a nanowire film in a Langmuir−Blodgett trough, followed by transfer of the film to a stretchable substrate. The resulting wavy nanowire networks exhibited much less fracture and greatly reduced resistance during stretching. A more practical approach to improved stretch ability is to use spray coating to form rings of Ag nanowires on the substrate. The Ag nanowires were apparently bent into ring structures inside the micrometer-sized liquid droplets rather than by the coffee ring effect during drying. The Ag nanowire rings exhibited a stable electrical resistance during 5000 cycles of mechanical stretching/releasing with 30% strain, whereas the randomly distributed Ag nanowires showed a dramatic increase in the electrical resistance with cycling. Different flexible metal nanowire based TCF devices are shown in Figure 1.10.

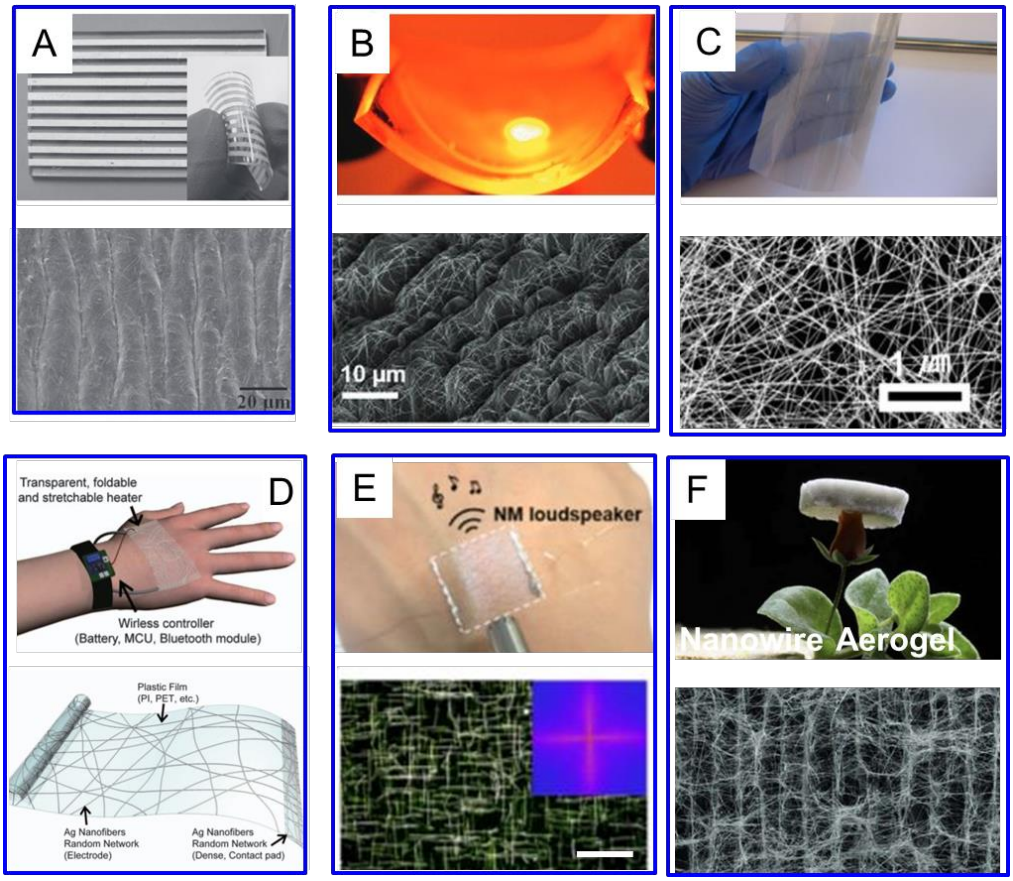

Figure 1.10. Flexibility test of the metal nanowire based transparent electrode devices. (A) Top: photograph of patterned parallel Ag nanowire/PDMS stretchable conductors. The inset shows the conductors deformed by hand. Bottom: SEM image of the Ag nanowire/PDMS surface after the stretching and releasing cycles86. (B) Top: photograph of a flexible LED cell using Ag nanowire network based transparent electrodes. Bottom: SEM image of the corresponding Ag nanowires coated on bubbled substrate87. (C) Top: a) Top: photograph of Ag nanowires film coated on PET substrate. Bottom: SEM image of the Ag nanowires film88. (D) Top: photograph of the wearable heater with a controller unit and wireless operation between a smartphone and the Bluetooth-integrated temperature controller circuits. Bottom: the stretchable transparent heater fabricated with Ag nanofibers89. (E) Top: Skin-attached loudspeaker mounted on the back of a hand. Bottom: Dark-field optical image of Ag nanowire arrays90. (F) Top: Photograph of ultra-light conductive Ag nanowire aerogel. Bottom: SEM image of Ag nanowire-based aerogel91. (A) Reprinted with permission from ref 86. Copyright 2012 Wiley. (B) Reprinted with permission from ref 87. Copyright 2016 Wiley. (C) Reprinted with permission from ref 88. Copyright 2016 American Chemical Society. (D) Reprinted with permission from ref 89. Copyright 2017 Nature. (E) Reprinted with permission from ref 90. Copyright 2018 Science. (F) Reprinted with permission from ref 91. Copyright 2017 American Chemical Society.

1.4 Fabrication Methods for flexible TCFs

Flexible transparent conducive films can be made from metal nanowires using a variety of different coating methods including dip coating, drop coating, spin coating, spray coating, vacuum filtration and coating with Meyer rod. All these fabrication methods can ensure that the nanowire based flexible TCFs have excellent electrical conductivity, optical transmittance, mechanical flexibility and even stretch ability performance.

1.4.1 Dip coating

Dip coating involves simply dipping a substrate into a suspension of the nanowires. The concentration of nanowires and the withdraw velocity can both control the thickness of nanowire film or the transmittance of nanowire based flexible TCFs. For example, Ma et al. developed a two-step dip-coating process to prepare an order-enhanced Ag nanowire networks on polyethylene terephthalate (PET) substrates using long and short Ag nanowires[92]. In this study, this order-enhanced Ag nanowire showed a typical sheet resistance of 35 Ω/sq. at 92% of transmittance much higher than random Ag nanowire networks (sheet resistance = 40 Ω/sq.; Transmission = 87%). And the resulting TCF was employed to construct polymer solar cells which could make the power efficiency up to 3.28%. Furthermore, Zhang and his co-workers developed a modified dip coating process with water-bath assisted convective self-assembly (Figure 1.11)[93]. In this work, the aligned Ag nanowire film was fabricated via three times orthogonal dip coating protocol at a water-bath temperature of 80°C that has a sheet resistance of 11.4Ω/sq with a transmittance of

89.9% at 550 nm and the root mean square of this aligned nanowire film was 15.6 nm which is much lower than the spin-coated random nanowire film (37.6 nm) with a similar sheet resistance.

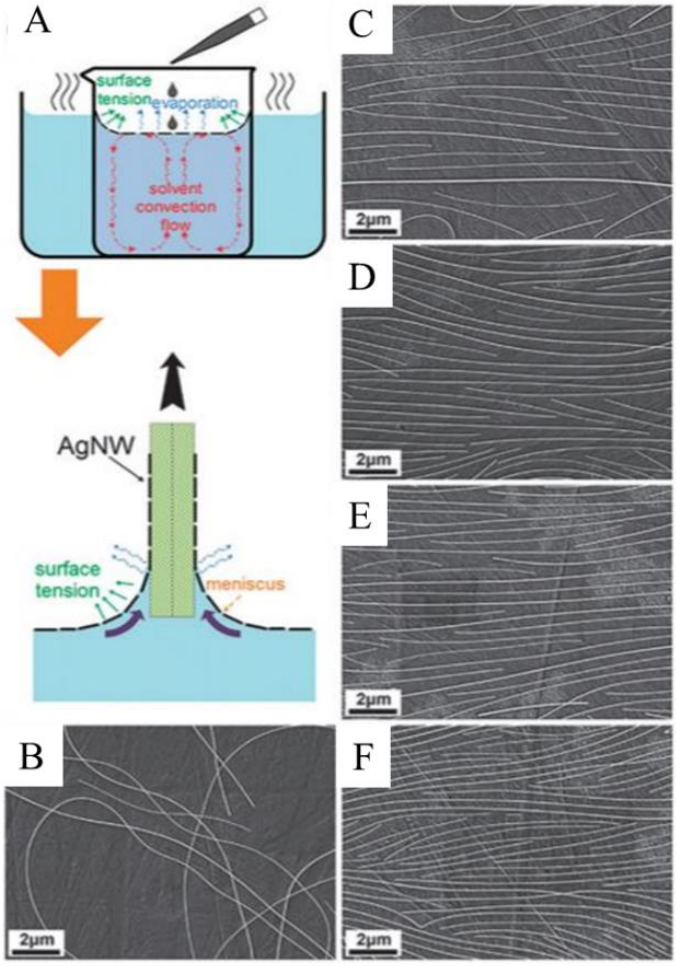

Figure 1.11 Water bath assisted assembly of ordered Ag nanowire based transparent conductive films. (A) Schematic illustration of the fabrication process of Ag nanowire network coated on a glass substrate assisted with water-bath assisted self-assembly by dip-coating. SEM images of the corresponding aligned Ag nanowire conductive films under different water-bath temperature: (B) room temperature, (C) 50 ℃, (D) 70 ℃, (E) 80 ℃ , and (F) 90 ℃, respectively[93]. Reprinted with permission from ref [93]. Copyright 2015 Royal Society of Chemistry.

1.4.2 Drop casting

Drop casting involves dropping a suspension of the nanowires on a substrate, and the nanowires can form a 2D network after the solvent has evaporated (Figure 1.12). Recently, ethanol, methanol, isopropanol, toluene, chloroform and even water are used as solvent to disperse metal nanowires. Zhang et al, reported that the polyimide/Ag nanowire composite transparent conductive film fabricated by drop casting technique can achieve a low sheet resistance of 20 Ω/sq combined with a high transmittance of 83% (Figure 3). And the polymer solar cell fabricated with this transparent electrode can make the power conversion efficiency comparable to the device fabricated with a commercial indium tin oxide electrode. Pei et al produced a stretchable transparent electrode consisting of Cu nanowires via drop casting process and this flexible electrode displayed a low sheet resistance (< 100 Ω/sq) at tensile strain up to 60%.[94]

Even though the drop casting allowed a facile synthetic process, it is difficult to obtain a uniform film with this method because the nanowires will likely move due to evaporative flows, resulting in a coffee-ring pattern. And the scalable active area was highly restricted which limits its further commercialization.

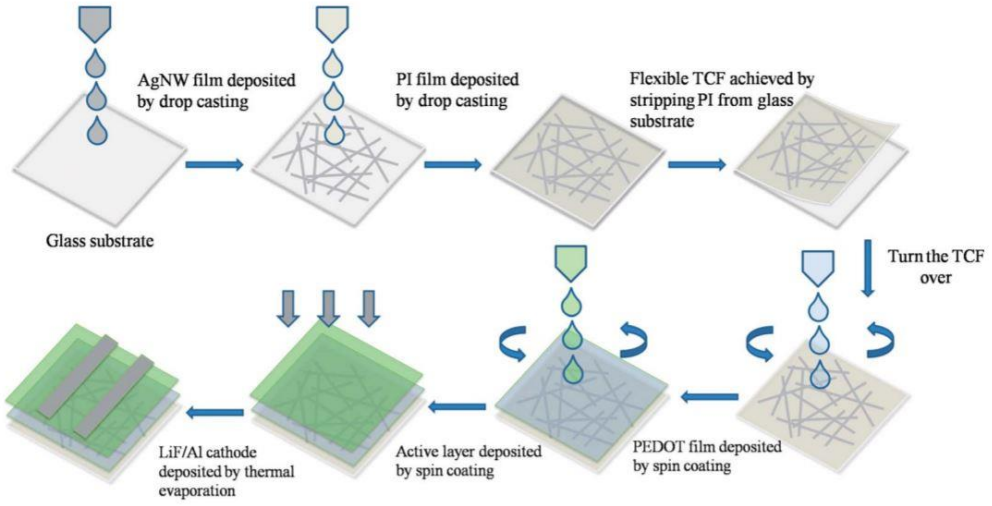

Figure 1.12. Fabrication of a flexible Ag nanowire/Polyimide composite transparent conductor via drop casting method[4]. Reprinted with permission from ref [4]. Copyright 2015 Royal Society of Chemistry.

1.4.3 Spin coating

Spin coating involves the placement of excessive amounts of metal nanowire suspension on a flat substrate, and the rotation to spread the nanowire solution evenly across the substrate through centrifugal force (Figure 1.13). The thickness of the metal nanowire based transparent conductive film can be tuned by varying the spin rate and the concentration of the nanowire suspension. Wu et al. demonstrated a highly transparent electrode based with Ag nanowire network, which was fabricated by a facile and efficacious two-step spin coating protocol. And this composite transparent electrode showed a 10 Ω/sq. at 90% of optical transmittance. Moreover, Nam et al developed an ultra-smooth, extremely deformable and shape recoverable Ag nanowire embedded transparent electrode with spin-coating method to embed a Ag nanowire film into a

transparent polymer matrix, which has sheet resistance and transmittance comparable to those of an ITO electrode.[95]

Spin coating process can be convenient for quickly checking samples in the laboratory; however, it is obviously not very scalable.

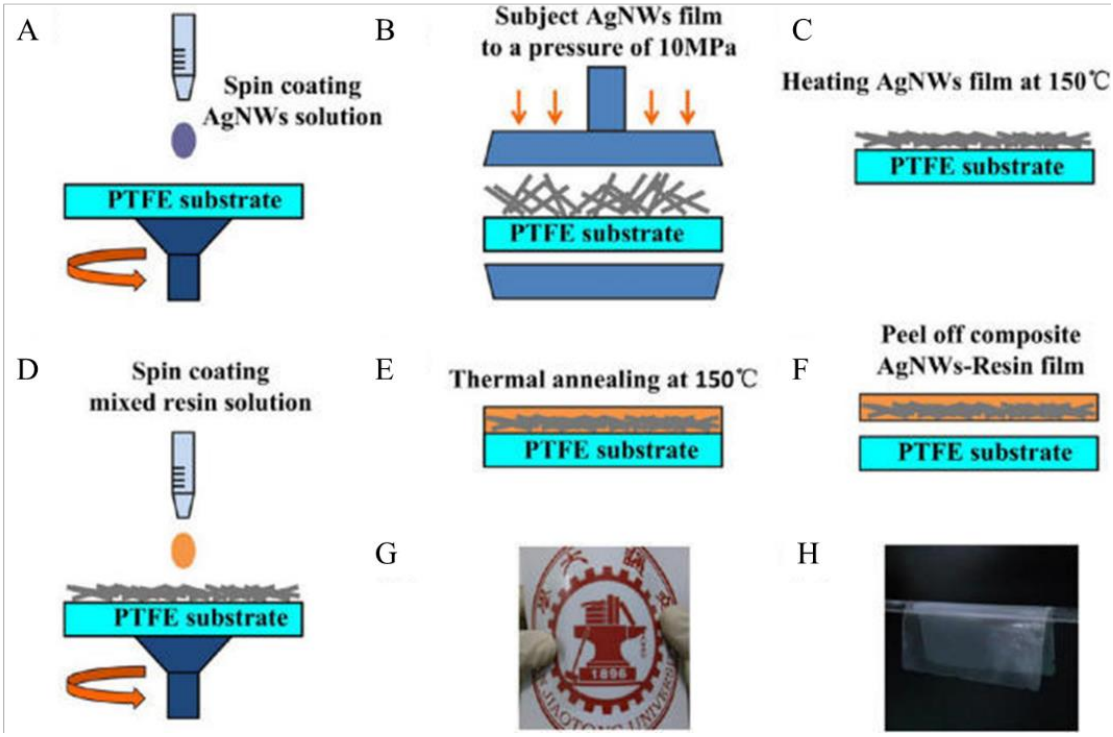

Figure 1.13 Fabrication of highly transparent conductive Ag nanowire embedded composite films. (A-F) Schematic of the procedure for fabrication process. (G-H) Photograph of this composite Ag nanowire-resin composite transparent electrodes[96]. Reprinted with permission from ref [96]. Copyright 2015 American Chemical Society.

1.4.4 Spray coating

Spray coating involves spraying a nanowire suspension with an air gun. The number of nanowires in the coating can be adjusted by the number of sprays passes and the concentration of the feed solution (Figure 1.14). This method sometimes requires that the substrate to be heated to evaporate the solvent, especially if the solvent is water. The spray pressure can be adjusted to produce small droplets to improve the uniformity of the film. For example, Kim et al reported the production of highly adhesive transparent and stretchable transparent electrode with spray-deposition of solution-based Ag nanowires onto a polydopamine-modified stretchable elastomeric substrate[97]. And this Ag nanowire coated elastomeric substrate exhibited 80% transmittance with an average sheet resistance of 35 Ω/sq. what's more, Jonathan et al presented a Ag nanowire based transparent electrode with large area (10 cm × 10 cm) via spray coating technique that has a sheet resistance of 50 Ω/sq at a transparency of 90%. However, spray coating protocol is relatively difficult to control and is low throughput relative to spin coating but can be used to apply nanowires to surfaces or substrates for which spin coating is not well-suited (i.e. surfaces that are not flat).

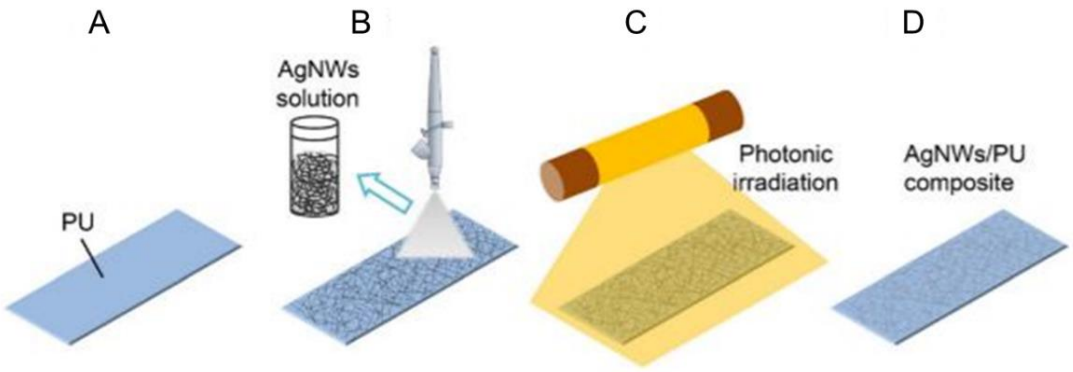

Figure 1.14. Schematic illustration of the fabrication process of Ag nanowire based transparent conductive electrodes via spray coating process. (A) flat clean PU substrate. (B) Spray deposition of Ag nanowires onto PU substrate. (C) Photonic sintering over the nanowire network deposited substrate. (D) The final Ag nanowire/PU composite transparent conductive electrode[98]. Reprinted with permission from ref [98]. Copyright 2012 Springer.

1.4.5 Vacuum filtration

Nanowire based flexible TCFs can be formed through vacuum filtration followed by transfer the nanowires from the filter membrane to various substrates (Figure 1.15). The substrates could be glass, silicon, polydimethylsiloxane (PDMS), and polyethylene terephthalate (PET).The filtration method can easily pattern the nanowires by filtering the solution with a patterned mask, and the number of nanowires in the film can be known and precisely controlled by changing the concentration of nanowires in the feed solution. Yang and his coworkers developed a copper nanowire based transparent electrode with vacuum filtration method. In this study, a Cu nanowire film was constructed by filtering down the nanowires from the dispersion onto a nitrocellose porous membrane via vacuum filtration and followed by transferring the nanowire network to the desired transparent substrate by

applying pressure to the back side of the filter membrane. The final transparent conductive film shows 90% in transmittance and 34.8 ohms/sq in sheet resistance. Moreover, the same group used the same vacuum filtering method to fabricate transparent electrode film but replace Cu nanowire with Cu@rGO core-shell nanowire, which can achieve a sheet resistance of ~28Ω/sq and a haze of ~2% at transmittance of 90%.[80]

However, the vacuum filtering method is not scalable that can be limited to the size of filter membrane or vacuum filter device. And it can be challenging to completely transfer the nanowires from the membrane filter to a target substrate.

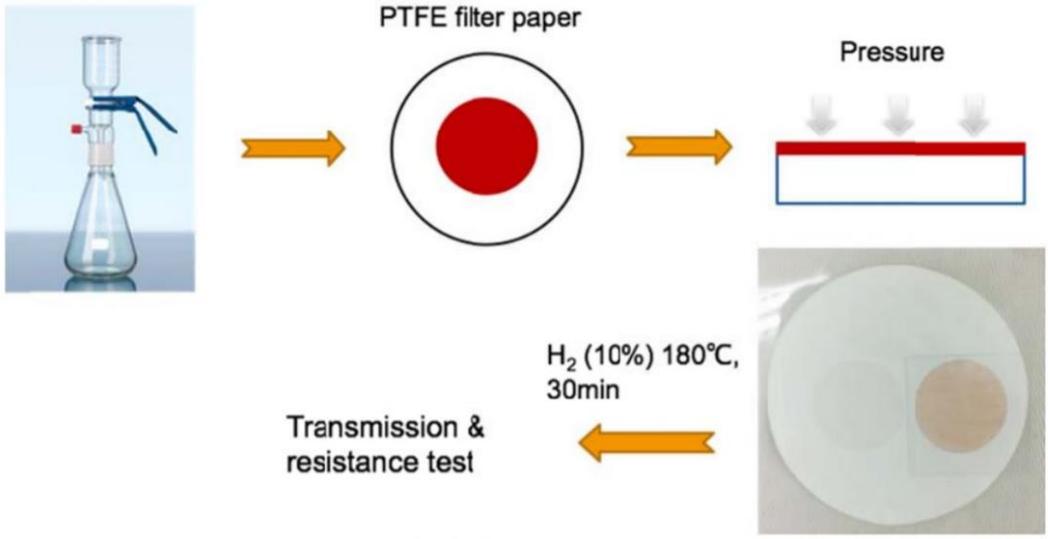

Figure 1.15. Schematic illustration of the transparent conductive film preparation process[31]. Reprinted with permission from ref [31]. Copyright 2015 American Chemical Society.

1.4.6 Meyer rod coating

Meyer rod coating involves spreading a nanowire suspension across a surface with a thickness of the wet film and thus the thickness of the nanowires film can be adjusted by using rods wrapped with wires of different sizes. These methods are compatible with large-scale, roll to roll coating processes. For example, Cui and his co-workers developed a transparent, flexible, Ag nanowire electrodes via Meyer rod coating [88]. In this study, Ag nanowire film can be coated directly from ethanol, then the Meyer rod is rolled over the drops to spread the Teflon solution evenly over the Ag nanowire film. Followed by heating the film at 120℃ for 10mins. Finally, the nanowires embedded Teflon transparent electrode was fabricated, and the performance of the resulted electrode film falls in the same range as the best indium tin oxide samples on plastic substrates for flexible electronics and solar cells. Besides, a nitrocellulose-based ink was developed for Meyer rod coating of Cu nanowires. Generally, Meyer rod coating is more scalable than spray coating as it enables faster deposition of metal nanowires to the film.

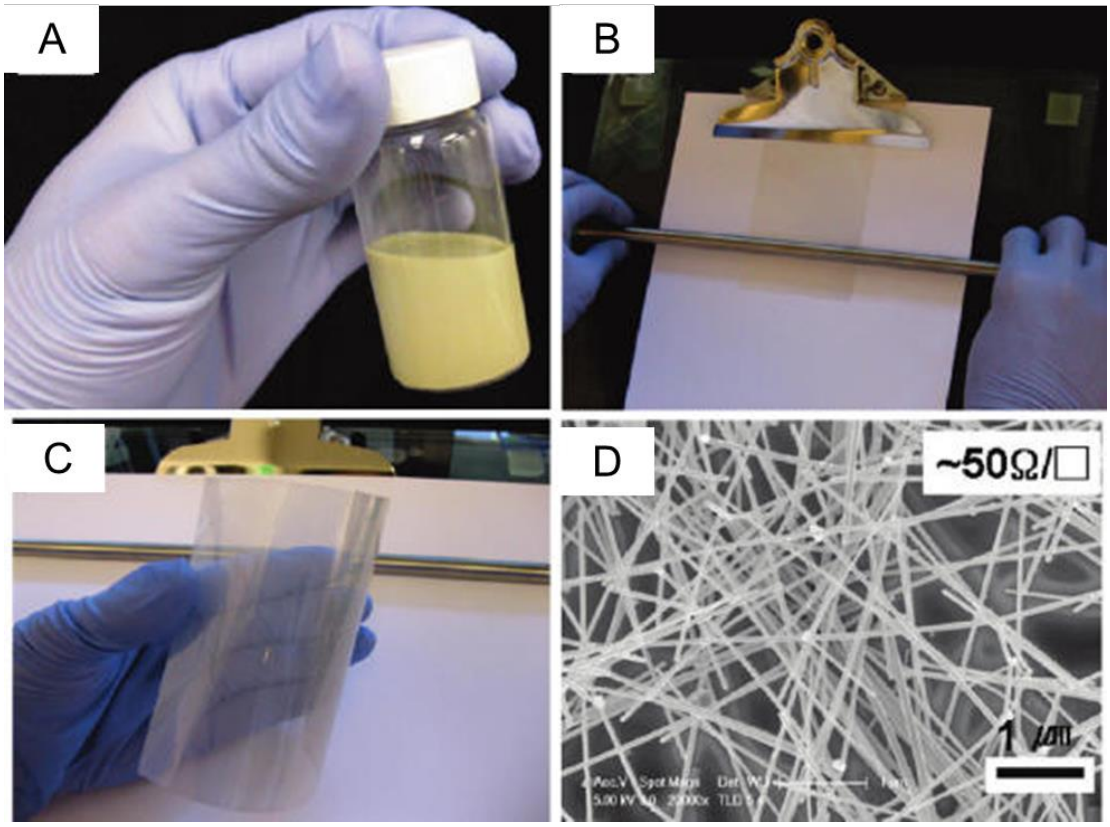

Figure 1.16. Scalable coating of Ag nanowire based flexible transparent electrodes. (A) Ag nanowire ink in ethanol. (B) Meyer rod coating set up for scalable Ag nanowire coating on plastic substrate. (C) the as-prepared Ag nanowire network coated PET substrate. (D) SEM image of Ag nanowire based transparent electrodes shown in figure C[88]. Reprinted with permission from ref [88]. Copyright 2010 American Chemical Society.

1.5 Methods to improve optoelectronic performance of FTCFs

1.5.1 Alignment of metal nanowires

As mentioned above, metal nanowire networks can be readily prepared by low-cost solution-based processes, such as drop-casting, spin-coating, vacuum filtration mentioned above, Meyer rod coating, and spray-coating. However, for the use of random metal nanowire networks in high-performance solar cells and OLEDs, the junction resistance

between nanowires and the large surface roughness are two critical issues that need to be addressed. Junction resistance prevents nanowire networks from achieving low R_s, while the high density of nanowires lowers the optical transmittance of the electrodes[99]. The protruding nanowires of overlapping random nanowire network structures can cause electrical short-circuits and leakages in multilayered device configurations. In addition, the optical haze of random nanowire networks may blur pixels or reduce the resolution in touch-screen and OLED devices[88].

To overcome the issue of junction resistance between nanowires, one approach uses lithographic or electrospinning techniques to design ordered metal nanowire networks, and this formation of junction-free nanowire networks has a very low sheet resistance. So, methods to align nanowires during coating have also been developed to improve the optoelectronic properties of the film.

Instead of using Meyer rod, Kang et al reported a highly aligned Ag nanowire transparent electrode prepared by capillary printing technique[100]. In this research, a polydimethylsiloxane (PDMS) stamp with 400 nm wide channels was dragged across a nanowire solution, resulting in their alignment. The alignment was presumably due to the confinement of the nanowires by the long channel and trapping them in the aligned state by removing the liquid. The alignment was also improved by applying a surface coating such as poly-lysine that promoted adhesion of the nanowires to the substrate. The aligned nanowires were about 4% more transparent than random nanowire networks at a sheet resistance of 20 Ω/sq. and, surprisingly, did not exhibit an anisotropic conductivity.

Except for the aforementioned capillary printing technique, microfluidic alignment, Langmuir-Blodgett alignment, bubble-blown technique, electric/magnetic field-assisted alignment, contact printing, stretching nanowire-polymer composites, substrate contraction/stretching, flow-assisted alignment, can all be employed to align metal nanowires as transparent conductive films.

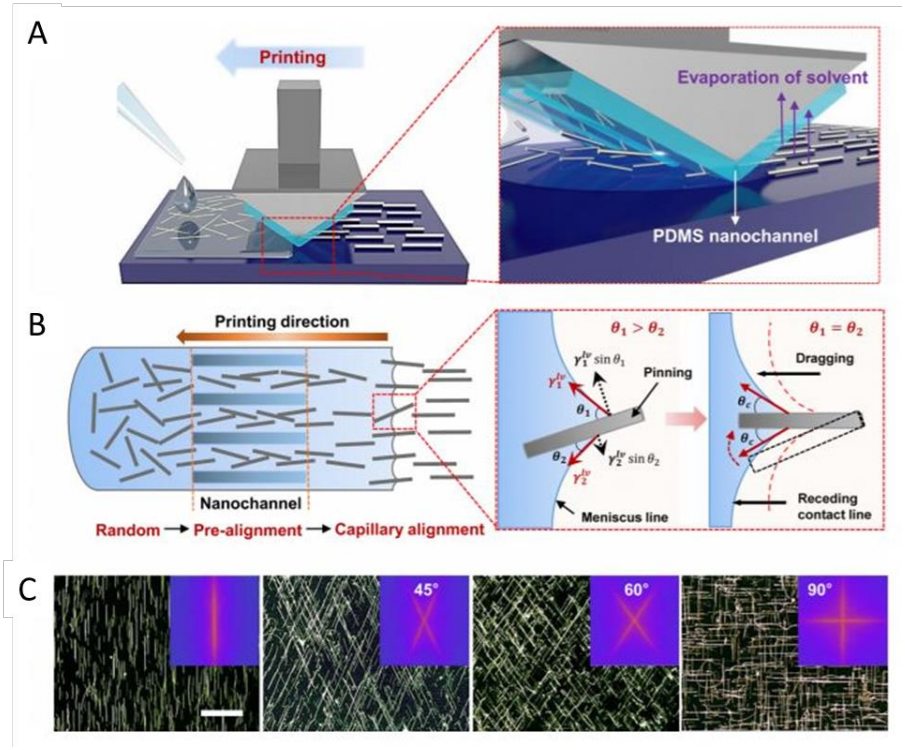

Figure 1.17. Solution-processed highly ordered Ag nanowire arrays. (A) Schematic illustration of the production of highly aligned Ag nanowire arrays assisted with capillary printing process made by a nanopatterned PDMS stamp. (B) Schematic displaying the alignment process during capillary printing of ordered Ag nanowire arrays. (C) Dark-field optical images of differently oriented Ag nanowire structures fabricated via one-step and multistep capillary alignments (0°C,45°, 60°, and 90° crossed). The scale bar is 40 μm[100]. Reprinted with permission from ref [100]. Copyright 2015 American Chemical Society.

1.5.2 Protection from corrosion

As discussed above, metal nanowires are the only materials that can be processed with low-cost, scalable solution-phase coating techniques while providing ITO-level performance[11]. However, the biggest issue that limits the commercial application of metal nanowire networks (e.g. Ag and Cu) is their long-term stability under operating conditions. Atmospheric sulfides will react with Ag, converting it into Ag_2S[48-49, 101], which are much less conductive and has a greater absorption cross-section. Unlike Ag, Cu reacts with oxygen at ambient conditions, and thus oxidizes and becomes non-conductive more quickly. Therefore, both Cu and Ag nanowires require protection from atmospheric corrosion, preferably through a low-cost, scalable solution-phase technique and without sacrificing film performance.

To solve this problem, several approaches have been reported: ***(1)*** using an overcoating layer on the Ag or Cu nanowire networks as a corrosion barrier. For example, PEDOT: PSS (Poly(3,4-ethylenedioxythio-phene):poly(styrenesulfonate))[102], reduced graphene oxide (rGO)[103] and ALD (atomic layer deposition) layer of aluminum-doped zinc oxide (AZO) and aluminum oxide (Al_2O_3) [44] have proven effective to increase the durability of metal nanowire network electrodes. However, PEDOT: PSS and rGO both have strong light absorption, which sacrifices the transmittance of metal nanowire networks. The ALD process will likely need to be replaced with a process that is less expensive to make it practical. ***(2)*** growing on the Cu nanowire a layer of a conductive yet chemically stable shell, such as Ni[73, 104-106] or rGO[80], which can both be achieved through a solution-phase

process. Coating Cu nanowires with Ni indeed improved their stability, however, both the total transparency and the overall conductivity of the films decreased significantly, which may be attributed to the increase in the diameter of the nanowires[73], as well as the formation of insulating NiO_x nanoparticles on the surface[105]. While an ultra-thin conformal rGO warping was proven effective to stabilize Cu nanowires without significant performance degradation[80], the long-term effectiveness of graphene for Cu protection is highly controversial[107-108]. Moreover, the overgrowth of a conductive protection layer on Ag nanowires has yet to be demonstrated in the context of transparent flexible conductors. More details can be found in section.

1.5.3 Post treatment of nanowire based flexible TCFs

Organic chemical from capping agent or surface oxides after the fabrication step may increase the contact resistance between each nanowire. The nanowire film is relative rough compared with ITO, and the nanowire network can easily be wiped off the substrate with a finger. So, in the following section, we will conclude a variety of recipes to improve the optoelectrical performance of flexible TCFs.

1.5.3.1 Improvement of junction resistance between nanowires

Based on the literatures, most of the sheet resistance of nanowires based FTCFs comes from the junction resistance between nanowires. So, it is necessary to minimize junction resistance between nanowires in order to reduce the total sheet resistance of nanowire based flexible TCFs.

1.5.3.1.1 Thermal annealing

Currently, thermal annealing is the method most commonly used for improving conductivity. The temperature between 140- 280 ℃ are sufficient to fuse metal nanowires together, and this annealing can generally be performed in a reducing environment such as forming gas (10%H_2 + 90% Ar) to remove surface oxides. For example, Yang et al found that thermal annealing of the copper nanowire network at a temperature of 200℃ for 30 min resulted in a dramatic decrease from 1000 Ω/sq to ~90 Ω/sq[31]. The reduction in the sheet resistance is attributed to the wielding of nanowires that can enhance the junction contact.

However, thermal annealing cannot be used with plastic substrates that deform at the annealing temperature, and thin nanowires are easily melted and fragmented into particles during thermal annealing. Therefore, the appropriate annealing conditions should be carefully determined to minimize thermal damage to the nanowires and substrates.

1.5.3.1.2 Mechanical Pressing

Mechanical pressing is another method to reduce junction resistance. In one example, the electrical conductivity of Ag nanowire transparent electrodes can be improved from 10000 Ω/sq to 10 Ω/sq by mechanical pressing at 25 MPa for 5s at room temperature[109]. This reduction in sheet resistance was like what was obtained when annealing the nanowire transparent electrode at 200 ℃. Another research showed that use of a rapid rolling pressure with moderate intensity, combined with heat over the back of Ag nanowire film on plastic substrate serves to weld the nanowires together[110]. The sheet resistance of the nanowire based transparent electrode drops dramatically to less than 20 Ω/sq while only annealing at 165℃ resulted in a sheet resistance of about 400 Ω/sq.

Mechanical pressing technique can also help to reduce the surface roughness of metal nanowire based conductive film; this is critical to the prevention of shorts when using the nanowire film as the transparent electrode in an organic solar cell.

1.5.3.1.3 Optical Thermal heating

Optical thermal heating is also an effective effort to reduce the junction resistance of metal nanowires and then the final optoelectrical performance of nanowire based transparent electrodes are enhanced. For example, Brongersma et al demonstrated an optical method for welding silver nanowires selectively at junction points by making use of plasmonic light, and the final sheet resistance of Ag nanowire film was reduced by three orders of

magnitude (Figure 1.18)[111]. It is thought that the concentration of the incident electromagnetic field in the nanoscale gap between nanowires results in a heating only at the junction where nanowires need to be joined, preventing the damage to the substrate or other parts of nanowires. Other works displayed that high intensity pulsed light sources such tungsten halogen lamp at a power density of 30 W/cm^2, can also reduce the sheet resistance in 1min[112].

All in all, this optical thermal technique hold promise for high speed roll to roll processing due to its fast processing.

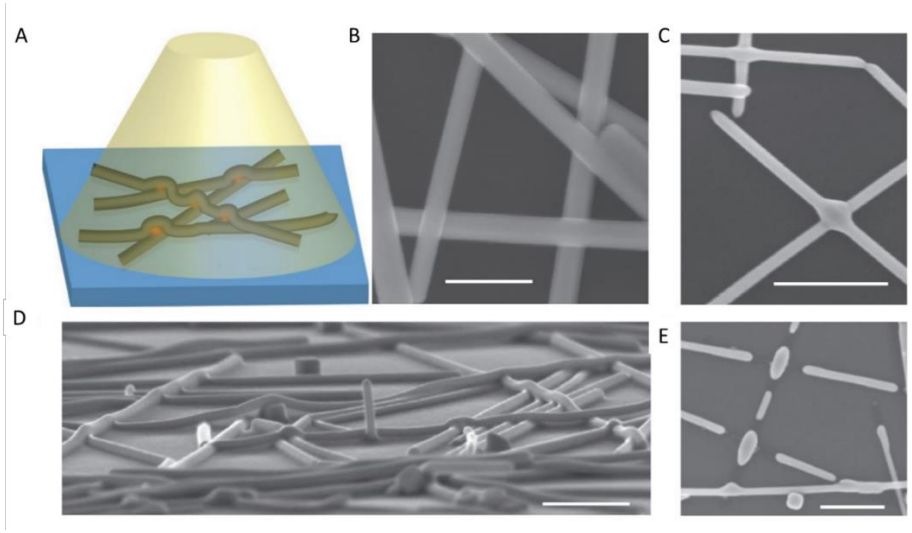

Figure 1.18. Self-limited plasmonic welding of Ag nanowire junctions. (A), Schematic illustration of the Ag nanowire junction plasmonic welding process with a silicon wafer for structural support. These small gaps enable extreme local heating due to the strong field concentration (red color). (B). SEM image of Ag nanowire junctions before welding. Scale bar is 200 nm. (C), SEM image of Ag nanowire junctions after optical welding with tungsten halogen lamp. Scale bar is 500 nm. (D) Tilted cross-section SEM image of the nanowire sample displayed in Figure C. Scale bar is 500 nm. (E), Plan-view SEM image of Ag nanowire junctions after uniform heating on a hotplate. This lack of control with uniform heating underscores the importance of the self-limited optical nanowelding process. Scale bar is 500 nm[111]. Reprinted with permission from ref [111]. Copyright 2012 Nature.

1.5.3.1.4 Cold welding

Recently, some researches showed that using capillary forces to join nanowires in a process which was referred to as cold-welding. For example, a moisture-treatment to introduce capillarity was used to improve the performance of Ag nanowire networks which showed a remarkable decrease in sheet resistance and a dramatic increase in mechanical stretch ability with negligible change in optical transmittance[113]. It is proposed that a liquid bridge forms at the nanowire junctions, resulting in a very strong capillary forces that drive the nanowires together during drying (Figure 1.19). In addition, capillary forces were also used to improve the adhesion of the metal nanowires to the substrate.

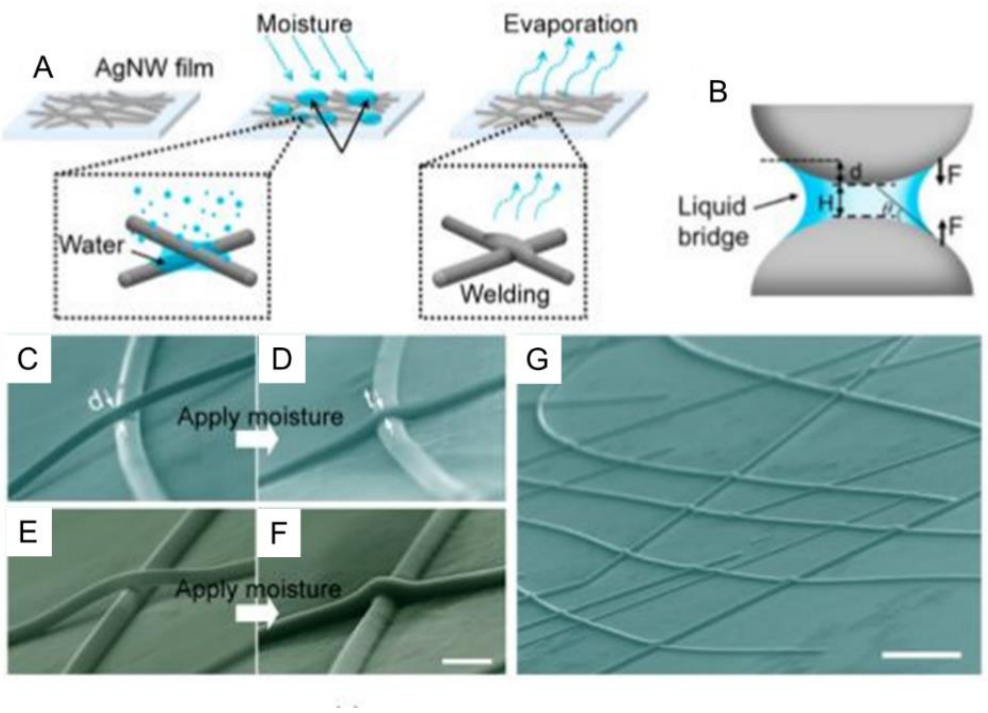

Figure 1.19. Capillary-force-induced cold welding of Ag nanowire network based flexible TCFs. (A) Schematic illustration of moisture treatment for the cold welding of Ag nanowire network. (B) Schematic illustration of the mechanism of capillary force induced between two particles connected with a liquid bridge. (C, D, E, F) Two types of SEM images of Ag nanowire junctions before and after moisture treatment. (G) SEM image of a large area of Ag nanowire network suggesting fine welded nanowire-nanowire junctions and very smooth surface induced by the moisture treatment. Scale bar: 1 μm[113]. Reprinted with permission from ref [113]. Copyright 2017 American Chemical Society.

1.5.3.1.5 Chemical treatment

The self-welding process of Ag nanowire network could also be fulfilled by simply dipping nanowire network in a solution of $NaBH_4$[114]. The resulted nanowire film showed much more efficient charge as a transparent electrode, without sacrificing transparency, flexibility and long-term stability. It is thought that PVP on the nanowire surface was replaced by hydride ions, which produce a clean Ag-Ag interface to allow direct welding of nanowire junctions via a room temperature solution process.

1.5.3.2 Increasing adhesion of nanowire network to substrate

As mentioned before, metal nanowire can be easily wiped off from the coated substrate if no more effort is achieved to improve adhesion between nanowires and the substrate. Embedding metal nanowire network into the inner surface of polymer matrix is the most common method to improve adhesion, as well as decrease surface roughness. Kim et al reported that the adhesion could be enhanced by coating a polydopamine layer on PDMS substrate prior to spray coating the Ag nanowires [115]. With this method, the Ag nanowire network could remain on the substrate even after a tape peel test. And the prepared transparent electrode displayed an average sheet resistance of 35 Ω/sq with 80% of optical transmittance. Carmichael et al improve the adhesion by embedding annealed Ag nanowire network into a polyurethane optical adhesive[116]. And moreover, this coating protocol can remain conductive at high bending strains and make the resulted transparent electrode more durable to scratch or marring than ITO. Lee and his coworkers demonstrated that poly (diallydimethyl-ammonium chloride) (PDDA) could increase the adhesion between Ag nanowire network and the substrate to form a uniform nanowire network and this composite electrode showed a sheet resistance as low as 10 Ω/sq at 91% of transmission[117].

1.5.3.3 Reducing the surface roughness

Commercial Indium Tin Oxide (ITO) presents a continuous, smooth surface that can make it compatible with thin organic electronic devices, such as organic light-emitting diode (OLEDs) and organic photovoltaics (OPVs). By contrast, nanowire surface is relatively rough, and based on the published literatures, the surface roughness of nanowire film typically has at least two nanowires diameters. Such a large roughness is on the order of the thickness of an OLED and OPV devices. So, such devices made with rough nanowire films often display short circuits.

Currently, several strategies are made to address the issue of surface roughness for metal nanowire based transparent conductive film. One method is mechanical pressing mentioned above, which can decrease the mean surface roughness from two nanowire diameters to as low as one diameter.

The other method is to embed the metal nanowire network into the inner surface of specific substrates which was illuminated before. Overall, these two methods can both decrease the surface roughness of nanowire based transparent conductive films.

1.6 Applications of flexible TCFs

Transparent conductors made of metal nanowires can now match the optoelectronic properties of ITO. The fabrication of a nanowire based flexible TCFs can be more cost-effective because they can be deposited from a suspension at high coating rates relative to the vapor-phase sputtering process for ITO. Furthermore, metal nanowire based TCFs are flexible and stretchable, whereas ITO is brittle. These advantages are motivating the study of metal nanowire based flexible TCFs in a wide range of applications, including touch panels, solar cells, OLEDs, super capacitors, transparent memory, air filters, transparent radio frequency antennas, electromagnetic interference shielding, and skin-attachable speakers and microphones (Figure 1.20). Here, we only highlight example applications of metal nanowire-based transparent conductors in touch screens, solar cells, OLEDs, and supercapacitors.

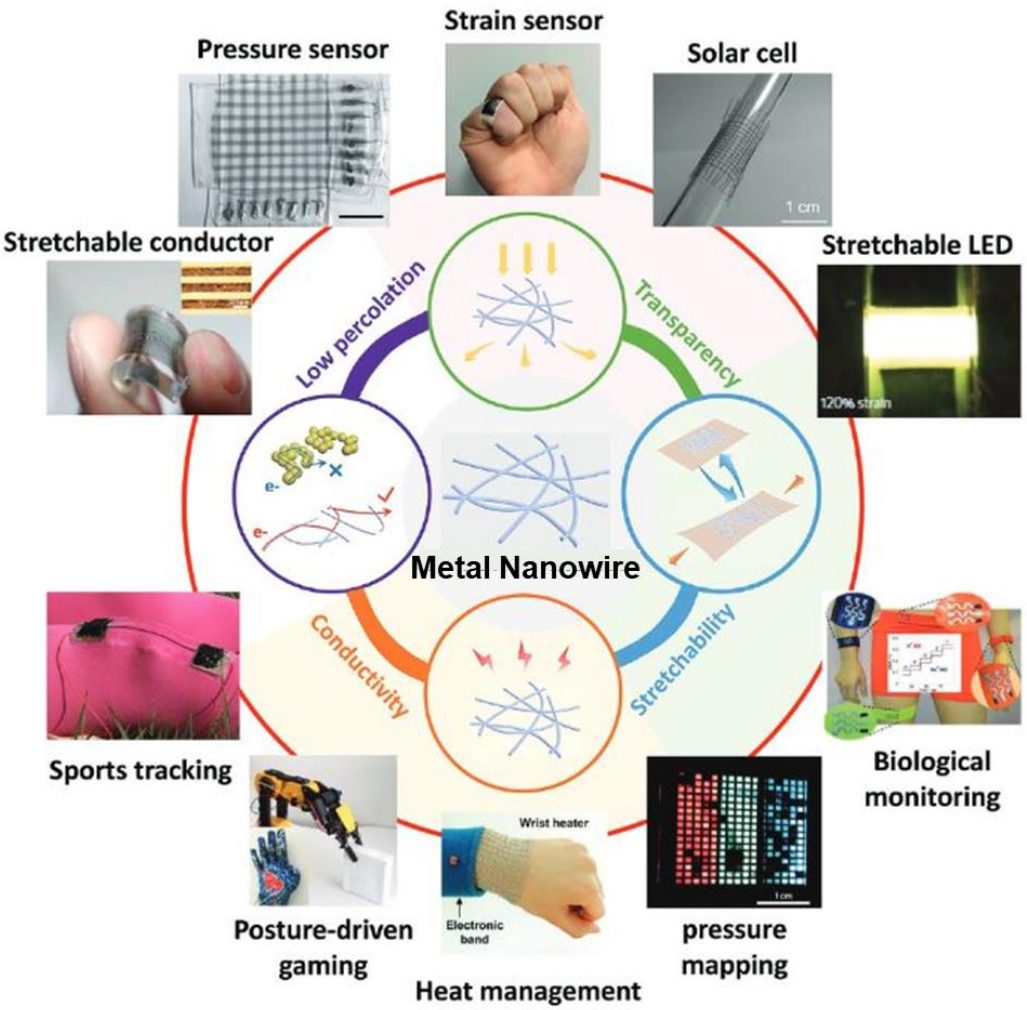

Figure 1.20. Characteristic properties and diverse devices or applications of soft electronics based on 1D nanomaterials. "Stretchable conductor" reprinted with permission from ref [118]. Copyright 2009 Nature Publishing Group. "Pressure sensor" reprinted with permission from ref [119]. Copyright 2011 Nature Publishing Group. "Sports tracking" reprinted with permission from ref [120]. Copyright 2011, Nature Publishing Group. "Strain sensor" reprinted with permission from ref [121]. "Solar cell" reprinted with permission from ref [122]. "Stretchable LED" reprinted with permission from ref [123]. Copyright 2013 Nature Publishing Group. "Pressure mapping" reprinted with permission from ref [124]. Copyright 2013 Nature Publishing Group. "Biological monitoring" reprinted with permission from ref [125]. "Heat management" reprinted with permission from ref [125]. Copyright 2015 American Chemical Society. "Posture-driven gaming" reprinted with permission from ref [126]. Copyright 2015, American Chemical Society.

1.6.1 Touch panels

Touch panel-based interfaces to satisfy the huge and high-speed growing commercial market for digital devices represents the most important commercial opportunity for metal nanowires. And as mentioned before, ITO has been the most common material used in this field because of the lower sheet resistance at a higher transmission. However, the comprehensive cost of ITO is increasing high because of the scarcity of indium element and its high fabrication cost. Motivated to the large scale and highly competitive characteristic of touch panel market, it is very necessary to lower costs in this field. Compared to vacuum-based ITO deposition, the low cost and scalable solution-based metal nanowire coating processes is one effective protocol for touch panel-based devices. Moreover, the greater mechanical durability and flexibility of metal nanowires based transparent electrodes is another merit to be the ideal ITO alternative and presents a high possibility to develop flexible touch-based devices that would not be possible for ITO due to its brittleness that is prone to cracking.

Metal nanowire-based touch screen panels are composed of two parallel metal nanowire-based transparent conductive films have been reported by several groups. The two transparent conductors were separated by a spacer or optically clear adhesive, while the driving and sensing lines were fabricated by metal evaporation or screen printing. In addition to touch screens that can detect the location of touch, a force-sensitive touch screen was recently reported. A composite film was added to a touch screen made of Ag nanowires. A touching force between 5 and 25 N was measured by analyzing the color change with a

spectroradiometer. This enabled the touch screen to measure the distribution of writing forces used to draw a single letter, potentially enabling screens that can verify the authenticity of personal signatures using such force distributions of writing forces used to draw a single letter, potentially enabling screens that can verify the authenticity of personal signatures using such force distributions.

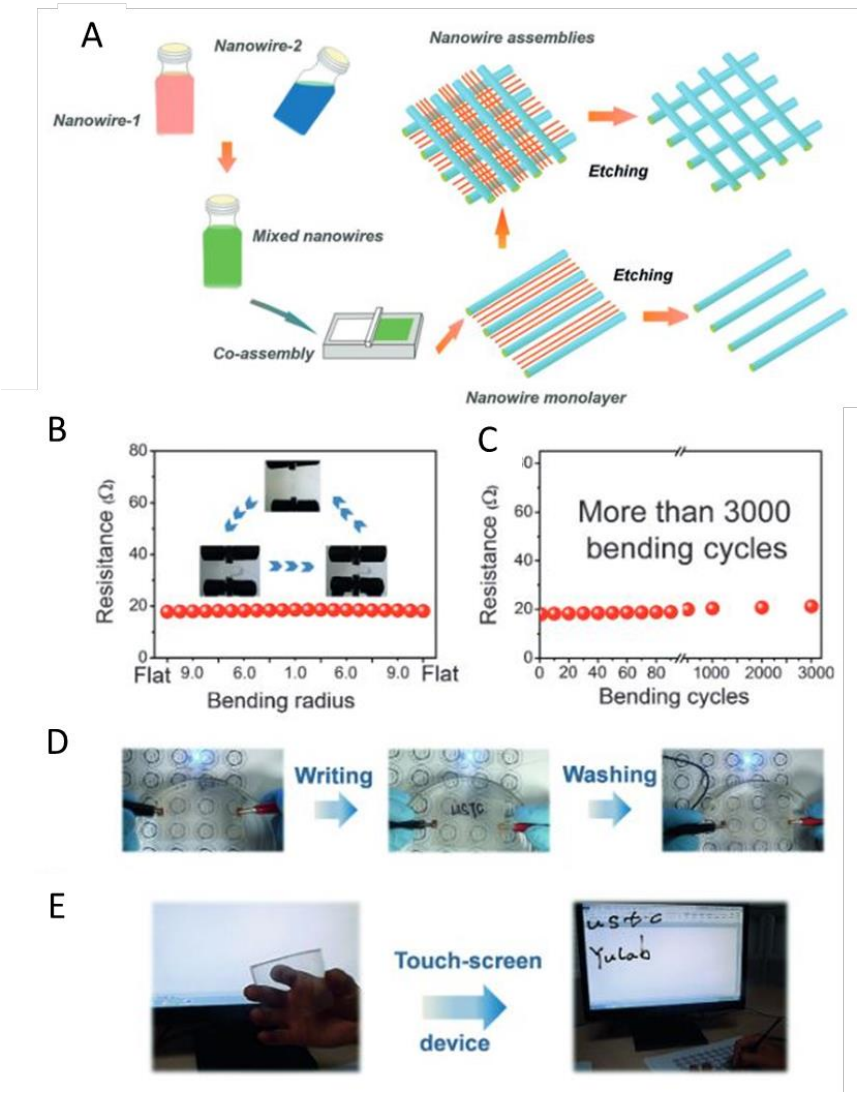

Figure 1.21. Manipulating nanowire assembly for flexible TCFs. (A) Schematic illustration of the fabrication process of aligned nanowire based flexible TCFs. (B, C) Mechanical flexibility and stability of the as-prepared based flexible TCFs. (D). Camera images of the Ag nanowire based transparent electrodes, immersion in liquid to show their mechanical properties. A blue LED light was connected by the flexible transparent electrodes with a battery pack. The LED remains lit during the immersion/bending process. (E) Photographs of the touch panel based on an assembled Ag nanowire network based TCFs. Text handwritten on the touch panel is then transferred to the computer screen[127]. Reprinted with permission from ref [127]. Copyright 2014 Wiley.

1.6.2 Solar cells

Many research groups have explored ITO alternatives in solar cells with metal nanowire-based transparent conductive films because of their potential to reduce the cost and enable the fabrication of much more flexible, durable solar cells. Metal nanowire based TCFs, however, have some disadvantages compared with ITO: 1. Unlike ITO, the metal nanowire based TCF is not continuous. Because highly transparent of metal nanowire-based films come from the truth that only a small area of the film surface is covered by metal nanowires, leaving behind micrometer-sized open areas in which charge carriers cannot be effectively collected. 2. The halide ions in perovskite solar cells can react with metal nanowires including Ag and Cu to form metal halides, leading to the performance degradation in the electrical conductivity of the metal nanowire based TCFs. 3, Metal nanowire network based TCFs usually has the relatively large surface roughness (on the order of two nanowire diameters) in comparison with ITO (less than 3 nm) can lead to the formation of electrical shorts in solar cells. Therefore, the poor adhesion and stability of metal nanowires to most substrates can lead to their detachment from the substrate during solution processing steps.

One protocol to addressing some of these disadvantages is the coat of an additional transparent conductive layer on top of the metal nanowire-based TCFs. Metal oxide, graphene or graphene oxide, ITO nanoparticles, and even conductive polymer such as PEDOT: PSS have all been employed to metal nanowire-based transparent conductive films to improve their performance in solar cells. The deposition of conductive layer fills

the metal nanowire-free open areas and enhance the probability of charge transfer. The function of metal nanowires in such composite films is to act as a highly conductive backbone that improves transport of charge carriers to busbars. Such inert transparent conductive layers can improve the adhesion of metal nanowires to the substrate and prevent possible reactions happened between metal nanowires and halide ions in solar cell system. The issue of surface roughness made by metal nanowire network could also be solved by embedding metal nanowires in a conductive polymer layer. These approaches enabled the construction of more cost-effective, flexible and durable solar cells with metal nanowire-based TCFs.

The improvement of haze index is another approach to improve the performance of a solar cell. A transparent conductive film with a higher haze factor can increase the light path length in the active material, leading to more light absorption. However, the haze factor increases when transmission decreases, this trade-off must be optimized to maximize the performance of a solar cell. Recent study suggested that thinner nanowires have a lower haze and can keep a lower transmittance as well. In one example, the optical haze factor of ITO film was below 1% at the wavelength of 550 nm, while an AgNW film with a 65% of transmittance exhibited a 59% of haze. Gao et al reported that a composite TCFs of Ag nanowires and fluorine doped ZnO displayed a sheet resistance of 17 Ω/sq with a haze of 37% at a transmittance of 84%. And they still exhibited a slightly improved power conversion efficiency of only 3.3%. Adding extra Ag nanowires to the top contact of conductive polymer PEDOT: PSS on a silicon substrate resulted in a higher conductivity, increased haze, and an increased power conversion efficiency of 10.1%[128].

The ability to coat metal nanowires from liquids can enable the TCFs more flexible. You et al displayed that a fully solution-processed polymer bulk heterojunction solar cells equipped with Ag nanowire-based anodes was fabricated with a structure of Ag nanowire/ PEDOT: PSS/ PCBM/ Ca/ Al, which revealed an efficiency of 2.8%. And the Ag nanowire network coated PET electrode could obtain a recoverable efficiency of 2.5% under large deformation up to 120° (Figure 1.22). Such bendable solar cells may someday be employed to power wearable electronics[3].

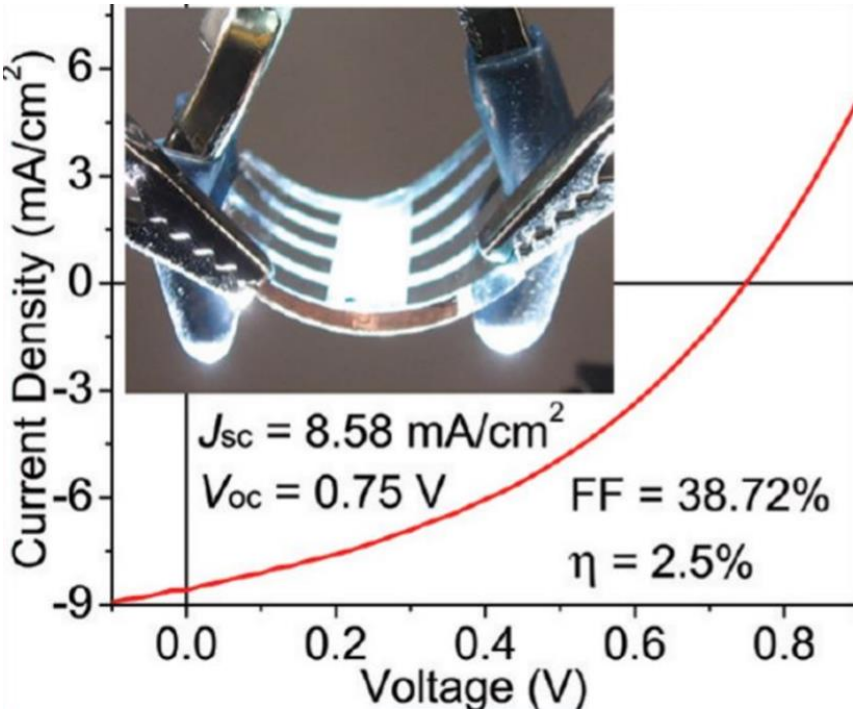

Figure 1.22. Solution-processed flexible polymer solar cells equipped with Ag nanowire network based transparent electrodes. The curve shows an efficiency of 2.5% was obtained even under the deformation process. And the inset shows that the direct contact of alligator clips to copper tape on Ag nanowire anode was used in order to confirm a good conductivity during the bending process[3]. Reprinted with permission from ref [3]. Copyright 2011 American Chemical Society.

1.6.3 OLEDs

Another promising application of the metal nanowire based TCFs is for OLEDs. Replacing ITO with a metal nanowire-based TCFs enables the fabrication of an OLED that is flexible and stretchable and can be potentially manufactured with roll-to-roll fabrication. The primary technical hurdle for using metal nanowires as the TCF in an OLED is the higher surface roughness of a metal nanowire-based TCF in comparison with ITO, which can result in the formation of electrical shorts and a degradation in the efficiency of the OLED device. Weak adhesion between metal nanowires and the substrate can also weaken the mechanical stability of the devices. Similar solutions to those discussed for solar cells were applied to fix these issues, including depositing an additional transparent conductive layer and embedding metal nanowires in a conductive polymer.

Another way to fill the open area in a nanowire electrode is to use a mixture of long, thick nanowires that act as highly conductive backbones, and short, thin nanowires that act as branches. Such dual-structure electrode was fabricated from Ag nanowire embedded in a transparent electrode for an OLED device. The current and power efficiency was increased by 40% and 70%, respectively, for OLED prepared with the composite electrode compared to previous work that used Ag nanowires with a smaller range of dimensions[8].

For example, Pei and his co-workers presented a composite TCF was fabricated by coating Ag nanowires on a glass substrate and then overcoating and polymerization of a vinyl monomer on the top of this Ag nanowire coated glass substrate (Figure 1.23). The composite electrode could then be peeled off from the glass to get an Ag nanowire network

embedded TCFs. The Ag nanowire based TCFs exhibited slightly improvements in their maximum current efficiency and a 20−50% higher luminance in comparison with ITO based OLEDs. Furthermore, Ag nanowire- based OLEDs could retain their performance even after 100 bending cycles[129]. Such metal nanowire-based OLEDs could be available in mobile and wearable electronic applications.

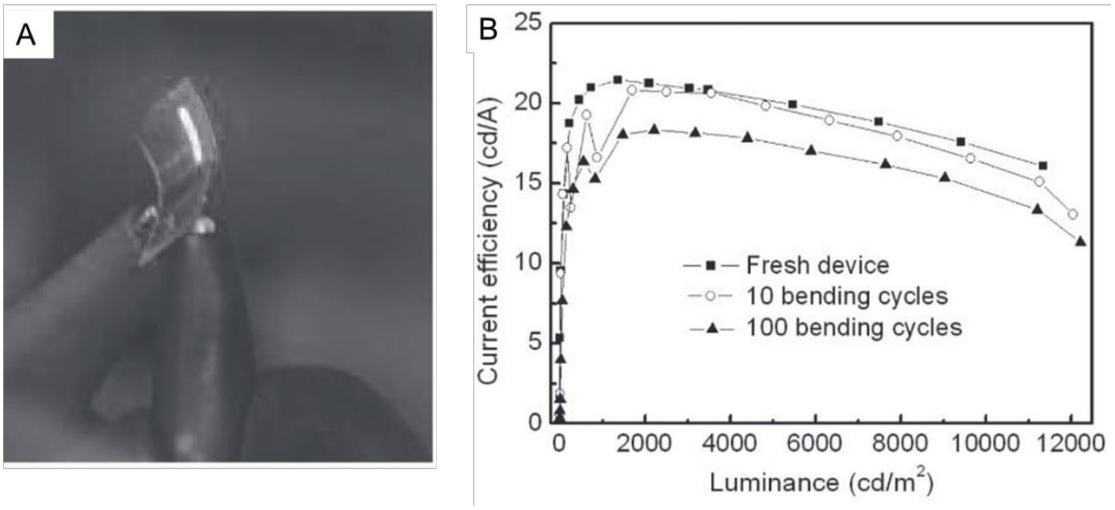

Figure 1.23. Flexible Ag nanowire based phosphorescent polymer LED. (A) Camera image of a bent device on Ag nanowire composite transparent electrode. (B) Current density- luminance performance of Ag nanowire based TCFs before, after 10 and 100 bending cycles[129]. Reprinted with permission from ref [129]. Copyright 2011 Wiley.

1.6.4 Transparent thermal heater

Transparent thermal heater is another typical application for metal nanowire network based TCF, since metal nanowire has high electrical and thermal conductivity. Therefore, previously mentioned Ag nanowire based transparent wearable electronics utilize the high electrical properties for input and output devices, touch screens and OLED devices. On the other hand, functional transparent wearable electronics such as a thermal heater utilizes the

high thermal conductivity. A fabricated Ag nanowire based TCF without additional processes can be converted for thermal heater application directly and easily. The thermal heater has been developed for defrosting purposes in smart windows initially, however the trend has now been directed towards wearable electronics which can be attached to the human body. As pointed out, the transparent thermal heater fabrication process is same as the general Ag nanowire based TCF fabrication process. Typically, Ag nanowire could be large scalable synthesized via the polyol-mediated solution process and be deposited on a specific substrate.

In one example, an optimal amount of clay platelet mixed with Ag nanowire ink was used to prevent conglomeration and to promote dispersion for thermal heater device fabrication. This method establishes a well dispersed Ag nanowire network even by Meyer bar coating, and therefore high optical transmittance and electrical conductivity can be obtained. In addition, high thermal conductivity enables fast heating up to 100 ℃ from room temperature with 7 V input voltage in 60 seconds and fast on/off switching at low input voltage. This result shows that the heating is significantly faster than a CVD grown graphene thermal heater at an input voltage of 30 V and heated up to 55 ℃. Therefore, an Ag nanowire based thermal heater is a prospective candidate for smart windows. The high thermal conductivity of an Ag nanowire enables fast switching when used as a thermal heater. A study has shown that a thermal heater which has a fast switching property can be linked to thermochromic display.

In another example. A graphene/Ag nanowire composite TCF was fabricated by mixing Ag nanowire and graphene oxide sheets and then followed by a subsequent thermal annealing process to reduce graphene oxide. The final graphene/Ag nanowire composite electrode shows good oxidation resistance and thermal stability even at high temperature without sacrificing the merit-of-figure performance of the pristine Ag nanowire. Other than graphene oxide, various materials have been used in hybrid film fabrication[130].

The research direction for Ag nanowire based transparent heaters is expected to have high electrothermal performance, fine stretch ability and long-term mechanical/Chemical stability. Moreover, a stretchable heater device integrated with other sensor modules will expanded its application to support a simultaneous monitoring and diagnostic system for future wearable applications.

Thermal therapy is another typical application for stretchable, conductive metal nanowires. Thermal therapy is often prescribed to alleviate the symptoms of painful or swollen joints, but current heat wraps are heavy, bulky, inconvenient, and do not maintain a desired temperature set point. Electrically programmable heaters on polyimide substrates cannot conform to the human body. To address this problem, researchers suspended Ag nanowires in an SBS elastomer, and molded the elastomer to create a stretchable, conductive serpentine mesh. This heater was connected to a battery and microcontroller to serve as a programmable heater for the wrist (Figure 1.24)[126]. An alternative approach to the construction of a stretchable heater is to start by creating stretchable, conductive yarn with Cu nanowires. A helical yarn composed of polyester microfibers was coated with Cu nanowires and then silicone by dip coating. A wearable heater was created by weaving the

conductive threads through the fabric, and its temperature could be controlled with a phone via Bluetooth. The fabrics created using this conductive yarn were washable, breathable, and highly deformable[131].

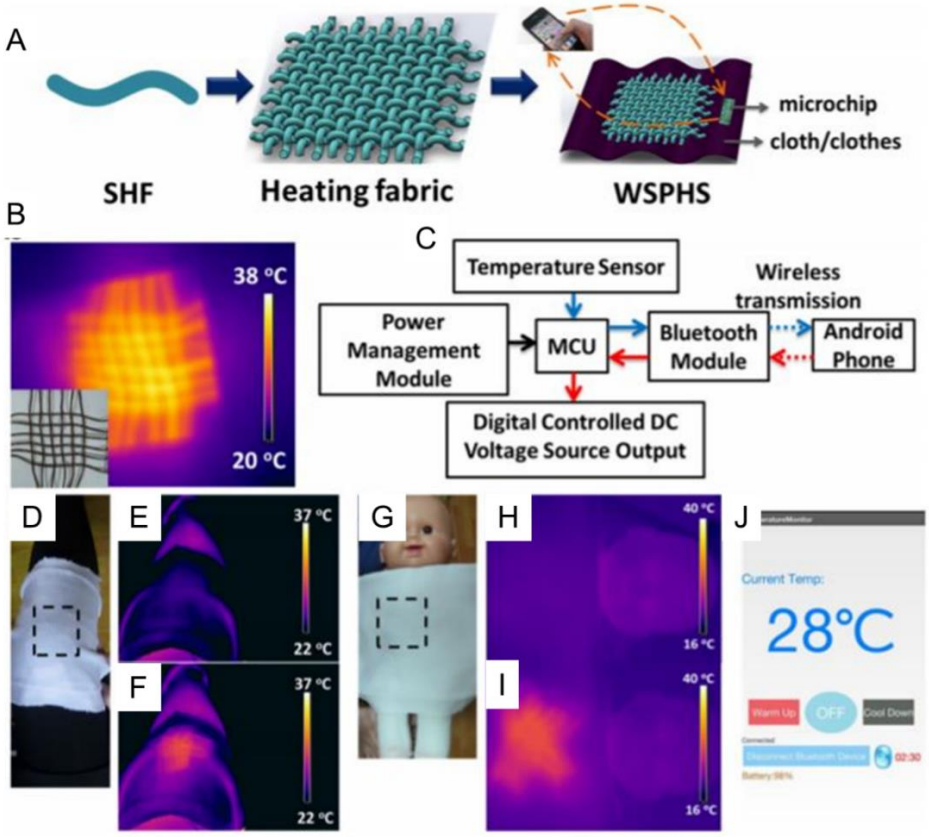

Figure 1.24. Stretchable Cu nanowire based wearable heaters. (A) Schematic illustration of the integration of wearable and smart personal heating system: weaving stretchable heating fibers into heating fabric and then integrating the heating fabric with cloth/clothes and a microcontroller chip. (B) IR thermal image of heating fabric under dc voltage of 1.8 V and photograph of heating fabric (Stretchable heating fabrics woven in a cross pattern). (C) Schematic illustration of the operation process of the wearable stretchable heating fibers. (D) Photograph of wearable stretchable heating fiber application at the knee position of a human body. IR thermal images before (E) and after (F) switching on the device. (G) Camera images of wearable stretchable heating fiber application at the chest position of an infant model. IR thermal images before (H) and after (I) switching on the device. (J) Software interface on an Android phone which read the body temperature and controlled the heating temperature[132]. Reprinted with permission from ref [132]. Copyright 2016 American Chemical Society.

1.7 Conclusion

While ITO has been the most widely used as transparent conductive film materials for decades, and will likely continue to play the role well into the future, metal nanowire especially for Ag nanowire and Cu nanowire represent the most ideal ITO replacement that can be produced from low cost solution phase processing and achieve optoelectronic performance that has comparable or even higher performance of ITO.

However, either Ag nanowire or Cu nanowire has the oxidation issue that limits their further commercialization process. We have systemically reviewed significantly progress that has been made in recent years to prevent oxidation from metal nanowire in the field of metal nanowire based flexible transparent electrodes. A variety of novel protocols especially for growing a conductive yet chemical stable layer on core nanowire surface to form core-shell nanostructure have been categorized and discussed in detail.

Given the potential importance of metal nanowire based flexible transparent electrodes for a range of applications, it is important to understand how to optimize the properties of metal nanowire based transparent conductive films. We have discussed the current models to affect the sheet resistance, optical property (light absorption, scattering, and even haze), and flexibility (stretch, bend ability) of metal nanowire based transparent conductive films. Based on these models, a variety of solutions including reducing the junction resistance of nanowire s, increasing adhesion of nanowire network to substrate and reducing the surface roughness have been proposed to improve the comprehensive performance of nanowire

based transparent conductive films. Followed then, we listed the stat of the art fabrication approaches of metal nanowire based flexible transparent electrodes such as dip coating, drop casting, spray coating, vacuum filtration, and Meyer rod coating.

In the end, various types of metal nanowire-based devices are also discussed and summarized. We believe that metal nanowire based transparent electrodes will lead to many real-world applications in the coming future; these may include touch panels, solar cells, transparent heaters, OLEDs, and even wearable electronic devices. And it is known that different devices may require different amount of metal nanowires. For instance, haze should be minimized for a touch panel while haze may desirable for the OPV devices. Further study is needed to better understand how we can control the structure and properties of metal nanowire based transparent electrodes to optimize the performances for a particular class of devices.

Reference

1. Laminating solution-processed silver nanowire mesh electrodes onto solid-state dye-sensitized solar cells. *Org. Electron.* **2011,** *12*, 875.

2. Highly transparent low resistance ZnO/Ag nanowire/ZnO composite electrode for thin film solar cells. *ACS nano* **2013,** *7*, 1081.

3. Solution-processed flexible polymer solar cells with silver nanowire electrodes. *ACS Appl. Mater. Interfaces* **2011,** *3*, 4075.

4. Guo, X.; Liu, X.; Luo, J.; Gan, Z.; Meng, Z.; Zhang, N., Silver nanowire/polyimide composite transparent electrodes for reliable flexible polymer solar cells operating at high and ultra-low temperature. *RSC Advances* **2015,** *5* (32), 24953-24959.

5. Very long Ag nanowire synthesis and its application in a highly transparent, conductive and flexible metal electrode touch panel. *Nanoscale* **2012,** *4*, 6408.

6. Hecht, D. S.; Thomas, D.; Hu, L.; Ladous, C.; Lam, T.; Park, Y.; Irvin, G.; Drzaic, P., Carbon-nanotube film on plastic as transparent electrode for resistive touch screens. *Journal of the Society for Information Display* **2009,** *17* (11), 941-946.

7. Madaria, A. R.; Kumar, A.; Zhou, C., Large scale, highly conductive and patterned transparent films of silver nanowires on arbitrary substrates and their application in touch screens. *Nanotechnology* **2011,** *22* (24), 245201.

8. Lee, J.; An, K.; Won, P.; Ka, Y.; Hwang, H.; Moon, H.; Kwon, Y.; Hong, S.; Kim, C.; Lee, C.; Ko, S. H., A dual-scale metal nanowire network transparent conductor for highly efficient and flexible organic light emitting diodes. *Nanoscale* **2017,** *9* (5), 1978-1985.

9. Tak, Y.-H.; Kim, K.-B.; Park, H.-G.; Lee, K.-H.; Lee, J.-R., Criteria for ITO (indium–tin-oxide) thin film as the bottom electrode of an organic light emitting diode. *Thin Solid Films* **2002,** *411* (1), 12-16.

10. Kang, M.-G.; Guo, L. J., Nanoimprinted Semitransparent Metal Electrodes and Their Application in Organic Light-Emitting Diodes. *Advanced Materials* **2007,** *19* (10), 1391-1396.

11. Ye, S.; Rathmell, A. R.; Chen, Z.; Stewart, I. E.; Wiley, B. J., Metal nanowire networks: the next generation of transparent conductors. *Adv Mater* **2014,** *26* (39), 6670-87.

12. Duong, T.-H.; Kim, H.-C., A high productivity and speedy synthesis process for copper nanowires via an ethylenediamine-mediated method. *International Nano Letters* **2017,** *7* (2), 165-169.

13. Ye, S.; Rathmell, A. R.; Chen, Z.; Stewart, I. E.; Wiley, B. J., Metal Nanowire Networks: The Next Generation of Transparent Conductors. *Advanced Materials* **2014,** *26* (39), 6670-6687.

14. Azzopardi, B.; Emmott, C. J. M.; Urbina, A.; Krebs, F. C.; Mutale, J.; Nelson, J., Economic assessment of solar electricity production from organic-based photovoltaic modules in a domestic environment. *Energy & Environmental Science* **2011,** *4* (10).

15. Zweibel, K., Issues in thin film PV manufacturing cost reduction. *Solar Energy Materials and Solar Cells* **1999,** *59* (1–2), 1-18.

16. Na, S.-I.; Kim, S.-S.; Jo, J.; Kim, D.-Y., Efficient and Flexible ITO-Free Organic Solar Cells Using Highly Conductive Polymer Anodes. *Advanced Materials* **2008,** *20* (21), 4061-4067.

17. Elschner, A.; Lövenich, W., Solution-deposited PEDOT for transparent conductive applications. *MRS Bulletin* **2011,** *36* (10), 794-798.

18. Transparent, conductive carbon nanotube films. *Science* **2004,** *305* (5688), 1273.

19. Zhou, Y.; Azumi, R., Carbon nanotube based transparent conductive films: progress, challenges, and perspectives. *Science and Technology of Advanced Materials* **2016,** *17* (1), 493-516.

20. Emerging transparent electrodes based on thin films of carbon nanotubes, graphene, and metallic nanostructures. *Adv. Mater.* **2011,** *23*, 1482.

21. A transparent and stretchable graphene-based actuator for tactile display. *Nanotechnology* **2013,** *24* (14).

22. Hatton, R. A.; Willis, M. R.; Chesters, M. A.; Briggs, D., A robust ultrathin, transparent gold electrode tailored for hole injection into organic light-emitting diodes. *Journal of Materials Chemistry* **2003,** *13* (4), 722-726.

23. Formica, N.; Ghosh, D. S.; Chen, T. L.; Eickhoff, C.; Bruder, I.; Pruneri, V., Highly stable Ag–Ni based transparent electrodes on PET substrates for flexible organic solar cells. *Solar Energy Materials and Solar Cells* **2012,** *107*, 63-68.

24. Kang, M. G.; Guo, L. J., Nanoimprinted Semitransparent Metal Electrodes and Their Application in Organic Light-Emitting Diodes. *Advanced Materials* **2007,** *19* (10), 1391-1396.

25. Guo, C. F.; Sun, T.; Liu, Q.; Suo, Z.; Ren, Z., Highly stretchable and transparent nanomesh electrodes made by grain boundary lithography. *Nature Communications* **2014,** *5*, 3121.

26. Electrospun metal nanofiber webs as high-performance transparent electrode. *Nano Lett.* **2010,** *10*, 4242.

27. Lee, Y.; Min, S.-Y.; Kim, T.-S.; Jeong, S.-H.; Won, J. Y.; Kim, H.; Xu, W.; Jeong, J. K.; Lee, T.-W., Versatile Metal Nanowiring Platform for Large-Scale Nano- and Opto-Electronic Devices. *Advanced Materials* **2016,** *28* (41), 9109-9116.

28. Song, M.; You, D. S.; Lim, K.; Park, S.; Jung, S.; Kim, C. S.; Kim, D.-H.; Kim, D.-G.; Kim, J.-K.; Park, J.; Kang, Y.-C.; Heo, J.; Jin, S.-H.; Park, J. H.; Kang, J.-W., Highly Efficient and Bendable Organic Solar Cells with Solution-Processed Silver Nanowire Electrodes. *Advanced Functional Materials* **2013,** *23* (34), 4177-4184.

29. Ye, S.; Rathmell, A. R.; Stewart, I. E.; Ha, Y.-C.; Wilson, A. R.; Chen, Z.; Wiley, B. J., A rapid synthesis of high aspect ratio copper nanowires for high-performance transparent conducting films. *Chemical Communications* **2014,** *50* (20), 2562-2564.

30. Araki, T.; Jiu, J.; Nogi, M.; Koga, H.; Nagao, S.; Sugahara, T.; Suganuma, K., Low haze transparent electrodes and highly conducting air dried films with ultra-long silver nanowires synthesized by one-step polyol method. *Nano Research* **2014,** *7* (2), 236-245.

31. Cui, F.; Yu, Y.; Dou, L.; Sun, J.; Yang, Q.; Schildknecht, C.; Schierle-Arndt, K.; Yang, P., Synthesis of Ultrathin Copper Nanowires Using Tris(trimethylsilyl)silane for High-Performance and Low-Haze Transparent Conductors. *Nano Lett* **2015,** *15* (11), 7610-5.

32. Roll-to-roll production of 30-inch graphene films for transparent electrodes. *Nature Nanotechnol.* **2010,** *5*, 574.

33. Becerril, H. A.; Mao, J.; Liu, Z.; Stoltenberg, R. M.; Bao, Z.; Chen, Y., Evaluation of Solution-Processed Reduced Graphene Oxide Films as Transparent Conductors. *ACS nano* **2008,** *2* (3), 463-470.

34. Ultrasmooth, large-area, high-uniformity, conductive transparent single-walled-carbon-nanotube films for photovoltaics produced by ultrasonic spraying. *Adv. Mater.* **2009,** *21*, 3210.

35. Geng, H.-Z.; Kim, K. K.; So, K. P.; Lee, Y. S.; Chang, Y.; Lee, Y. H., Effect of Acid Treatment on Carbon Nanotube-Based Flexible Transparent Conducting Films. *Journal of the American Chemical Society* **2007,** *129* (25), 7758-7759.

36. Lee, J. H.; Jeong, Y. R.; Lee, G.; Jin, S. W.; Lee, Y. H.; Hong, S. Y.; Park, H.; Kim, J. W.; Lee, S.-S.; Ha, J. S., Highly Conductive, Stretchable, and Transparent PEDOT:PSS Electrodes Fabricated with Triblock Copolymer Additives and Acid Treatment. *ACS Applied Materials & Interfaces* **2018,** *10* (33), 28027-28035.

37. Wang, Y.; Zhu, C.; Pfattner, R.; Yan, H.; Jin, L.; Chen, S.; Molina-Lopez, F.; Lissel, F.; Liu, J.; Rabiah, N. I.; Chen, Z.; Chung, J. W.; Linder, C.; Toney, M. F.; Murmann, B.; Bao, Z., A highly stretchable, transparent, and conductive polymer. *Science Advances* **2017,** *3* (3), e1602076.

38. Highly transparent and conductive films of densely aligned ultrathin Au nanowire monolayers. *Nano Lett.* **2012,** *12*, 6066.

39. O'Connor, B.; Haughn, C.; An, K.-H.; Pipe, K. P.; Shtein, M., Transparent and conductive electrodes based on unpatterned, thin metal films. *Applied Physics Letters* **2008,** *93* (22), 223304.

40. Lee, D.; Paeng, D.; Park, H. K.; Grigoropoulos, C. P., Vacuum-Free, Maskless Patterning of Ni Electrodes by Laser Reductive Sintering of NiO Nanoparticle Ink and Its Application to Transparent Conductors. *ACS nano* **2014,** *8* (10), 9807-9814.

41. Ghosh, D. S.; Martinez, L.; Giurgola, S.; Vergani, P.; Pruneri, V., Widely transparent electrodes based on ultrathin metals. *Opt. Lett.* **2009,** *34* (3), 325-327.

42. Liu, Y.; Li, Y.; Zeng, H., ZnO-Based Transparent Conductive Thin Films: Doping, Performance, and Processing. *Journal of Nanomaterials* **2013,** *2013*, 9.

43. Bhosle, V.; Prater, J. T.; Yang, F.; Burk, D.; Forrest, S. R.; Narayan, J., Gallium-doped zinc oxide films as transparent electrodes for organic solar cell applications. *Journal of Applied Physics* **2007,** *102* (2), 023501.

44. Hsu, P.-C.; Wu, H.; Carney, T. J.; McDowell, M. T.; Yang, Y.; Garnett, E. C.; Li, M.; Hu, L.; Cui, Y., Passivation Coating on Electrospun Copper Nanofibers for Stable Transparent Electrodes. *ACS Nano* **2012,** *6* (6), 5150-5156.

45. Ma, X.; Zhu, Y.; Kim, S.; Liu, Q.; Byrley, P.; Wei, Y.; Zhang, J.; Jiang, K.; Fan, S.; Yan, R.; Liu, M., Sharp-Tip Silver Nanowires Mounted on Cantilevers for High-Aspect-Ratio High-Resolution Imaging. *Nano Letters* **2016,** *16* (11), 6896-6902.

46. Li, B.; Ye, S.; Stewart, I. E.; Alvarez, S.; Wiley, B. J., Synthesis and Purification of Silver Nanowires To Make Conducting Films with a Transmittance of 99%. *Nano Letters* **2015,** *15* (10), 6722-6726.

47. Guo, H.; Lin, N.; Chen, Y.; Wang, Z.; Xie, Q.; Zheng, T.; Gao, N.; Li, S.; Kang, J.; Cai, D.; Peng, D.-L., Copper Nanowires as Fully Transparent Conductive Electrodes. *Scientific reports* **2013,** *3*, 2323.

48. Elechiguerra, J. L.; Larios-Lopez, L.; Liu, C.; Garcia-Gutierrez, D.; Camacho-Bragado, A.; Yacaman, M. J., Corrosion at the Nanoscale: The Case of Silver Nanowires and Nanoparticles. *Chemistry of Materials* **2005,** *17* (24), 6042-6052.

49. Bennett, H. E.; Peck, R. L.; Burge, D. K.; Bennett, J. M., Formation and Growth of Tarnish on Evaporated Silver Films. *Journal of Applied Physics* **1969,** *40* (8), 3351-3360.

50. The effect of nanowire length and diameter on the properties of transparent, conducting nanowire films. *Nanoscale* **2012,** *4* (6), 1996.

51. Uniform silver nanowires synthesis by reducing AgNO3 with ethylene glycol in the presence of seeds and poly(vinyl pyrrolidone). *Chem. Mater.* **2002,** *14*, 4736.

52. Polyol synthesis of uniform silver nanowires: a plausible growth mechanism and the supporting evidence. *Nano Lett.* **2003,** *3*, 955.

53. Large-scale synthesis of uniform silver nanowires through a soft, self-seeding, polyol process. *Adv. Mater.* **2002,** *14*, 833.

54. Sun, Y.; Gates, B.; Mayers, B.; Xia, Y., Crystalline Silver Nanowires by Soft Solution Processing. *Nano Letters* **2002,** *2* (2), 165-168.

55. Korte, K. E.; Skrabalak, S. E.; Xia, Y., Rapid synthesis of silver nanowires through a CuCl- or CuCl2-mediated polyol process. *Journal of Materials Chemistry* **2008,** *18* (4), 437-441.

56. Uniform silver nanowires synthesis by reducing AgNO 3 with ethylene glycol in the presence of seeds and poly(vinyl pyrrolidone). *Chem. Mater.* **2002,** *14* (11), 4736.

57. da Silva, R. R.; Yang, M.; Choi, S. I.; Chi, M.; Luo, M.; Zhang, C.; Li, Z. Y.; Camargo, P. H.; Ribeiro, S. J.; Xia, Y., Facile Synthesis of Sub-20 nm Silver Nanowires through a Bromide-Mediated Polyol Method. *ACS Nano* **2016,** *10* (8), 7892-900.

58. Rapid synthesis of silver nanowires through a CuCl- or CuCl2-mediated polyol process. *J. Mater. Chem.* **2008,** *18*, 437.

59. Schuette, W. M.; Buhro, W. E., Polyol Synthesis of Silver Nanowires by Heterogeneous Nucleation; Mechanistic Aspects Influencing Nanowire Diameter and Length. *Chemistry of Materials* **2014,** *26* (22), 6410-6417.

60. Zhang, Y.; Guo, J.; Xu, D.; Sun, Y.; Yan, F., One-Pot Synthesis and Purification of Ultralong Silver Nanowires for Flexible Transparent Conductive Electrodes. *ACS Applied Materials & Interfaces* **2017,** *9* (30), 25465-25473.

61. Liu, S.; Sun, B.; Li, J.-g.; Chen, J., Silver nanowires with rounded ends: ammonium carbonate-mediated polyol synthesis, shape evolution and growth mechanism. *CrystEngComm* **2014,** *16* (2), 244-251.

62. Silver nanowires: from scalable synthesis to recyclable foldable electronics. *Adv. Mater.* **2011,** *23*, 3052.

63. Lee, E.-J.; Chang, M.-H.; Kim, Y.-S.; Kim, J.-Y., High-pressure polyol synthesis of ultrathin silver nanowires: Electrical and optical properties. *APL Materials* **2013,** *1* (4), 042118.

64. Large-scale synthesis and characterization of very long silver nanowires via successive multistep growth. *Cryst. Growth Des.* **2012,** *12*, 5598.

65. Rathmell, A. R.; Wiley, B. J., The Synthesis and Coating of Long, Thin Copper Nanowires to Make Flexible, Transparent Conducting Films on Plastic Substrates. *Advanced Materials* **2011,** *23* (41), 4798-4803.

66. Chang, Y.; Lye, M. L.; Zeng, H. C., Large-Scale Synthesis of High-Quality Ultralong Copper Nanowires. *Langmuir : the ACS journal of surfaces and colloids* **2005,** *21* (9), 3746-3748.

67. Ye, S.; Rathmell, A. R.; Stewart, I. E.; Ha, Y. C.; Wilson, A. R.; Chen, Z.; Wiley, B. J., A rapid synthesis of high aspect ratio copper nanowires for high-performance transparent conducting films. *Chem Commun (Camb)* **2014,** *50* (20), 2562-4.

68. Jin, M.; He, G.; Zhang, H.; Zeng, J.; Xie, Z.; Xia, Y., Shape-Controlled Synthesis of Copper Nanocrystals in an Aqueous Solution with Glucose as a Reducing Agent and Hexadecylamine as a Capping Agent. *Angewandte Chemie International Edition* **2011,** *50* (45), 10560-10564.

69. Mohl, M.; Pusztai, P.; Kukovecz, A.; Konya, Z.; Kukkola, J.; Kordas, K.; Vajtai, R.; Ajayan, P. M., Low-Temperature Large-Scale Synthesis and Electrical Testing of Ultralong Copper Nanowires. *Langmuir : the ACS journal of surfaces and colloids* **2010,** *26* (21), 16496-16502.

70. Synthesis of ultralong copper nanowires for high-performance transparent electrodes. *J. Am. Chem. Soc.* **2012,** *134*, 14283.

71. Pate, J.; Zamora, F.; Watson, S. M. D.; Wright, N. G.; Horrocks, B. R.; Houlton, A., Solution-based DNA-templating of sub-10 nm conductive copper nanowires. *Journal of Materials Chemistry C* **2014,** *2* (43), 9265-9273.

72. Niu, Z.; Cui, F.; Yu, Y.; Becknell, N.; Sun, Y.; Khanarian, G.; Kim, D.; Dou, L.; Dehestani, A.; Schierle-Arndt, K.; Yang, P., Ultrathin Epitaxial Cu@Au Core–Shell Nanowires for Stable Transparent Conductors. *Journal of the American Chemical Society* **2017,** *139* (21), 7348-7354.

73. Synthesis of oxidation-resistant cupronickel nanowires for transparent conducting nanowire networks. *Nano Lett.* **2012,** *12*, 3193.

74. Stewart, I. E.; Ye, S.; Chen, Z.; Flowers, P. F.; Wiley, B. J., Synthesis of Cu–Ag, Cu–Au, and Cu–Pt Core–Shell Nanowires and Their Use in Transparent Conducting Films. *Chemistry of Materials* **2015,** *27* (22), 7788-7794.

75. Chen, Z.; Rathmell, A. R.; Ye, S.; Wilson, A. R.; Wiley, B. J., Optically Transparent Water Oxidation Catalysts Based on Copper Nanowires. *Angewandte Chemie International Edition* **2013,** *52* (51), 13708-13711.

76. Chen, Z.; Ye, S.; Stewart, I. E.; Wiley, B. J., Copper Nanowire Networks with Transparent Oxide Shells That Prevent Oxidation without Reducing Transmittance. *ACS nano* **2014,** *8* (9), 9673-9679.

77. <OA_10.1021jacs.6b12143.pdf>.

78. Yoon, H.; Shin, D. S.; Kim, T. G.; Kim, D.; Park, J., Facile Synthesis of Graphene on Cu Nanowires via Low-Temperature Thermal CVD for the Transparent Conductive Electrode. *ACS Sustainable Chemistry & Engineering* **2018,** *6* (11), 13888-13896.

79. Ahn, Y.; Jeong, Y.; Lee, D.; Lee, Y., Copper Nanowire–Graphene Core–Shell Nanostructure for Highly Stable Transparent Conducting Electrodes. *ACS nano* **2015,** *9* (3), 3125-3133.

80. Dou, L.; Cui, F.; Yu, Y.; Khanarian, G.; Eaton, S. W.; Yang, Q.; Resasco, J.; Schildknecht, C.; Schierle-Arndt, K.; Yang, P., Solution-Processed Copper/Reduced-Graphene-Oxide Core/Shell Nanowire Transparent Conductors. *ACS nano* **2016,** *10* (2), 2600-2606.

81. Huo, D.; Kim, M. J.; Lyu, Z.; Shi, Y.; Wiley, B. J.; Xia, Y., One-Dimensional Metal Nanostructures: From Colloidal Syntheses to Applications. *Chemical Reviews* **2019**.

82. Flexible transparent PES/silver nanowires/PET sandwich-structured film for high-efficiency electromagnetic interference shielding. *Langmuir : the ACS journal of surfaces and colloids* **2012,** *28*, 7101.

83. The synthesis and coating of long, thin copper nanowires to make flexible, transparent conducting films on plastic substrates. *Adv. Mater.* **2011,** *23*, 4798.

84. Highly flexible transparent film heaters based on random networks of silver nanowires. *Nano Res.* **2012,** *5*, 427.

85. Highly flexible silver nanowire electrodes for shape-memory polymer light-emitting diodes. *Adv. Mater.* **2011,** *23* (5), 664.

86. Xu, F.; Zhu, Y., Highly conductive and stretchable silver nanowire conductors. *Adv Mater* **2012,** *24* (37), 5117-22.

87. Sannicolo, T.; Lagrange, M.; Cabos, A.; Celle, C.; Simonato, J.-P.; Bellet, D., Metallic Nanowire-Based Transparent Electrodes for Next Generation Flexible Devices: a Review. *Small* **2016,** *12* (44), 6052-6075.

88. Scalable coating and properties of transparent, flexible, silver nanowire electrodes. *ACS nano* **2010,** *4*, 2955.

89. Jang, J.; Hyun, B. G.; Ji, S.; Cho, E.; An, B. W.; Cheong, W. H.; Park, J.-U., Rapid production of large-area, transparent and stretchable electrodes using metal nanofibers as wirelessly operated wearable heaters. *Npg Asia Materials* **2017,** *9*, e432.

90. Kang, S.; Cho, S.; Shanker, R.; Lee, H.; Park, J.; Um, D.-S.; Lee, Y.; Ko, H., Transparent and conductive nanomembranes with orthogonal silver nanowire arrays for skin-attachable loudspeakers and microphones. *Science Advances* **2018,** *4* (8), eaas8772.

91. Qian, F.; Lan, P. C.; Freyman, M. C.; Chen, W.; Kou, T.; Olson, T. Y.; Zhu, C.; Worsley, M. A.; Duoss, E. B.; Spadaccini, C. M.; Baumann, T.; Han, T. Y.-J., Ultralight Conductive Silver Nanowire Aerogels. *Nano Letters* **2017,** *17* (12), 7171-7176.

92. Pu, D.; Zhou, W.; Li, Y.; Chen, J.; Chen, J.; Zhang, H.; Mi, B.; Wang, L.; Ma, Y., Order-enhanced silver nanowire networks fabricated by two-step dip-coating as polymer solar cell electrodes. *RSC Advances* **2015,** *5* (122), 100725-100729.

93. Duan, S.-k.; Niu, Q.-l.; Wei, J.-f.; He, J.-b.; Yin, Y.-a.; Zhang, Y., Water-bath assisted convective assembly of aligned silver nanowire films for transparent electrodes. *Physical Chemistry Chemical Physics* **2015,** *17* (12), 8106-8112.

94. Smooth nanowire/polymer composite transparent electrodes. *Adv. Mater.* **2011,** *23*, 2905.

95. Nam, S.; Song, M.; Kim, D.-H.; Cho, B.; Lee, H. M.; Kwon, J.-D.; Park, S.-G.; Nam, K.-S.; Jeong, Y.; Kwon, S.-H.; Park, Y. C.; Jin, S.-H.; Kang, J.-W.; Jo, S.; Kim, C. S., Ultrasmooth, extremely deformable and shape recoverable Ag nanowire embedded transparent electrode. *Scientific reports* **2014,** *4*, 4788.
96. Jiang, Y.; Xi, J.; Wu, Z.; Dong, H.; Zhao, Z.; Jiao, B.; Hou, X., Highly Transparent, Conductive, Flexible Resin Films Embedded with Silver Nanowires. *Langmuir : the ACS journal of surfaces and colloids* **2015,** *31* (17), 4950-4957.

97. Akter, T.; Kim, W. S., Reversibly Stretchable Transparent Conductive Coatings of Spray-Deposited Silver Nanowires. *ACS Applied Materials & Interfaces* **2012,** *4* (4), 1855-1859.

98. Yang, Y.; Ding, S.; Araki, T.; Jiu, J.; Sugahara, T.; Wang, J.; Vanfleteren, J.; Sekitani, T.; Suganuma, K., Facile fabrication of stretchable Ag nanowire/polyurethane electrodes using high intensity pulsed light. *Nano Research* **2016,** *9* (2), 401-414.

99. Solution-processed flexible transparent conductors composed of silver nanowire networks embedded in indium tin oxide nanoparticle matrices. *Nano Res.* **2012,** *5*, 805.

100. Kang, S.; Kim, T.; Cho, S.; Lee, Y.; Choe, A.; Walker, B.; Ko, S. J.; Kim, J. Y.; Ko, H., Capillary Printing of Highly Aligned Silver Nanowire Transparent Electrodes for High-Performance Optoelectronic Devices. *Nano Lett* **2015,** *15* (12), 7933-42.

101. Graedel, T. E., Corrosion Mechanisms for Silver Exposed to the Atmosphere. *Journal of The Electrochemical Society* **1992,** *139* (7), 1963-1970.

102. Choi, D. Y.; Kang, H. W.; Sung, H. J.; Kim, S. S., Annealing-free, flexible silver nanowire–polymer composite electrodes via a continuous two-step spray-coating method. *Nanoscale* **2013,** *5* (3), 977-983.

103. Ahn, Y.; Jeong, Y.; Lee, Y., Improved Thermal Oxidation Stability of Solution-Processable Silver Nanowire Transparent Electrode by Reduced Graphene Oxide. *ACS Applied Materials & Interfaces* **2012,** *4* (12), 6410-6414.

104. Song, J.; Li, J.; Xu, J.; Zeng, H., Superstable Transparent Conductive Cu@Cu4Ni Nanowire Elastomer Composites against Oxidation, Bending, Stretching, and Twisting for Flexible and Stretchable Optoelectronics. *Nano Letters* **2014,** *14* (11), 6298-6305.

105. Kim, T. G.; Park, H. J.; Woo, K.; Jeong, S.; Choi, Y.; Lee, S. Y., Enhanced Oxidation-Resistant Cu@Ni Core–Shell Nanoparticles for Printed Flexible Electrodes. *ACS Applied Materials & Interfaces* **2018,** *10* (1), 1059-1066.

106. Wang, X.; Wang, R.; Zhai, H.; Shen, X.; Wang, T.; Shi, L.; Yu, R.; Sun, J., Room-Temperature Surface Modification of Cu Nanowires and Their Applications in Transparent

Electrodes, SERS-Based Sensors, and Organic Solar Cells. *ACS Applied Materials & Interfaces* **2016,** *8* (42), 28831-28837.

107. Schriver, M.; Regan, W.; Gannett, W. J.; Zaniewski, A. M.; Crommie, M. F.; Zettl, A., Graphene as a Long-Term Metal Oxidation Barrier: Worse Than Nothing. *ACS nano* **2013,** *7* (7), 5763-5768.

108. Zhou, F.; Li, Z.; Shenoy, G. J.; Li, L.; Liu, H., Enhanced Room-Temperature Corrosion of Copper in the Presence of Graphene. *ACS nano* **2013,** *7* (8), 6939-6947.
109. Fabrication of silver nanowire transparent electrodes at room temperature. *Nano Res.* **2011,** *4*, 1215.

110. Hauger, T. C.; Al-Rafia, S. M. I.; Buriak, J. M., Rolling Silver Nanowire Electrodes: Simultaneously Addressing Adhesion, Roughness, and Conductivity. *ACS Applied Materials & Interfaces* **2013,** *5* (23), 12663-12671.
111. Garnett, E. C.; Cai, W.; Cha, J. J.; Mahmood, F.; Connor, S. T.; Greyson Christoforo, M.; Cui, Y.; McGehee, M. D.; Brongersma, M. L., Self-limited plasmonic welding of silver nanowire junctions. *Nature materials* **2012,** *11*, 241.

112. Jiu, J.; Sugahara, T.; Nogi, M.; Araki, T.; Suganuma, K.; Uchida, H.; Shinozaki, K., High-intensity pulse light sintering of silver nanowire transparent films on polymer substrates: the effect of the thermal properties of substrates on the performance of silver films. *Nanoscale* **2013,** *5* (23), 11820-11828.

113. Liu, Y.; Zhang, J.; Gao, H.; Wang, Y.; Liu, Q.; Huang, S.; Guo, C. F.; Ren, Z., Capillary-Force-Induced Cold Welding in Silver-Nanowire-Based Flexible Transparent Electrodes. *Nano Letters* **2017,** *17* (2), 1090-1096.

114. Kang, H.; Kim, Y.; Cheon, S.; Yi, G.-R.; Cho, J. H., Halide Welding for Silver Nanowire Network Electrode. *ACS Applied Materials & Interfaces* **2017,** *9* (36), 30779-30785.

115. Reversibly stretchable transparent conductive coatings of spray-deposited silver nanowires. *ACS Appl. Mater. Int.* **2012,** *4* (4), 1855.

116. Miller, M. S.; O'Kane, J. C.; Niec, A.; Carmichael, R. S.; Carmichael, T. B., Silver Nanowire/Optical Adhesive Coatings as Transparent Electrodes for Flexible Electronics. *ACS Applied Materials & Interfaces* **2013,** *5* (20), 10165-10172.

117. Li, Y.; Cui, P.; Wang, L.; Lee, H.; Lee, K.; Lee, H., Highly Bendable, Conductive, and Transparent Film by an Enhanced Adhesion of Silver Nanowires. *ACS Applied Materials & Interfaces* **2013,** *5* (18), 9155-9160.

118. Sekitani, T.; Nakajima, H.; Maeda, H.; Fukushima, T.; Aida, T.; Hata, K.; Someya, T., Stretchable active-matrix organic light-emitting diode display using printable elastic conductors. *Nature materials* **2009,** *8*, 494.

119. Lipomi, D. J.; Vosgueritchian, M.; Tee, B. C. K.; Hellstrom, S. L.; Lee, J. A.; Fox, C. H.; Bao, Z., Skin-like pressure and strain sensors based on transparent elastic films of carbon nanotubes. *Nature Nanotechnology* **2011,** *6*, 788.

120. Yamada, T.; Hayamizu, Y.; Yamamoto, Y.; Yomogida, Y.; Izadi-Najafabadi, A.; Futaba, D. N.; Hata, K., A stretchable carbon nanotube strain sensor for human-motion detection. *Nature Nanotechnology* **2011,** *6*, 296.

121. Gong, S.; Lai, D. T. H.; Su, B.; Si, K. J.; Ma, Z.; Yap, L. W.; Guo, P.; Cheng, W., Highly Stretchy Black Gold E-Skin Nanopatches as Highly Sensitive Wearable Biomedical Sensors. *Advanced Electronic Materials* **2015,** *1* (4), 1400063.

122. Pan, S.; Yang, Z.; Chen, P.; Deng, J.; Li, H.; Peng, H., Wearable Solar Cells by Stacking Textile Electrodes. *Angewandte Chemie International Edition* **2014,** *53* (24), 6110-6114.

123. Elastomeric transparent capacitive sensors based on an interpenetrating composite of silver nanowires and polyurethane. *Appl. Phys. Lett.* **2013,** *102*.

124. Wang, C.; Hwang, D.; Yu, Z.; Takei, K.; Park, J.; Chen, T.; Ma, B.; Javey, A., User-interactive electronic skin for instantaneous pressure visualization. *Nature materials* **2013,** *12*, 899.

125. Parrilla, M.; Cánovas, R.; Jeerapan, I.; Andrade, F. J.; Wang, J., A Textile-Based Stretchable Multi-Ion Potentiometric Sensor. *Advanced Healthcare Materials* **2016,** *5* (9), 996-1001.

126. Choi, S.; Park, J.; Hyun, W.; Kim, J.; Kim, J.; Lee, Y. B.; Song, C.; Hwang, H. J.; Kim, J. H.; Hyeon, T.; Kim, D.-H., Stretchable Heater Using Ligand-Exchanged Silver Nanowire Nanocomposite for Wearable Articular Thermotherapy. *ACS nano* **2015,** *9* (6), 6626-6633.

127. Liu, J.-W.; Wang, J.-L.; Wang, Z.-H.; Huang, W.-R.; Yu, S.-H., Manipulating Nanowire Assembly for Flexible Transparent Electrodes. *Angewandte Chemie International Edition* **2014,** *53* (49), 13477-13482.

128. Chen, T.-G.; Huang, B.-Y.; Liu, H.-W.; Huang, Y.-Y.; Pan, H.-T.; Meng, H.-F.; Yu, P., Flexible Silver Nanowire Meshes for High-Efficiency Microtextured Organic-Silicon Hybrid Photovoltaics. *ACS Applied Materials & Interfaces* **2012,** *4* (12), 6857-6864.

129. Efficient flexible phosphorescent polymer light-emitting diodes based on silver nanowire–polymer composite electrode. *Adv. Mater.* **2011,** *23*, 5563.

130. Zhang, X.; Yan, X.; Chen, J.; Zhao, J., Large-size graphene microsheets as a protective layer for transparent conductive silver nanowire film heaters. *Carbon* **2014,** *69*, 437-443.

131. Doganay, D.; Coskun, S.; Genlik, S. P.; Unalan, H. E., Silver nanowire decorated heatable textiles. *Nanotechnology* **2016,** *27* (43), 435201.

132. Cheng, Y.; Zhang, H.; Wang, R.; Wang, X.; Zhai, H.; Wang, T.; Jin, Q.; Sun, J., Highly Stretchable and Conductive Copper Nanowire Based Fibers with Hierarchical Structure for Wearable Heaters. *ACS Applied Materials & Interfaces* **2016,** *8* (48), 32925-32933.

Chapter 2. Epitaxial, ultra-thin Au coating as a barrier for oxidation damages for silver nanowires

2.1 Introduction

Crystalline Ag nanowire is known to have the highest electrical and thermal conductivity among metals, which make them receive significant attention in transparent conductor technologies, including thin-film solar cells, super capacitor, transparent heaters, touch panels, organic light-emitting diodes (OLEDs). Furthermore, Ag nanowires also own high surface to volume ratio, low defect level and atomically flat surface, all of which enable Ag nanowires hold promise for numerous emerging applications such as sensors (e.g. bio-sensor, strain or pressure sensor), plasmonic device (e.g. surface enhanced Raman spectroscopy (SERS), subwavelength optoelectronics), scanning tunneling microscopies (STM), artificial skin and even wearable electronics.

Across all these above applications, the major challenge for Ag nanowire is the long-term stability issue which means their susceptibility to damage from oxidation has limited its further commercialization. The morphology structure and electrical (optical, chemical or mechanical) properties of Ag nanowire can be deteriorated when exposed to water, acids, oxidative agents and even in the ambient condition, A Heat and UV irradiation can play a damaging role as well. Therefore, there is an outgoing drive to avoid oxidation of Ag nanowire.

However, every application actually has their own specific requirements for the protection of Ag nanowires. For the transparent conductors, it requires large-area process-ability and cost-effectiveness with high optical transmittance (%T) and low sheet resistance (R_s). So far, the dominant approaches have been reported to address this long-term stability issue in the field of transparent conductor, which can be concluded into two methods: (1) Using an over-coated layer on the Ag nanowire networks as a corrosion barrier. For example, Polydimethylsiloxane (PDMS),[1] Poly (methyl methacrylate) (PMMA),[2] Poly(3,4-ethylenedioxythio-phene): poly(styrenesulfonate) (PEDOT: PSS), reduced graphene oxide (rGO)[3] and atomic layer deposition (ALD) layer of aluminum-doped zinc oxide (AZO) and aluminum oxide (Al_2O_3)[3]. (2) Growing a layer of a conductive yet chemically stable shell on the Ag nanowire surface, such as Ni,[4] C[5] and Zn, Sn, Pt. which can be achieved through a solution-phase process. Both methods have been proven effective in improving the electrical and optical durability of Ag nanowire networks for transparent conductors to some extent. However,

For sensor application, maintaining both sensitivity and flexibility (stretch or strain sensor) or chemical stability (bio-sensor) are the critical performance criteria. For example, Morteza et al. fabricated the sandwich-structured PDMS/Ag nanowire/PDMS nanocomposite sensor[6]. Although the obtained sensor showed excellent flexibility, stretch-ability and bendability, the coating of nonconductive layer (PDMS) on the surfaces of Ag nanowire network can significantly weaken the overall conductivity and moreover, the oxygen from the air can still penetrate into polymer PDMS during the stretch/release cycle in the long-term run, which oxidant the silver paste or Ag nanowire network and thus the

electrical resistance of this composite increased irreversibly, which deteriorate the sensor performance finally. So, the long-term effectiveness of over-coated non-conducting layer for Ag nanowire protection is highly controversial. Mao et al. reported a solution-processed Ag/C nanowire decorated with Au nanoparticles to form Ag/C/Au nanocomposites and this composite was employed as enzymatic hydrogen peroxide biosensor[7]. It can exhibit good electrocatalytic activity to the reduction of H_2O_2. However, the galvanic replacement reaction happened during the reduction of Au nanoparticles which was found in TEM image, which means incompletely or imperfect coating of carbon on Ag nanowires. So, it is still a big challenge for this Ag/C nanowire to exist in a strong oxidant H_2O_2,

For SERS application, it requires this protection not only can retain strong enhancement of Raman scattering same as Ag, but also should make this Ag nanowire substrate robust, stable and recycle. Zhou et al prepared TiO_2 coated Ag nanowire arrays via anodic aluminum oxide (AAO) template[8]. Although TiO_2 layer make this substrate have a good photocatalysis performance of organic pollutants, it also greatly cripples the high SERS enhancement efficiency of Ag nanowire.

For AFM probe application, mechanical stability is the majority concern, Ag nanowires, benefiting from the stiffening size effect, can reach 160 GPa of the Young's modulus, which exceeds that of silicon nanowires. Ma et al. developed an Ag nanowire-based probe by attaching a sharp-tip Ag nanowire to ordinary AFM tips which can achieve the lateral resolution of 8 nm[9]. However, Ag nanowire is vulnerable to oxidize even in the ambient condition and thus the Ag nanowire tip would become fragile without standing the desired force AFM probe need. Thus, in order to extend this long life of Ag nanowire-based and

make Ag nanowire more commercial in AFM probe, it is very necessary to develop a route to mitigate the oxidation issue and retain a stable mechanical performance.

Based on the aforementioned description, in order to fulfilling further commercialization of Ag nanowires, there is a need for to seek for an effective, universal and economical approach to stop Ag nanowires from oxidative etching without sacrificing the intrinsic property of Ag nanowires in all the mentioned applications such as transparent conductors, sensors, plasmonic device and STM (e.g. AFM probe) technologies. Therefore, the core-shell nanostructure that encapsulates Ag with a noble metal shell has been exploited to greatly maintain the intrinsic characteristics of Ag nanowire. A recent research was made by Yang et al. deposited Au on Ag nanowire surface,[10] the resulted Ag@Au nanowires with a shell thickness of ~1 nm exhibited slightly improved performance compared to pristine Ag nanowires. However, the protection is impaired due to the incompletely or imperfect coverage of Au shell on Ag nanowire surface and the indefinite interface between Ag core and Au shell. We envision that this stability issue can be solved via the epitaxial growth of a uniform and conformal shell of noble metal on Ag nanowires.

However, the challenge mainly comes from the galvanic replacement reaction when depositing a stable metal onto a less stable metal surface, which causes nanoscale etching of the original Ag nanowires and finally leads to severe surface roughness, or even the formation of hollow alloys nanotubes.[5, 11-12] The surface roughness is easily found on the order of the Fermi wavelength of an electron (~0.5 nm), resulting in an increased electron scattering and decreased conductivity. Gao et al. suggested that galvanic replacement reaction between Ag nanowire and Au precursor can be avoided in the presence of stronger

reducing agent such as ascorbic acid (AA).[13] Liu et al. confirmed that galvanic replacement reaction can be blocked through both decreasing the reduction potential of Au precursors and offering sufficient protection on the Ag nanoplate surface.[14] Yin group reported the preparation of Au coated Ag nanoplates by applying stronger reducing agent (AA) and lessening the reducing potential through complexion with SO_3^{2-} which leads to galvanic replacement free deposition of Au on Ag nanoplate surface.[14] Motivated by these work, herein, we propose a single-step, solution-phase, etch-free, epitaxial deposition technique to grow an ultra-thin (~6 nm), conformal, single-crystalline and atomically smooth Au layer on AgNW surface on the basis of introducing SO_3^{2-} ions, which acts as a reliable and economical anti-oxidation barrier to provide long-term device stability. The Ag@Au nanowires can keep excellent stability in air and even in harsh environment such as PBS and H_2O_2 solution as well. Transparent electrode films prepared with Ag@Au nanowires can also display perfect optical, electrical performance. More surprisingly, the highly good performance can be stained for more than 84 days under 80% of humidity and 80 ℃ of temperature in the duration test, this is the first demonstration of this level of long-term stability to the best of our knowledge.

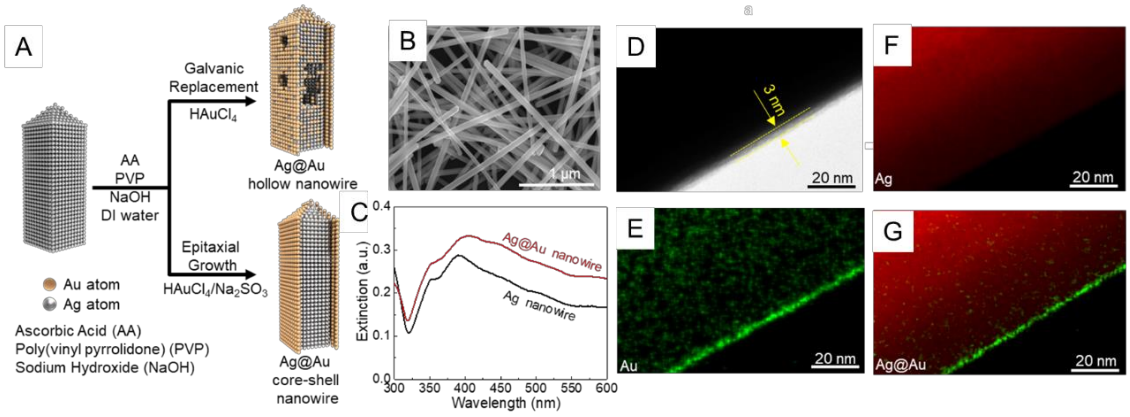

Figure 2.1. Synthesis of the Ag@Au (~3 nm Au) core-shell nanowires. (A) Schematic illustration of the two possible products for syntheses that involve Ag nanowires and $HAuCl_4$ with and without ligand Na_2SO_3. the morphology structure of the resulted product is determined by lowering reduction potential relative to the added appropriate ligand SO_3^{2-}. (B) SEM image of Ag@Au core-shell nanowires. (C) UV-vis extinction spectrum of Ag nanowire before (black line) and after (red line) coating gold. (D) TEM image of Ag@Au core-shell nanowire (~3 nm Au). (E-G) Elemental mapping of both Ag and Au (Ag@Au core-shell nanowire (~3 nm Au)). The red color indicates Ag, whereas the green color indicates Au.

2.2 Results and Discussion

Our attempts to achieve the etch-free deposition of Au on Ag nanowires in an aqueous solution is to introduce a strong reducing power (AA) to compete with Ag and an appropriate ligand SO_3^{2-} which could be complexed with Au^{3+} ions to retard the reduction potential of Au and this recipe could block the galvanic replacement reaction completely, which was illustrated in Figure 2.1a. Figure 2.1b depicts the Ag-like surface morphology of Ag@Au nanowires which indicates the possible conformal growth of Au on Ag nanowire surface. The corresponding transmission electron microscopy (TEM) image of the Ag@Au core-shell nanowire obtained from the optimized synthetic recipe was showed

in figure 2.1d. The obvious contrast between Ag and Au in TEM image suggests a core-shell nanostructure of this resulted samples. The core-shell nanostructure feature was furtherly confirmed by element dispersive spectroscopy (EDS) mapping (Figure 2.1e-g). Ag (red color) is mainly located in the central zone of the nanowire while Au (green color) is distributed in the outer edge. The Au nano-shell thickness was estimated to be about 3 nm. UV-vis spectra (Figure 2.1c) also shows that the similar peak intensity and position could be found compared with pristine AgNW which means a possible epitaxial growth of Au on Ag nanowire. Compared with Au coated Ag nanoplates, growing Au on Ag nanowires is more challenging. Firstly, Ag nanowires are prone to aggregate in aqueous solution because of the high aspect ratio (~2000) and this feature may result in insufficient coverage of Au on Ag nanowire surface.[15] Secondly, Ag nanowire was known to have five facets on side surfaces with corresponding {111} facets on the end part and the energy difference for Au coating between the different facets of Ag nanowire would also lead to nonuniform deposition of Au.[13] To handle these two issues, we therefore kept stirring to promote homogeneously mass transfer during the whole process and also introduced polyvinylpyrrolidone (PVP, MW=55000) as a capping reagent to stabilize Ag nanowires against aggregation by making full use of the robust coordination between the oxygen and nitrogen atoms of the pyrrolidone ring and AgNW surface.[13] Moreover, specific amount of diethylamine was also to help minimize the energy difference of two different lattice facets of AgNWs[16]. Meanwhile, the Au growth solution was slowly fed into the reaction solution system via syringe pump with the a relatively slow rate of 0.05 mL/min, this is because if Au precursor was rapidly added to the reaction system, instantaneous reduction

of Au ions could lead to a fast-increased amount of the Au atoms, initiating the self-nucleation and finally Au nanoparticles were grown.

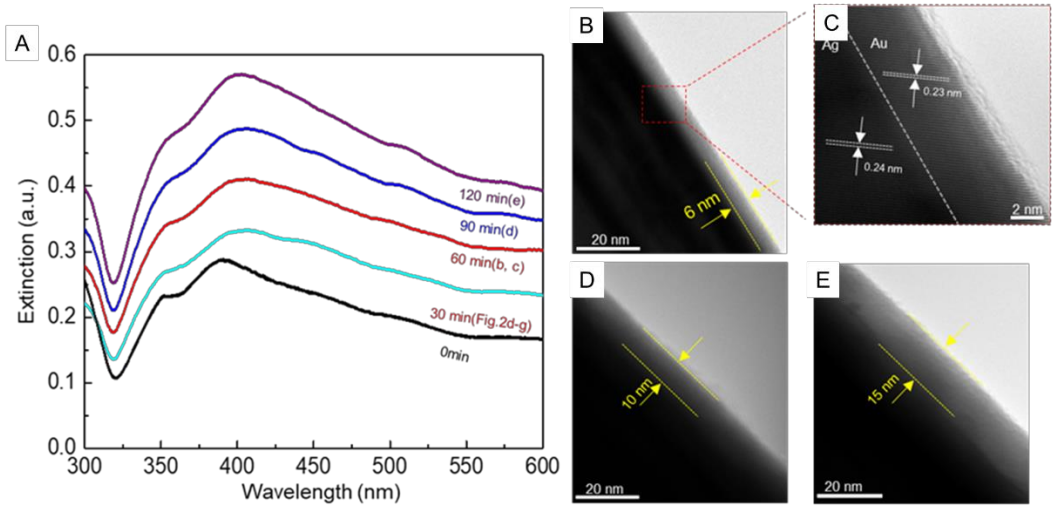

Figure 2.2. Synthesis of Ag@Au core-shell nanowires with varying thickness of Au nanoshell. (A) UV-vis extinction spectrum of Ag@Au nanowires with different reaction time; (B, C) HRTEM image of Ag@Au nanowire (~6 nm Au) and corresponding atomic resolution TEM image; (D, E) TEM image of Ag@Au Nanowire (10 nm Au) and Ag@Au nanowire (~15 nm Au) respectively.

In our work, SO_3^{2-} ions act as not only a ligand but also a reducing agent to form particularly high stable complex $[Au\ (SO_3)_2]^{2-}$. Considering the slow injection method of Au growth solution into AgNW aqueous solution, we cannot simply set the regular ratio between Na_2SO_3 and $HAuCl_4$ to 2:1 as evidenced in Figure 2.3a. By tuning the ratio between Au^{3+} and SO_3^{2-} to optimize the minimal reduction potential to avoid galvanic etching between Ag and Au (Figure 2.3), we found that when the ratio (Na_2SO_3:$HAuCl_4$) was increased to 150:1, highly smooth surface was obtained on the final Ag@Au nanowire samples while voids or pores could be glimpsed on core-shell nanowire surface especially

on the end part of nanowires when the ratio was lower than 150, indicating a galvanic replacement reaction could easily happen if insufficient sulfite ligands were presented in the growth solution. And this observation could also confirm the truth that SO_3^{2-} do served as the capping reagent specially to the {100} facets of the Ag nanowires, which provide enough protection on the side part of Ag nanowires that possess a large fraction of the {100} facets, which suppressed galvanic replacement reaction between Ag and Au. However, it cannot offer enough protection on the end parts of Ag nanowires that are usually composed of {111} facets.[17] So the ratio should be increased up to at least 150, then the galvanic reaction could be fully suppressed both on side parts and end parts of AgNWs. With this optimized condition, the added gold sulfite complex was exclusively reduced by AA rather than contributing to the galvanic reaction with AgNWs. So, with this optimized recipe, we could control the thickness of Au shell varied from 3 nm, 6 nm and even to 15 nm via increasing the injection time of Au growth solution into the original AgNW solution, which could be evidenced by the UV-vis spectroscopy (Figure 2.2A) and the corresponding TEM image (Figure 2.2B-E). From UV-vis spectra, we observed a continuous increase in the intensity with increasing injection time. We may ascribe this phenomenon to the increase in the aspect ratio of the Ag@Au nanowires during the epitaxial growth. And this increase in the intensity could be owing to the effective separation of localized surface plasmon resonance (LSPR) band from the inter-band transitions and to the expanding volume of nanowires[14]. The varied thickness of the Au shell can also be confirmed by the brighter contrast on the edge of the nanowires shown in TEM images (Figure 2.2B-E), suggesting a local deposition of the heavier Au atoms. High-resolution TEM (HRTEM) image of the

core-shell nanowire (Figure 2.2C) displays that the Au layer was grown on the Ag nanowire surface in a conformal manner with single crystallinity. This uninterrupted lattice fringes from the core to the boundary indicates the epitaxial overgrowth of Au on Ag. This is of vital importance for the stability of the nanowires and the electrical properties as well. Because rough surface within nanoscale can result in a decreased mean free path (λ) and then finally leads to an increased resistance[18]. In addition, the distance between the adjacent lattice fringes in the cores are measured to 0.24 nm for samples, in good agreement with the lattice spacing of the Ag (111) plane, while the lattice distance in the shell was measured to 0.23 nm which in accordance with the lattice spacing of the corresponding Au (111) plane.

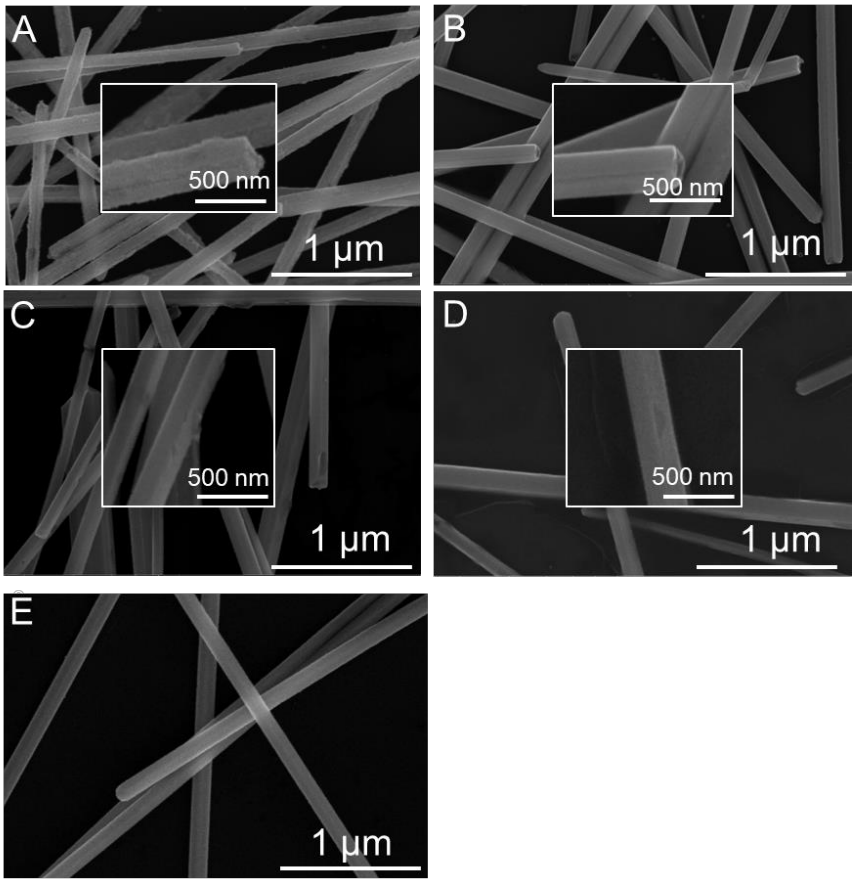

Figure 2.3. The surface morphology of as-prepared Ag@Au nanowires changing with molar ratio of Na_2SO_3 to $HAuCl_4$ with (a) 2:1, (b) 18:1, (c)50:1, (d) 100:1, (e) 150:1. With increasing molar ratio, enough ligand SO_3^{2-} could coordinate to the Au precursor to form highly stable complex and this gold sulfite complex significantly decreased reduction potential of Au and thus galvanic replacement reaction was reliably avoided. When the molar ratio was up to 150:1, highly smooth surfaces of Ag@Au nanowires were found in the final samples, indicating a conformal and uniform deposition of Au on AgNW.

Following the synthesis, we evaluated the chemical stability of the Ag@Au core-shell nanowires by benchmarking against the Ag nanowires in different harsh environment. Our results suggest that with a 3 nm of thickness, the Au nanoshell could be effectively served as barrier to prevent oxidation for AgNWs. Figure 2.4A and Figure 2.4B depicts scanning

electron microscopy (SEM) images of the Ag@Au core-shell nanowire (~3 nm Au) samples, these nanowires are kept intact without any new formed voids or pores even in the air for 183 days. By contrast, Ag NWs without Au protection was oxidized gradually as shown in Figure 2.2C and Figure 2.2D. The results showed AgNWs became severely oxidized which were kept in the ambient condition for only 21 days. It is worth noting that the Ag@Au core-shell nanowires also displayed excellent chemical stability against phosphate-buffered saline (PBS) etching due to the presence of the conformal Au layer (~3 nm Au) on their surfaces (Figure 2.4A), UV-vis extinction spectrum was used to monitor the stability when they were exposed to PBS solution which was commonly used in biological research. It was found that the LSPR peak position and peak intensity remained essentially unchanged in PBS solution for 21 days or longer. Control experiments were carried out for comparison if no Au layer was protected on AgNW surface, the original AgNW sample was gradually destroyed by PBS (Figure 2.4B and its inset) as evidenced by significant shift LSPR peak position and a dramatic decrease in the intensity within a week. It is especially astonishing that the Ag@Au core-shell nanowires (~3 nm Au) are highly stable in H_2O_2 (2%) which is a strong oxidant that can easily destroy pristine AgNWs. The Ag@Au nanowires was kept in H_2O_2 for overnight appeared to be similar in surface morphology to the fresh Ag@Au nanowires without oxidative etching (Figure 2.5E, inset), thus confirming that this decent chemical stability could be against strong etching agents such as H_2O_2. Moreover, no obvious surface morphology change was observed in the UV-vis spectra after etching by H_2O_2 (2%).

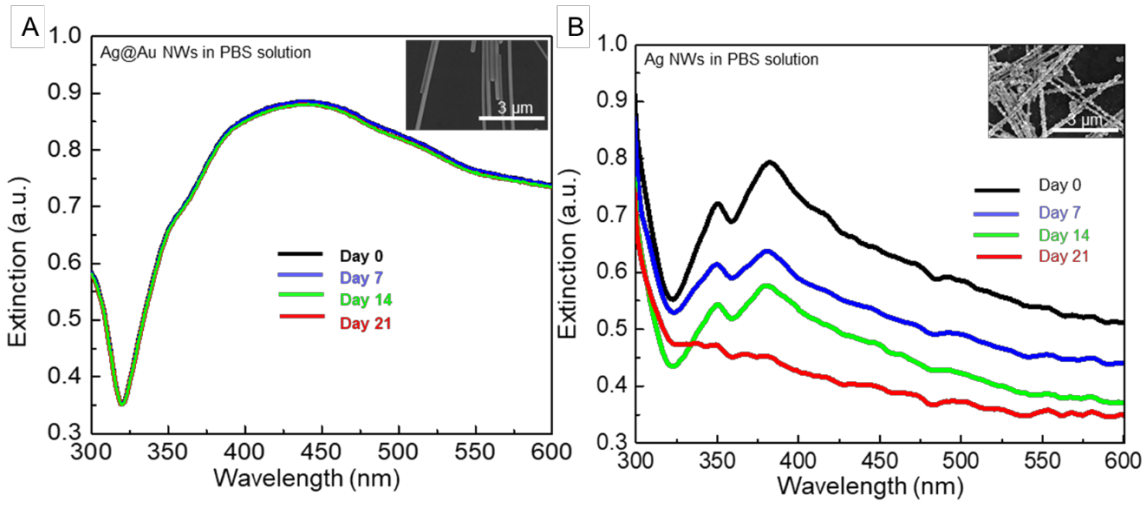

Figure 2.4. Chemical stability of Ag@Au nanowires (~3 nm) in phosphate-buffered saline (PBS) solution. (A) Chemical stability of Ag@Au nanowires (3 nm Au) in a PBS solution detected by UV/vis spectrophotometry. No obvious change could be found in UV-vis measurement even after 21 days in terms of intensity and position. Inset is the SEM image of the Ag@Au nanowires (3 nm Au) kept in PBS solution for 21 days. (B) chemical stability of original Ag nanowires after treatment in PBS solution for 21 days. The peak intensity significantly decayed with time goes by because of the damaged structure etched by PBS. Inset is the SEM image of pristine Ag nanowires kept in PBS solution for 21 days.

Aside from chemical stability, Ag@Au NWs displayed excellent electrical stability as well. This is critical for AgNW-based transparent electrodes because Ag is prone to oxidative deterioration which limits their commercialization. Figure 2.6B shows the optical image and SEM image of the Ag@Au NW based transparent electrode films with different loading amount of nanowires. Figure 2.6A displayed its corresponding transmittance spectra and measured sheet resistance. Moreover, the transparent electrode films displayed outstanding performance in the trade-off between sheet resistance and transparency as plotted in Figure 2.6A. For a transparent conductive film with transmittance of 75%, the sheet resistance is as low as 4.67 Ω/sq. And even the transmittance increases to 95%, the sheet resistance increases only slightly to 37.41 Ω/sq. This feature may be ascribed to high

aspect ratio (L/D) of nanowires. Thick nanowires could block light more efficiently than thin nanowires due to their larger extinction cross-sections. Besides, high L/D can maximize the number of connections between nanowires, which could favor decreasing the sheet resistance. The plot of specular transmittance (%T) versus sheet resistance (R_s) for the AgNW networks was shown in Figure 2.6C, along with some of the best previous literature results. The transparent electrode films made of long, thin Ag@Au NWs has a comparable performance with commercial ITO [19] and a much better performance than other ITO-replacements such as copper nanowire, [20]graphene,[18] carbon nanotube (CNT) [21]and PEDOT[22] in terms of transparency and its corresponding conductivity (see Figure 2.6C). Figure 2.6D depicted the harsh environment aging behavior of the conductive electrode films made from AgNWs and Ag@Au nanowires. The unprotected Ag nanowire film shows a severely conductivity fade. After 4 days of exposure, the sheet resistance increased to several hundred Ω/sq (see Figure 2.6D, inset). The sheet resistance raised to over 20 kΩ/sq for AgNW based electrode film within a week. However, the Ag@Au core-shell nanowire-based electrode film (Figure 2.6C) reported here appear to be much more durable compared with other reports on AgNW-like based electrode film, the Ag@Au NW (~6 nm Au) based electrodes showed no sign of degradation after being exposed to high temperature and high humidity (80 ℃ of temperature, 80% of humidity) even after 7 days. And what is more, the sheet resistance increased by only 25% throughout the whole 84 days of testing. The supreme stability could be mainly attributed to the epitaxial overgrowth of Au on Ag nanowires. This synthesis recipe provides a route to fulfil a complete and uniform deposition of Au atoms on AgNW surface.

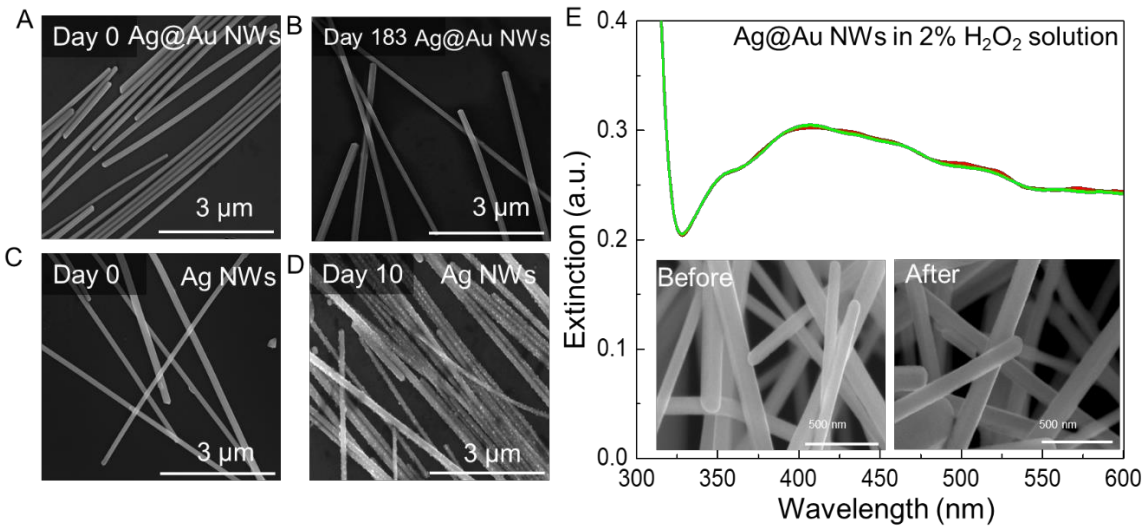

Figure 2.5. Chemical stability of Ag@Au nanowires (3 nm Au) in harsh environment (2% H_2O_2 aqueous solution, and air). (A, B) SEM images of the Ag@Au nanowires (3 nm Au) when exposed to air for 0 and 183 days, respectively. (C, D) SEM images of pristine Ag nanowires when exposed to air for 0 and 10 days, respectively. (E) UV-vis extinction spectrum of Ag@Au nanowires before (red line) and after (green line) immersing with H_2O_2 (2%) for overnight. The inset is the corresponding SEM images of Ag@Au nanowires before (left inset) and after (right inset) etching with H_2O_2 (2%).

Moreover, AgNWs have atomically smooth surface and this can ensure the smaller propagation loss, thus this character makes them of great attractive for nanoscale confinement and guiding of light to nanoscale area.[23] Scattering of plasmons to light was known to occur only on the tip of AgNW, making sure plasmons to be excited at the one end of AgNW and then transmitted with much lower loss to the other end of AgNW. We measured propagation length based on the reported work[24]. Figure 2.7A schematically depicts a dark-field optical image of tapered fiber tip was put in physical contact with nanowire (AgNW or Ag@Au NW) on the PDMS substrate. Figure 2.7B is the corresponding waveguiding image, where the laser (532 nm/671 nm) coupled to the optical

fiber was on, and microscope illumination was off. The image clearly shows that the coupling efficiency between fiber and the nanowire was good enough to allow a tip emission intensity. The nanowire tip emission intensity, which was measured by integrating the total counts of the emission spot, was strongly correlated with the surface plasmon polariton (SPP) propagation distance, which was characterized by the separation between the scattering spot at the nanowire-fiber junction (large white spot on the lower left) and the emission spot at the nanowire tip (small white spot on the upper right). As shown in Figure 2.7C,D, Ag@Au NW (~3 nm Au) only has 4.47% propagation loss compared with pristine Ag nanowire for 671 nm laser excitation while Ag@Au (~3 nm Au) has 69.91% propagation loss for 532 nm laser excitation, this is because Au nanoshell can absorb 543 nm of laser energy which accelerate decreasing propagation length. Both results can also be confirmed by our simulation data (Figure 2.7E, F).

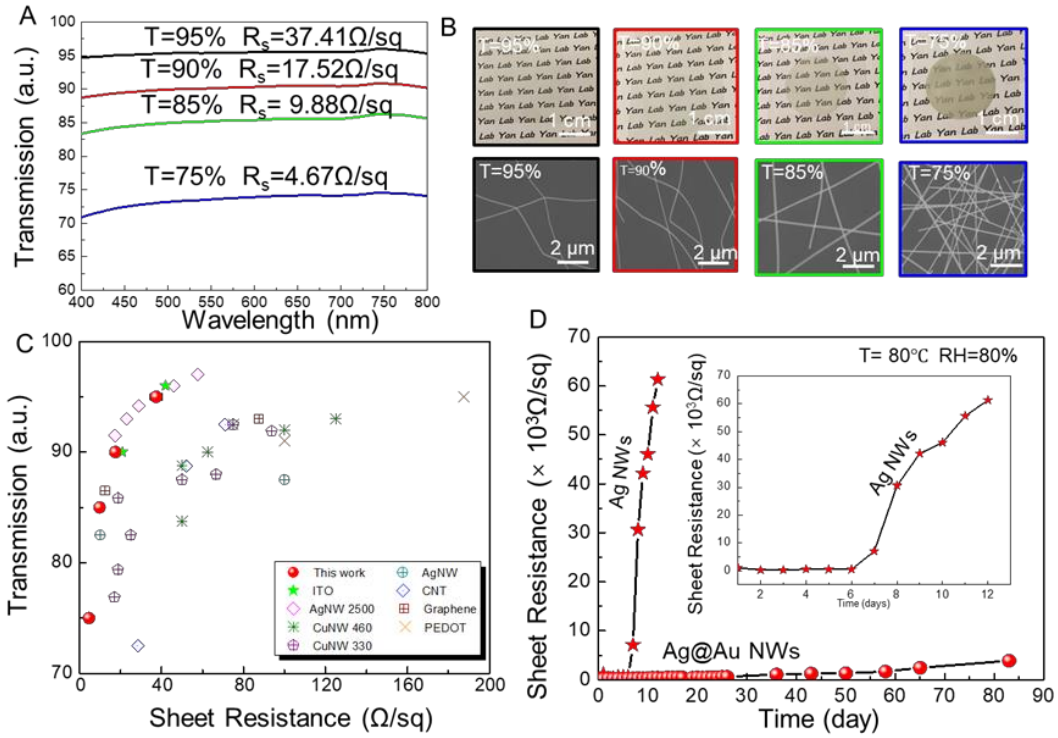

Figure 2.6. Ag@Au core shell nanowire based transparent electrode films and its optical and electrical performance. (A, B) Wavelength-dependent transmittance, sheet resistance, corresponding SEM images and optical images of transparent conductors with increasing Ag@Au Nanowire density (from left to right), Substrate contribution is excluded. (C) Transmission vs. Sheet resistance of Ag@Au nanowire network. comparison data are shown representing current state of art transparent conductors, including ITO, carbon nanotubes (CNT, L/D=1600), PEDOT, Ag nanowires (L/D=2500) and Cu nanowires (L/D=330, 460). (D) Long term stability of Ag@Au core-shell nanowire (~3 nm Au) and Ag nanowire mesh films in high temperature environment (temperature=80℃, relative humidity=80%).

Our results also showed that the thin Au coating does not have adverse effects on the coupling of surface plasmon polariton in AgNW waveguides, and the device performance is stable in air for at least 21 days. As shown in Figure 2.8A and Figure 2.8F, we attached one single AgNW and Ag@Au NW to a tapered optic fiber separately and then guided laser light form optic fiber to nanowire tip and measured the coupling efficiency over a time

period. It is found that the laser light propagates from the optic fiber into Ag@Au NW and the maximum output was observed on the end of the nanowire, indicating that almost all of the laser light was coupled into nanowire end without scattering loss and no obvious coupling loss was found even after 21 days (Figure 2.8G-J), which means optical coupling efficiency is still retained almost 100% over time and this can be accredited to the protective Au layer on AgNW surface. As a contrast, AgNW was used as a control experiment (Figure 2.8B-E), If no Au protection was present, the evident light scattering loss was found only after 7 days and became severely worse with over time, this should be ascribed to the severe oxidation of AgNW surface in the air over time, and thereby results in a lower and worse coupling efficiency of the AgNW probe with time goes by, which was in accordance with the analysis illuminated above.

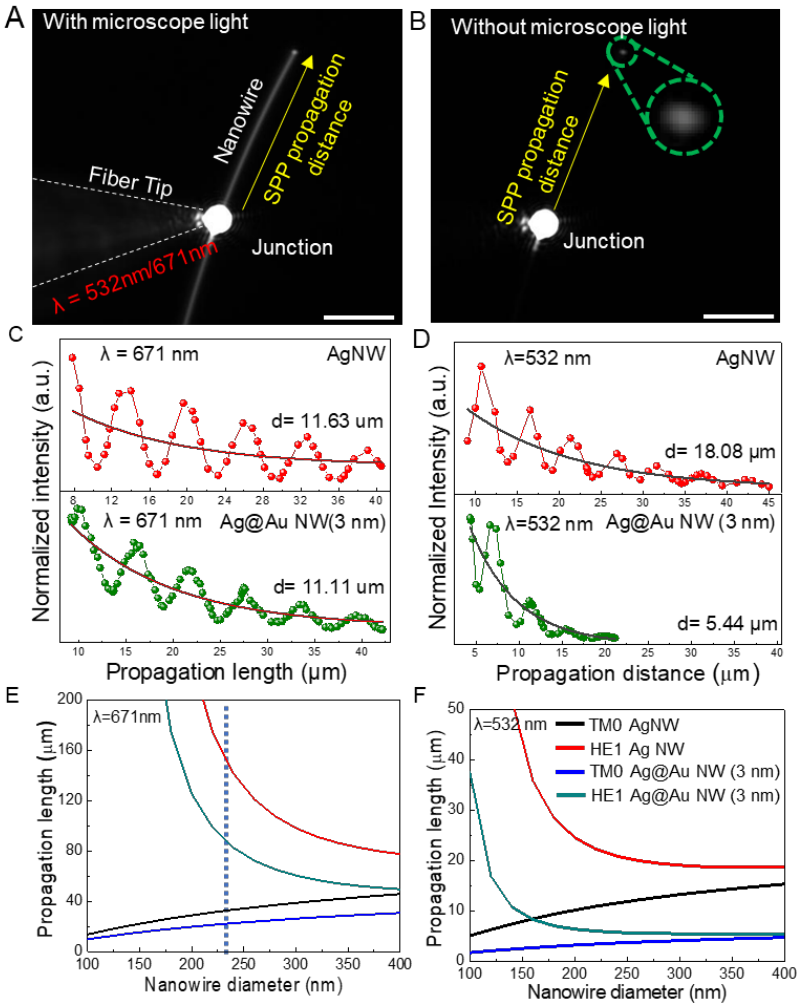

Figure 2.7. Measurement of the SPP propagation length in a free-standing nanowire (Ag nanowire or Ag@Au nanowire (~3 nm Au)). (A) Dark-field optical image of the measurement setup. A nanowire was placed on a PDMS substrate. The tapered tip of a laser-coupled optical fiber was put into physical contact with the nanowire to excite its SPPs. The SPPs propagated along the nanowire to its distal end, where they were scattered back into free space. The far-field emission at the suspended Ag nanowire tip was collected as the optical fiber tip was slid along the nanowire. (B) Waveguide images (back illumination off, laser on) of the nanowire at specific SPP propagation distances. Insets: enlarged images of the tip emission spot. (C, D) Tip emission intensity measured as a function of x under 671 nm (c: top is Ag nanowire while bottom is Ag@Au nanowire (~3 nm Au)) and 532 nm (d: top is Ag nanowire while bottom is Ag@Au nanowire (3 nm Au)) excitation. (E, F) simulation study about the relationship between nanowire diameter and propagation length under 671 nm (E) and 532 nm (F) wavelength of laser. All scale bars are 200 μm. Note: the diameter of nanowire used in this experiment is about 250 nm.

Not even this, Ag nanostructures are widely used as a surface-enhanced Raman scattering (SERS) substrate due to their better performance of surface plasmon resonance (SPR) compared with traditional metallic materials. AgNWs can be used as an ideal SERS substrate for large-scale sensing application. However, Ag is susceptible to oxidation damage which greatly shorten its lifetime. The Ag@Au nanowires (3 nm Au) can not only enhanced the stability but also are closely equivalent to Ag nanowire in SPR property. This can be proved by Raman spectrum measured on single Ag nanowire (Ag@Au nanowire (3 nm Au)) functionalized with 4-ATP (4-aminothiophenol) (the top is Ag nanowire while the bottom is Ag@Au nanowire (3 nm Au)). Generally, Au has fluorescence at about 520 nm. However, no obvious fluorescence peak found in the Raman spectra. This can be ascribed to the thin Au layer grown on AgNW surface. In addition, the Ag@Au nanowires (~3 nm Au) exhibit a similar surface enhanced Raman spectra (SERS) performance like pristine AgNWs, which confirms that the epitaxial ultra-thin Au coating on AgNW offers a promising way to protect Ag nanowires from degradation without compromising device performance.

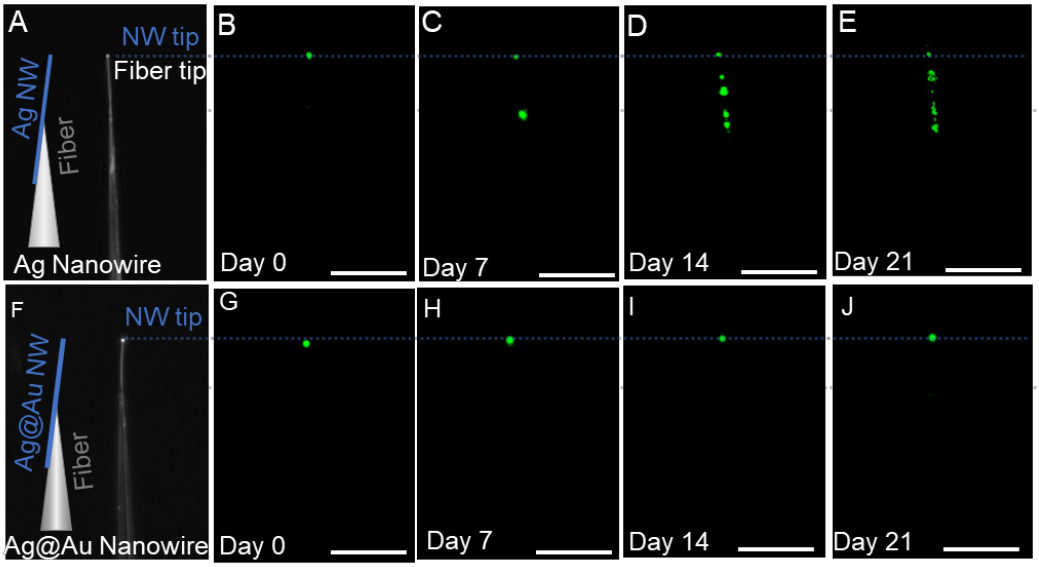

Figure 2.8. Coupling point of nanowire (Ag nanowire, Ag@Au nanowire (~3 nm Au)). (A) Dark field optic image of tapered optic fiber/Ag nanowire probe, (B-E) Coupling point of Ag nanowire when optical fiber/AgNW probe was kept in the air for 0, 7, 14 and 21 days, respectively. (F) Dark field optic image of tapered optic fiber/Ag@Au nanowire (3 nm Au) probe. (G-J) Coupling point of Ag@Au core-shell nanowire when optical fiber/Ag@Au nanowire probe was kept in the air for 0, 7, 14 and 21 days, respectively.

Beyond demonstrating optoelectronic performance of the Ag@Au nanowire, there is a real lack of information in the literature concerning the mechanical property of Ag nanowire. In our previous work,[25-26] AgNW based AFM probe was used for high-aspect-ratio high resolution imaging via improved mechanical performance and tunability of tip morphology. However, the vulnerability to oxidation for AgNW lead to a shorter lifetime. Ag@Au NWs with conformal, epitaxial ultra-thin Au coating layer reported here can help avoid this concern. The Ag@Au nanowire-based AFM probe shown in Figure 2.9A was fabricated based on our previous work [9]. Figure 2.9B and Figure 2.8 represents the tapping mode scanning images obtained with the Ag@Au based AFM probe, corresponding to the height,

magnitude and phase images measured from the same area of the sample, respectively. It is worth noting that high quality image could still be obtained when scanned with the Ag@Au nanowire-based AFM probe which was kept in the air for 21 days, confirming the good image reproducibility and high stability of using Ag@Au nanowire-based probes. To illustrate it more convincingly, An AgNW based AFM probe was prepared for comparison. If no protection provided by the Au shell was present, the quality of AFM image decayed gradually and became severely worse when the AgNW was kept in the air after 21 days as shown in the Figure 2.9C. This can be explained by the fact that the AgNW based AFM probe was significantly oxidized and thus the nanowire tip became fragile and easily die.

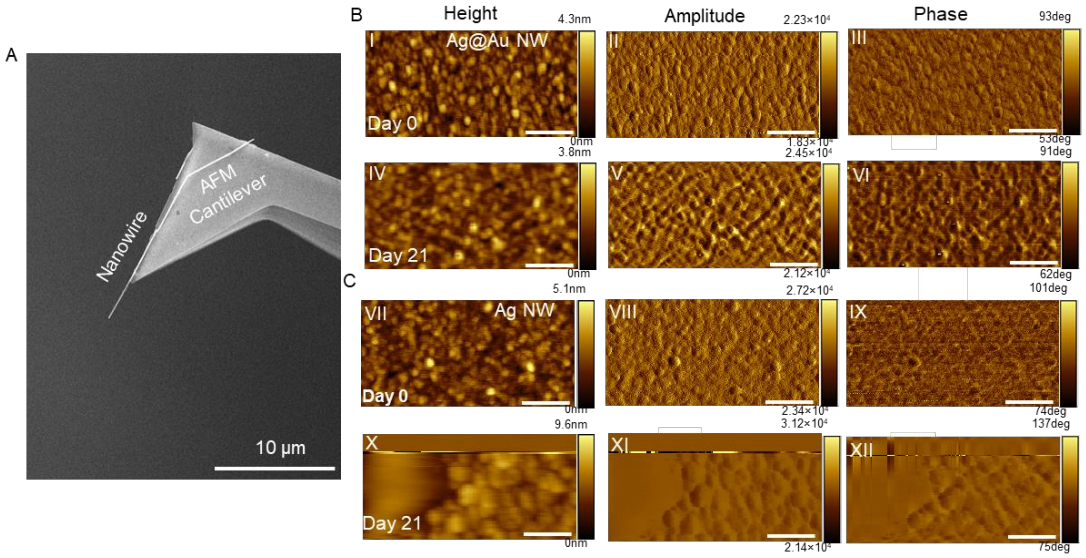

Figure 2.9. Tapping mode AFM topography images of a gold film with 40 nm thickness prepared by electron beam thermal deposition on a quartz substrate. (A) SEM image of nanowire-based AFM probe (B) AFM image scanned by Ag@Au nanowire (3 nm Au) based probe. (I, II, III) are Height, Amplitude, Phase imaging scanned by Ag@Au NW based probe which was kept in the air for 0 day. (IV, V, VI) are Height, Amplitude, Phase imaging obtained by Ag@Au NW based probe which was kept in the air for 21 days. (C) AFM image scanned by Ag nanowire-based probe. (VII, VIII, IX) are Height, Amplitude, Phase imaging scanned by AgNW based probe, which was kept in the air for 0 day, respectively. (X, XI, XII) are Height, Amplitude, Phase imaging scanned by AgNW based probe, which was kept in the air for 21 days, respectively. All scale bars are 200nm.

2.2. Conclusion

In summary, we have demonstrated a single-step, solution-phase, galvanic-replacement-free, epitaxial deposition technique to grow an ultra-thin, single-crystalline and atomically smooth layer of Au on AgNW surface, which acts as a reliable and economical anti-oxidation barrier to provide long-term device stability. This versatile recipe can make it to preparing core-shell nanostructures with tunable Au shell thickness and this conformal and complete coverage of Au shell could be served as a barrier for oxidation damage without severely sacrificing the intrinsic property of Ag nanostructure. By solving the long-standing stability issue, this project will facilitate the realization of the full commercial potential of AgNWs. It will inspire those novel flexible optoelectronic devices that are based on AgNWs, such as foldable displays, E-textiles, digital clothing, smart-glasses, 3D-shaped touch-sensing surfaces, wearable electronic sensors for safety and healthy living.

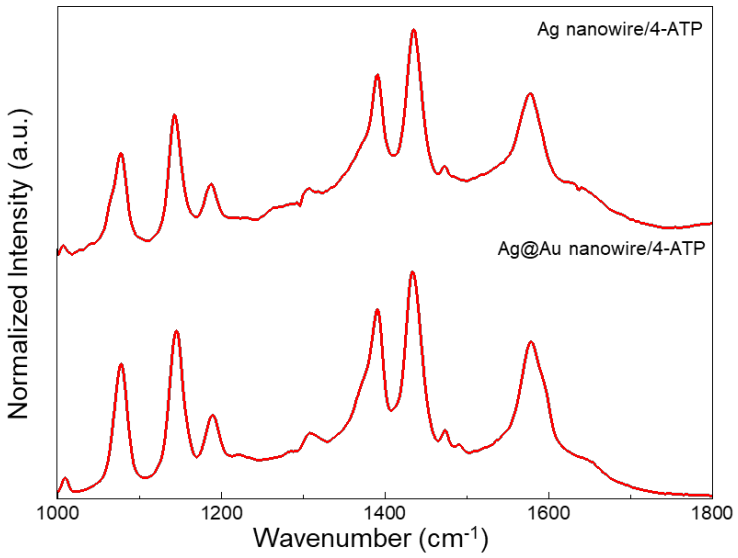

Figure 2.10. Raman spectra recorded from the 4-ATP-functionalized Ag nanowires and Ag@Au nanowires (~3 nm Au), respectively. Silicon was used as the substrate in this experiment.

Reference

1. Lee, W. J.; Lee, M. Y.; Roy, A. K.; Lee, K. S.; Park, S. Y.; In, I., Poly(dimethylsiloxane)-protected Silver Nanowire Network for Transparent Conductor with Enhanced Oxidation Resistance and Adhesion Properties. *Chemistry Letters* **2013,** *42* (2), 191-193.

2. Ma, J.; Zhan, M.; Wang, K., Ultralightweight silver nanowires hybrid polyimide composite foams for high-performance electromagnetic interference shielding. *ACS Appl Mater Interfaces* **2015,** *7* (1), 563-76.

3. Meenakshi, P.; Karthick, R.; Selvaraj, M.; Ramu, S., Investigations on reduced graphene oxide film embedded with silver nanowire as a transparent conducting electrode. *Solar Energy Materials and Solar Cells* **2014,** *128*, 264-269.

4. Eom, H.; Lee, J.; Pichitpajongkit, A.; Amjadi, M.; Jeong, J. H.; Lee, E.; Lee, J. Y.; Park, I., Ag@Ni core-shell nanowire network for robust transparent electrodes against oxidation and sulfurization. *Small* **2014,** *10* (20), 4171-81.

5. Zhu, Y.; Li, X.; He, G.; Qi, X., Magnetic C-C@Fe3O4 double-shelled hollow microspheres via aerosol-based Fe3O4@C-SiO2 core-shell particles. *Chem Commun (Camb)* **2015,** *51* (14), 2991-4.

6. Amjadi, M.; Pichitpajongkit, A.; Lee, S.; Ryu, S.; Park, I., Highly Stretchable and Sensitive Strain Sensor Based on Silver Nanowire–Elastomer Nanocomposite. *ACS nano* **2014,** *8* (5), 5154-5163.

7. Mao, C.-J.; Chen, X.-B.; Niu, H.-L.; Song, J.-M.; Zhang, S.-Y.; Cui, R.-J., A novel enzymatic hydrogen peroxide biosensor based on Ag/C nanocables. *Biosensors and Bioelectronics* **2012,** *31* (1), 544-547.

8. Multifunctional TiO2-coated Ag nanowire arrays as recyclable SERS substrates for the detection of organic pollutants. *Eur. J. Inorg. Chem.* **2012,** *2012*, 3176.

9. Ma, X.; Zhu, Y.; Kim, S.; Liu, Q.; Byrley, P.; Wei, Y.; Zhang, J.; Jiang, K.; Fan, S.; Yan, R.; Liu, M., Sharp-Tip Silver Nanowires Mounted on Cantilevers for High-Aspect-Ratio High-Resolution Imaging. *Nano Letters* **2016,** *16* (11), 6896-6902.

10. Yang, M.; Hood, Z. D.; Yang, X.; Chi, M.; Xia, Y., Facile synthesis of Ag@Au core-sheath nanowires with greatly improved stability against oxidation. *Chem Commun (Camb)* **2017,** *53* (12), 1965-1968.

11. Au, L.; Lu, X.; Xia, Y., A Comparative Study of Galvanic Replacement Reactions Involving Ag Nanocubes and AuCl(2) or AuCl(4). *Adv Mater* **2008,** *20* (13), 2517-2522.

12. Yang, Y.; Zhang, Q.; Fu, Z. W.; Qin, D., Transformation of Ag nanocubes into Ag-Au hollow nanostructures with enriched Ag contents to improve SERS activity and chemical stability. *ACS Appl Mater Interfaces* **2014,** *6* (5), 3750-7.

13. Gao, C.; Lu, Z.; Liu, Y.; Zhang, Q.; Chi, M.; Cheng, Q.; Yin, Y., Highly stable silver nanoplates for surface plasmon resonance biosensing. *Angew Chem Int Ed Engl* **2012,** *51* (23), 5629-33.

14. Liu, H.; Liu, T.; Zhang, L.; Han, L.; Gao, C.; Yin, Y., Etching-Free Epitaxial Growth of Gold on Silver Nanostructures for High Chemical Stability and Plasmonic Activity. *Advanced Functional Materials* **2015,** *25* (34), 5435-5443.

15. Cobley, C. M.; Campbell, D. J.; Xia, Y., Tailoring the Optical and Catalytic Properties of Gold-Silver Nanoboxes and Nanocages by Introducing Palladium. *Adv Mater* **2008,** *20* (4), 748-752.

16. Gao , C.; Lu , Z.; Liu , Y.; Zhang, Q.; Chi, M.; Cheng, Q.; Yin, Y., Highly Stable Silver Nanoplates for Surface Plasmon Resonance Biosensing. **2012,** *51* (23), 5629-5633.

17. da Silva, R. R.; Yang, M.; Choi, S. I.; Chi, M.; Luo, M.; Zhang, C.; Li, Z. Y.; Camargo, P. H.; Ribeiro, S. J.; Xia, Y., Facile Synthesis of Sub-20 nm Silver Nanowires through a Bromide-Mediated Polyol Method. *ACS Nano* **2016,** *10* (8), 7892-900.

18. Xia, F.; Perebeinos, V.; Lin, Y. M.; Wu, Y.; Avouris, P., The origins and limits of metal-graphene junction resistance. *Nat Nanotechnol* **2011,** *6* (3), 179-84.

19. Ye, S.; Rathmell, A. R.; Stewart, I. E.; Ha, Y. C.; Wilson, A. R.; Chen, Z.; Wiley, B. J., A rapid synthesis of high aspect ratio copper nanowires for high-performance transparent conducting films. *Chem Commun (Camb)* **2014,** *50* (20), 2562-4.

20. Rathmell, A. R.; Wiley, B. J., The Synthesis and Coating of Long, Thin Copper Nanowires to Make Flexible, Transparent Conducting Films on Plastic Substrates. *Advanced Materials* **2011,** *23* (41), 4798-4803.

21. Hecht, D. S.; Heintz, A. M.; Lee, R.; Hu, L.; Moore, B.; Cucksey, C.; Risser, S., High conductivity transparent carbon nanotube films deposited from superacid. *Nanotechnology* **2011,** *22* (7), 075201.

22. Ye, S.; Rathmell, A. R.; Chen, Z.; Stewart, I. E.; Wiley, B. J., Metal nanowire networks: the next generation of transparent conductors. *Adv Mater* **2014,** *26* (39), 6670-87.

23. Pyayt, A. L.; Wiley, B.; Xia, Y.; Chen, A.; Dalton, L., Integration of photonic and silver nanowire plasmonic waveguides. *Nat Nanotechnol* **2008,** *3* (11), 660-5.

24. Kim, S.; Bailey, S.; Liu, M.; Yan, R., Decoupling co-existing surface plasmon polariton (SPP) modes in a nanowire plasmonic waveguide for quantitative mode analysis. *Nano Research* **2017,** *10* (7), 2395-2404.

25. Ma, X.; Zhu, Y.; Kim, S.; Liu, Q.; Byrley, P.; Wei, Y.; Zhang, J.; Jiang, K.; Fan, S.; Yan, R.; Liu, M., Sharp-Tip Silver Nanowires Mounted on Cantilevers for High-Aspect-Ratio High-Resolution Imaging. *Nano Lett* **2016,** *16* (11), 6896-6902.

26. Ma, X.; Zhu, Y.; Yu, N.; Kim, S.; Liu, Q.; Apontti, L.; Xu, D.; Yan, R.; Liu, M., Toward high-contrast AFM-TERS imaging: nano-antenna-mediated remote-excitation on sharp-tip silver nanowire probes. *Nano Lett* **2018**.

Chapter 3. Tailoring the scalable aqueous synthesis of copper@reduced graphene oxide core-shell nanowires for flexible transparent electrodes

3.1. Introduction

So far, great efforts have been to prepare HARCuNWs. Cui et al. prepared CuNWs with 997 of aspect ratio (~17 μm long; ~20 nm wide) with the oleylamine-mediated approach, However, this synthesis is time-consuming (~10 h) and costly, because of high operation temperature (~165) and using highly expensive organic chemical (tris(trimethylsily)silane).[17] Ye et al. increased the aspect ratio up to 2280 (80 μm long and 35 nm wide) by modifying the ethylenediamine-mediated synthesis. However, the yield of CuNWs is restively low in the final resulted sample and the reducing agent (N_2H_4) used in this recipe was highly toxic that is not environmentally friendly.[19] As a result, there is an ongoing drive to find an economical, green chemistry, scalable route to prepare HARCuNWs with high yield.

Therefore, there is an on-going drive to replace ITO with a flexible material that gives comparable performance. Over the last decade, different ITO alternatives, including conducting polymers, carbon nanotubes, graphene and metal nanowires, were extensively studied. However, by far, metal nanowire especially for silver nanowire (AgNW) networks are the dominant alternative that can provide comparable or better performance to ITO, while being processable with low-cost, scalable solution-phase synthesis techniques[14-15]. And recently, high aspect ratio silver nanowires (AgNWs) have been synthesized and they

have been already demonstrated superior levels of performance for transparent electrodes[6]. However, Ag is a noble metal on the earth and thus the cost is too high to limit its further commercialization.

Motivated by the balance between the cost and electrode performance, copper nanowires (CuNWs) are an attractive replacement to Ag. Copper (Cu) is known as 1000 times more abundant than silver or 22000 times abundant more than gold and copper has the second-best intrinsic conductivity and only 6% less conductive than silver while 30% more conductive than gold (Au)[16-17]. Meanwhile, Cu is much cheaper than Ag or indium by 100 times. And high aspect ratio CuNW could provide comparable ITO levels of electrode performance at a lower cost which was demonstrated in the previous work[15]. However, the long-term stability limits the commercial application of CuNW networks. Because CuNWs are prone to oxidative deterioration and therefore it requires surface protection to avoid atmospheric corrosion. To address this challenge, several approached have been conducted and they can be concluded into two solutions: one is to employ an overcoating layer on the CuNWs as a corrosion barrier such as atomic layer deposition (ALD) layer of aluminum-doped zinc oxide and aluminum oxide (Al_2O_3)[18]; the other is to grow a layer of a conductive yet chemically stable shell on the CuNW surface like Zn[19-20], Sn[20], Pt[21], Ni[22], Ag[21] and Au[16, 23-24]. Although both methods could indeed improve the chemical stability to some extent, either the fabrication cost furtherly increased or the transparency (the conductivity) severely decreased. Graphene is known to have remarkable in-plane stiffness to prevent mechanical deformation, impermeability to prevent Cu from exposed chemical or Oxygen-like gaseous species[25-26]. These properties make graphene a noninteracting barrier for

CuNWs to prevent oxidation. So recently, coating graphene on CuNWs have been employed to fix this issue. Yumi Ahn, et al first applied plasma-enhanced chemical vapor deposition (PECVD) method (at 400℃) to grow the thin graphene layer on the CuNWs[25]. However, this procedure is not scalable via the low-cost high-throughput production which limit its practical applications. Letian Dou, et al demonstrated a new solution-based recipe to wrap GO nanosheets on CuNW surface, and then GO was reduced to form Cu@rGO core-shell nanowires[27]. The facile route could significantly decrease the fabrication cost compared with the PECVD method.

Herein, we modified this solution-processed technique to wrap GO layer on the high aspect ratio CuNW that we prepared in our previous work, GO layer coating thickness could be tuned by controlling the mass ratio of CuNW and GO. With the optimum coating thickness (6 nm), we then fabricated flexible transparent electrode films using this nanowire solution which display excellent conductivity and chemical stability toward oxidation. Moreover, the transparent films also show good flexibility even after the bending or stretching test for 1000 cycles. This is the first time to report a systematic study of exploring the relationship between the GO layer coating thickness and sheet resistance via solution-based GO wrapping method and testing the flexibility performance of transparent electrode films prepared with the optimized Cu@rGO core-shell nanowires.

3.2 Results and Discussion

Figure 1 shows an illustration of the wrapping strategy of GO coating on CuNW surface. The CuNWs with a high aspect ratio (L/D=2738) were prepared using our recently pH-tuned method. to achieve uniform surface coating, GO nanosheets with an average of several hundred nanometers were synthesized (see Figure 1d) based on modified hummer method. The as-synthesized CuNWs were dispersed in toluene solution (Figure 1g, Middle), and as-prepared GO nanosheets were kept in DI-water (Figure1g, Left). Then the mixing and wrapping process occur effectively in methanol with ultrasonication, and the high-quality Cu@GO nanowire can be formed subsequently (see figure 1g, Right). This coating mechanism could be attributed to the fact that the thin native oxide layer (2-3nm) on CuNW surface, which was confirmed in Figure S1, could have a strong interaction with hydroxyl and carboxyl groups. Since GO is highly oxidized, it could be served as an effective ligand and interacts much stronger with the oxide surface of CuNWs. The scanning electron microscopy (SEM) image (Figure 1h) shows the resulted Cu@GO NWs with scalable synthesis and Cu-like morphology, and the transmission electron microscopy (TEM) image (Figure 1i) displays a uniform and smooth coating of GO layer on CuNW surface. Figure 2 shows the structure characterization and performance evaluation of the as-prepared Cu@GO nanowires with different GO coating thickness. Figure 2d-f show the TEM image of different GO coating thickness, it can bee seen that a layer of GO with average thickness of 3.3nm, 5.9nm and 11.9nm have been coated uniformly along the CuNW surface separately. They all show a very clear interface between crystalline Cu and amorphous GO layer. Furthermore. The energy-dispersive X-ray spectroscopy (EDS)

mapping on a single wire confirms the proposed core-shell structure. As shown in Figure 2g-k, Cu exists only in the core of the nanowire while carbon and oxygen form a uniform thicker shell around the sides of CuNW. Overall, these results indicate that the GO layer could be homogeneously coated onto the high aspect ratio CuNW surface without changing the morphology of CuNWs.

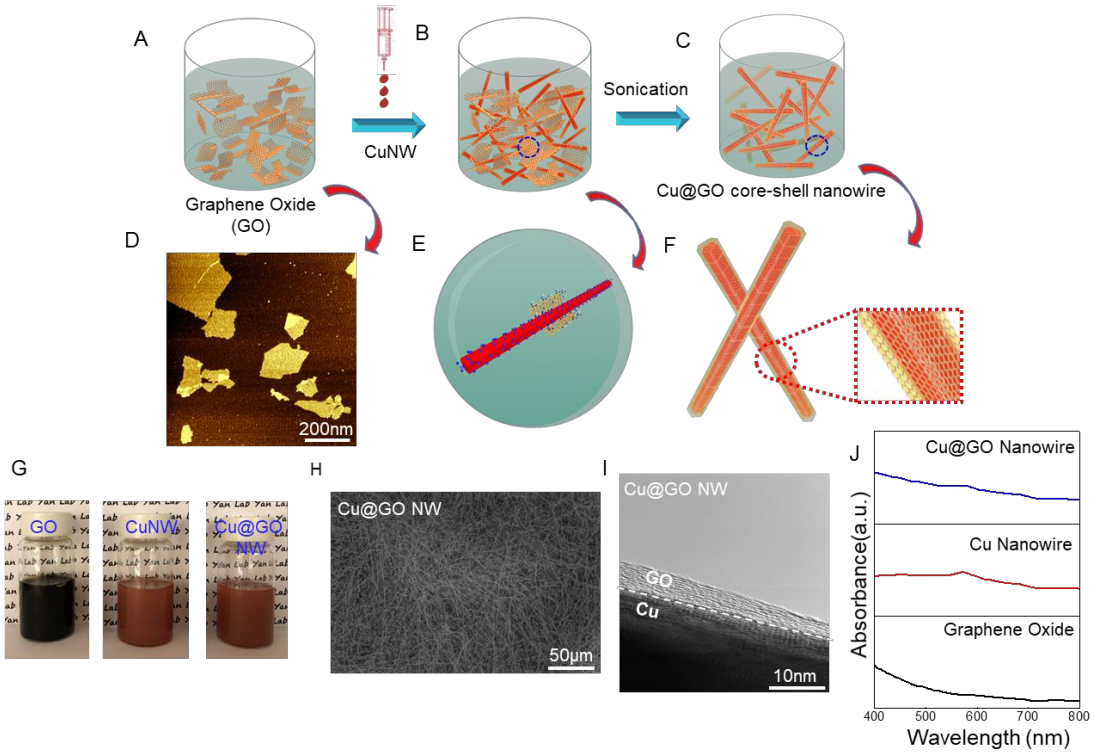

Figure 3.1. Schematic illustration for the development of solution-processed Cu@GO core-shell nanowires. (A) GO nanosheet aqueous solution was homogeneously dispersed into methanol solution. (B) CuNW toluene solution was added to this diluted GO solution with stirring. (C) The mixture was sonicated for several minutes to form the Cu@GO core–shell nanowires. (D) Atomic force image (AFM) images of as-grown graphene oxide nanosheet. (E) The magnified view of graphene oxide nanosheets wrapped on Cu nanowire surface during sonication. (F) The zoomed in image of Cu@GO core-shell nanowires. (G) Digital images displaying GO nanosheet solution (in DI water), pristine Cu nanowire solution (in ethanol), as-grown Cu@GO nanowire solution (in isopropyl alcohol (IPA)). (H) Low magnification SEM image of Cu@GO NW samples. (I). High Magnification TEM image of Cu@GO NW which confirms a very uniform GO layer coated on CuNW surface. (J) UV-vis spectra of graphene oxide, Cu Nanowire, Cu@GO nanowire.

Having demonstrated the ability to form the core-shell nanostructures of Cu@GO NW, we fabricated flexible transparent electrode films with the core-shell nanowires via vacuum filtration method. The schematic of the fabrication process can be found in Figure 3.5, a dilute solution of Cu@GO nanowires in isopropyl alcohol was vacuum filtered onto polytetrafluoroethylene porous membrane (pore size 450nm) and then the nanowire network was transferred onto polyethylene terephthalate (PET) substrate by applying pressure to the backside of filter membrane and forcing an intimate contact with the PET substrate. Followed then, the Cu@GO NW film was annealed under forming gas to reduce GO to rGO, remove copper oxides and create an intimate contact junction between overlapping nanowires. In order to improve the performance of transparent electrode films, we annealed the films at different annealing temperature. As shown in Figure 3.6, an increased sheet resistance was approached when annealed below 200℃, this may because GO cannot be thermally reduced at this lower temperature, and therefore the insulating layer stops efficient electron transfer from nanowire network. A significantly decreased sheet resistance was found when the annealing temperature increased to 280℃ while the sheet resistance increased dramatically due to the damage of Cu@GO nanowires. Figure S4 shows the SEM images of the films annealed at different temperature. The nanowire morphology is well kept below 280℃. At 320℃, the nanowires start to melt. At even higher temperature of 360℃, all the nanowires melt and lose the initial morphology. Thereby the optimal annealing temperature was set to 280℃. Under this condition, the GO nanosheets can be thermally reduced to form rGO, as confirmed by the color of samples and the XRD measurement. The XRD result shows a peak shifted from 10° to 23°,

indicating the π-π stacking distance decreased from 1.0nm to 0.4nm due to the removal of C=O ad OH groups on GO. Based on this optimal recipe, the Cu@rGO nanowire-based electrode films show enhanced performance than with CuNW based films without rGO coating in terms of sheet resistance and transparency (see Figure 3.2A). The sheet resistance of Cu@rGO NW (3nm and 6nm of GO layer coating thickness) based electrode films show a better conductivity than the uncoated CuNW based films. The improvement can be attributed to the following facts. First, the thin GO coating layer improves the junction and electric conduction from nanowire to nanowire. the nanowire was picked up by using our previously reported method to put in the gap between two separate gold electrodes. According to the results, the junction resistance was found to obviously decrease after a thin GO coating on nanowire surface, which means that like the graphene coated CuNWs, the rGO coating also improve the electric conductivity of the single junction of NW itself. Second, the CuNWs with thin GO coated nanoshell form a more homogeneously dispersion, indicating less aggregation for Cu@rGO nanowire samples. Therefore, during filtration, fewer large bundles form compared with the pristine CuNW samples. Figure 3.2C shows a plot of transmittance versus sheet resistance for the Cu@rGO nanowire network, along with some of the best previous reference results. The high aspect ratio Cu@rGO nanowire (6 nm) network exhibit excellent conductivity and transparency: sheet resistance of at transmission of , sheet resistance of at transmission of , sheet resistance of at transmission of , sheet resistance of at transmission of were achieved, which close to the commercial ITO or AgNW electrode films (green star and blue-white hexagon in Figure 3.2C).

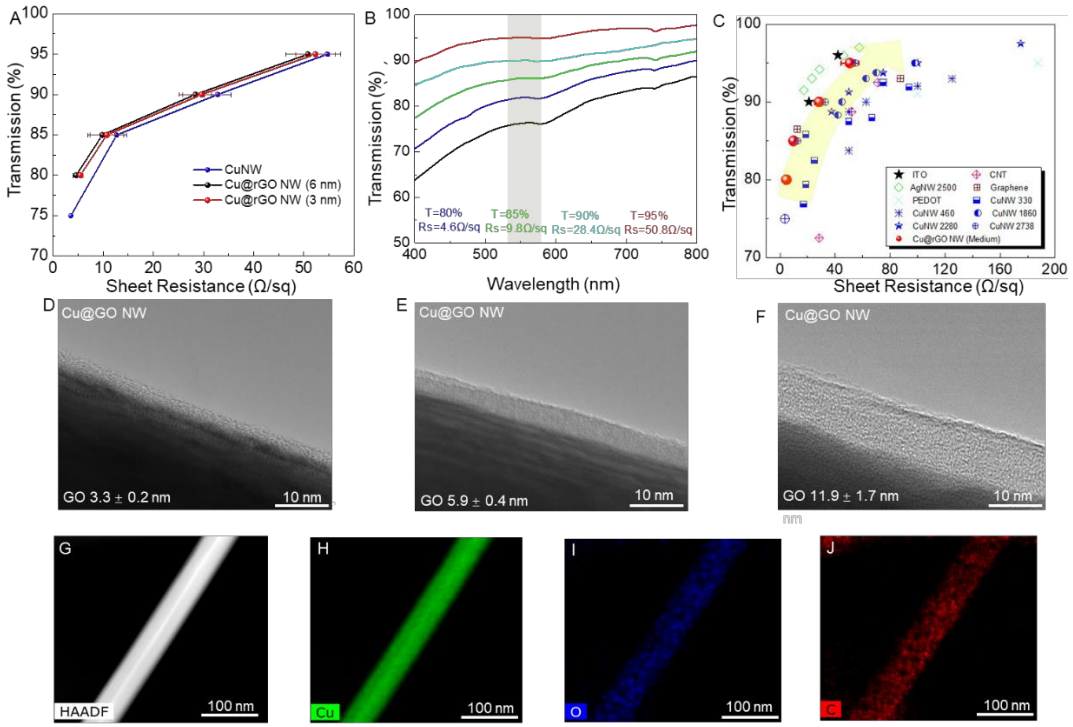

Figure 3.2. Structure characterization of the Cu@GO core-shell nanowires. (A) Transmittance versus the sheet resistance of types of films (CuNW, Cu@rGO NW (~3.3 nm), Cu@rGO NW (~6 nm), Cu@rGO NW (~11.9 nm)). (B) Transmittance spectra of the film from UV-vis device). (C) Transmittance vs. Sheet resistance of Cu@rGO NW networks based on high aspect ratio CuNW reported in our previous work. Comparison data was also shown representing current progress of the transparent conductors, including CuNWs (L/D=330,460,1860,2280), carbon nanotube, AgNW(L/D=2500), Graphene, Graphene, PEDOT, ITO. (D-F). TEM image of the Cu@GO core-shell nanowire with different coating thickness (GO= ~3.3 nm, 5.9nm, 11.9 nm). (G-J) EDS analysis of a core-shell nanowire showing the elemental distribution of copper, oxygen and carbon that reconfirm a uniform GO coating on CuNW surface.

The stability performance of Cu@rGO nanowire electrode films was evaluated in the air or even in high temperature with high relative humidity (80°C,80% of RH). Two types of electrode films (CuNW and Cu@rGO nanowire samples were recorded and the results were shown in Figure 3.5A, B. The CuNW film show poor stability than Cu@rGO NW (6 nm) film, and the sheet resistance hugely increased within 30 days and became even worse

after then in the air environment. In comparison, the rGO coated CuNW samples display excellent stability and no obvious degradation was found up to 362 days, indicating rGO shell do act as an effective barrier to prevent CuNW oxidation. Furthermore, in order to accelerate the oxidation, we also tested the long-term stability for CuNW and Cu@rGO NW samples in high temperature and high humidity (80℃,80% of RH). Figure 3.5A shows the results that the sheet resistance of CuNW sample hugely increased within few hours and no conductivity was tracked only after 122h at 80℃ of temperature with 80% of relative humidity. However, the Cu@rGO nanowire sample can keep stable without obvious degradation even after 600h at the same environment, this improvement is probably due to the completely coated rGO nanoshell could stop oxygen from diffusing to etch the copper core.

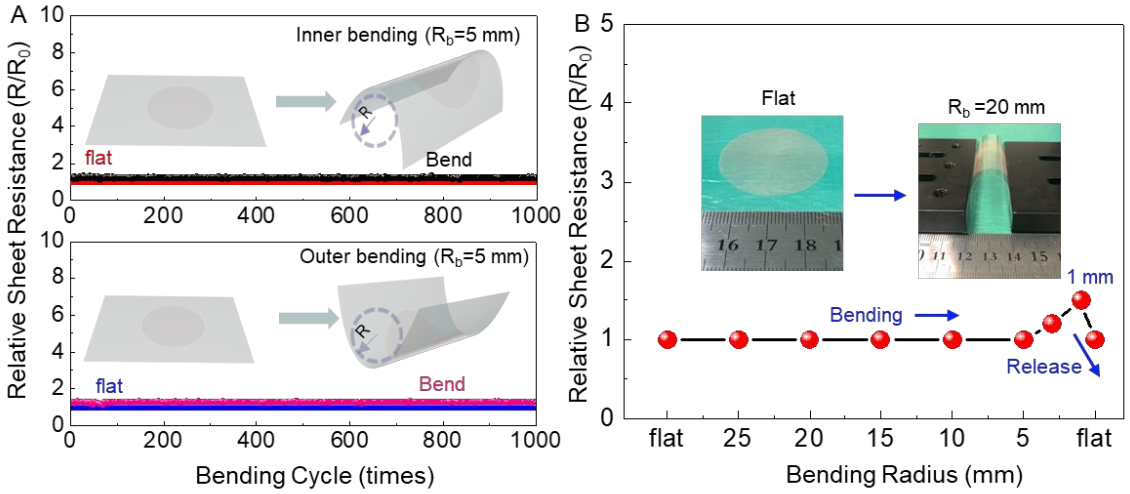

Figure 3.3. Conductivity performance of CuNW conductive film upon mechanical deformation (Bending). (a) Electrical- resistance change of a CuNW based electrode film when bending to a 5 mm of bending radius (Inner & outer bending) and then strengthening each cycle. The resistance becomes stable after several cycles. The inset shows the bending process. (b) Conductivity variation of electrode film at a bending radius up to 1 mm in the first cycle. The inset shows the digital images of flat and bended conducive film (PET as a substrate). The transmittance in this electrode film is 80% for all the films. R_0 refers to electrical resistance of the pristine electrode film.

Flexibility is another vital parameter that evaluate the quality of flexible transparent electrode films.

We then transferred the nanowire network onto flexible polydimethylsiloxane (PDMS) substrate with vacuum filtration recipe mentioned above. The electrical resistance shows a slightly increase up to a bending radius of 1mm and can perfectly recover after straightening (Figure 3.3B). Regardless of the bending mode (Inner & outer bending), only less than 10% of increased sheet resistance was achieved even after 1000cycles of bending when bending radius was fix to 5mm. Figure 3.3A shows the outer/inner bending tests of

transparent electrode film prepared with Cu@rGO nanowire sample. The relative resistance of the test samples can be expressed as R/R0, where R0 is the initial measured sheet resistance and R is the measured resistance after the film bending. Regardless of the bending mode (Inner or outer bending), a constant resistance change occurred even after 1000cylces of bending when the bending radius was fixed to 5mm. Figure 3.3A, inset shows the illustration of bending process. These results display the excellent electromechanical stability of Cu@rGO nanowire electrode film. We further investigated the electromechanical ability of electrode film by measuring their sheet resistance as a function of tensile strain (Figure 3.4). A negligible resistance change was found in one stretch-release cycle (the maximum strain is 50%), and the electrical resistance was recovered to the original value after the strain was released, which was shown in Figure 6a, inset. Moreover, the resistance of the as-prepared electrode film slightly increases with stretching even after 1000 cycles of test, this is possible because of high tensile property of nanowire network. To our surprise, the resistance change could keep stable even the strain increased as much as 400% and become slightly larger when it was up to 600%, but the resistance could almost come back to the initial value after the strain was released. All the results suggest a great potential of Cu@rGO nanowire electrode film for high performance elastic conductive electrode.

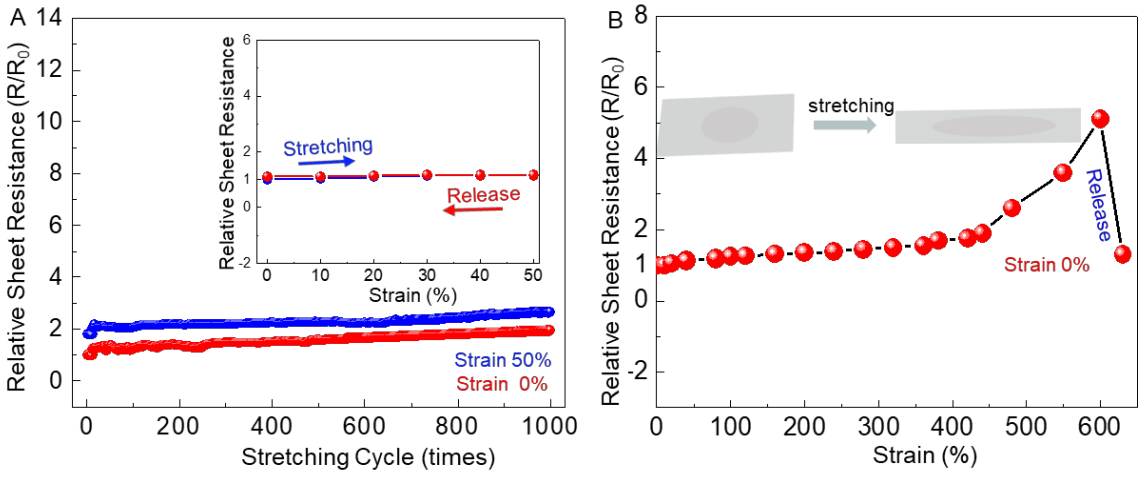

Figure 3.4. Conductivity performance of CuNW conductive film upon mechanical deformation (stretching). (A) Conductivity change of a CuNW based electrode film (PDMS as a substrate) after 50% stretching and then releasing for each cycle. In each cycle, the electrode film was gradually stretched to a strain of 50% and then released to zero strain with same stretching rate. The inset shows the resistance change of electrode film in a typical stretch/release cycle after becoming stable. (B) Conductivity variation of the electrode film as a function of tensile strain until fracture. The inset shows the stretching process. Multiple CuNW electrode films were measured and the conductivity performance shows a good reproducibility under the same mechanical deformation. The transmittance in this electrode film is 80% for all the films. R_0 refers to electrical resistance of the pristine electrode film. All the tests were conducted using a simple device constructed in-house that uses a syringe pump (NE-1000X) to produce repetitive motion.

3.3 Conclusion

In summary, we reported a facile solution-processed method to coat GO nanosheets on the surface of high aspect ratio of copper nanowires. The GO layer on CuNW surface could be reduced with thermal annealing process and thus Cu@rGO core-shell nanostructure was achieved. And this work also systematically studied the regular pattern between the film performance (transparency & sheet resistance) and GO layer coating thickness. The Cu@rGO nanowire samples suggest a long-term stability in air and even in high

temperature and humidity. High performance transparent electrode films were then fabricated with these core-shell nanowires that show a comparable ITO level of optical and electric performance. These transparent electrode films display an excellent flexibility in terms of stretching and bending. This work confirms a new and economical route to stabilize metal nanowire, which hold promise for the commercialization of copper nanowires used as optoelectronic devices.

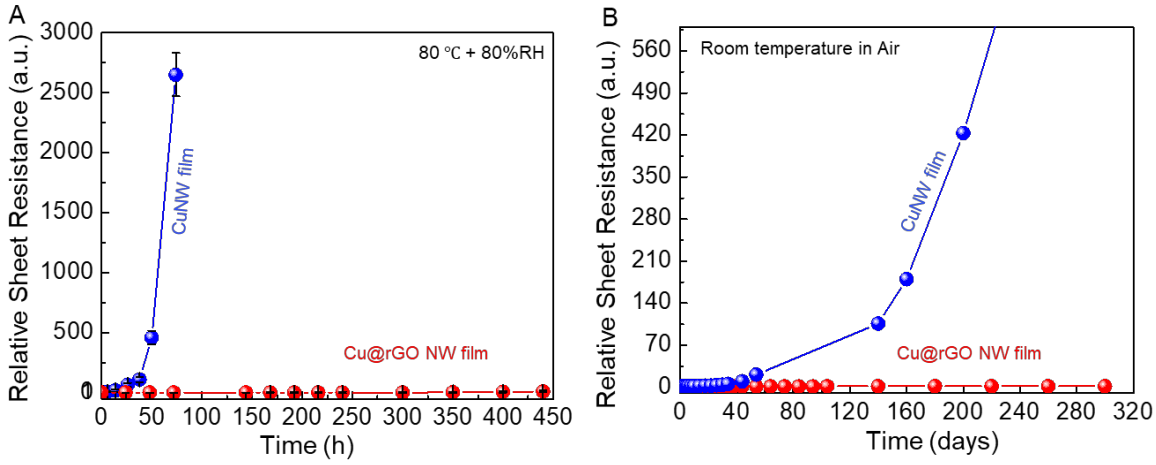

Figure 3.5. Stability of the nanowire-based transparent conducting films. (A) Different types of CuNW (Cu@rGO NW) based conductive films tracked at a temperature of 80 °C and 80% of relative humidity. (B) The Cu@rGO NW based conductive films showing long-term stability in air after storage for over 320 days while the CuNW based conductive films degraded after 1 month when stored in air. Note: CuNW film was dead after 122 h in 80 °C of temperature and 80% of relative humidity.

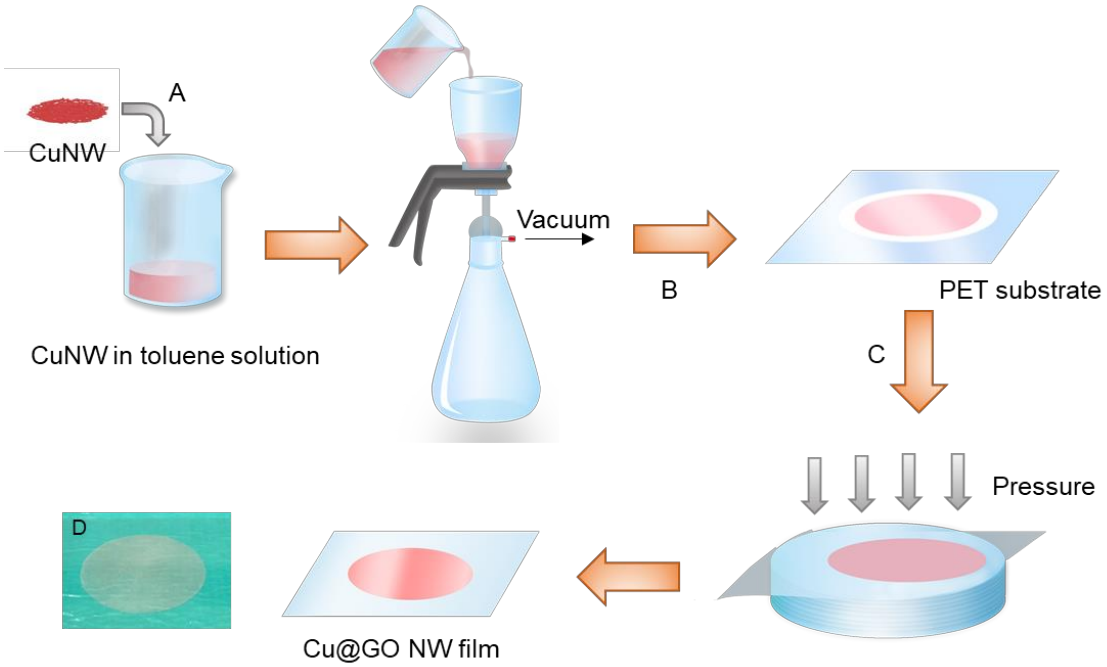

Figure 3.6. Schematic illustration of transparent electrode film fabrication. (A) The as-grown CuNW was dispersed into toluene solution. (B) Vacuum filtration. (C) Pressure transfer process. (D) Optical image of flexible transparent conductive film based on CuNW (PET substrate). Cellulose Nitrate membrane (450 nm of pore size) were used as filter in this experiment.

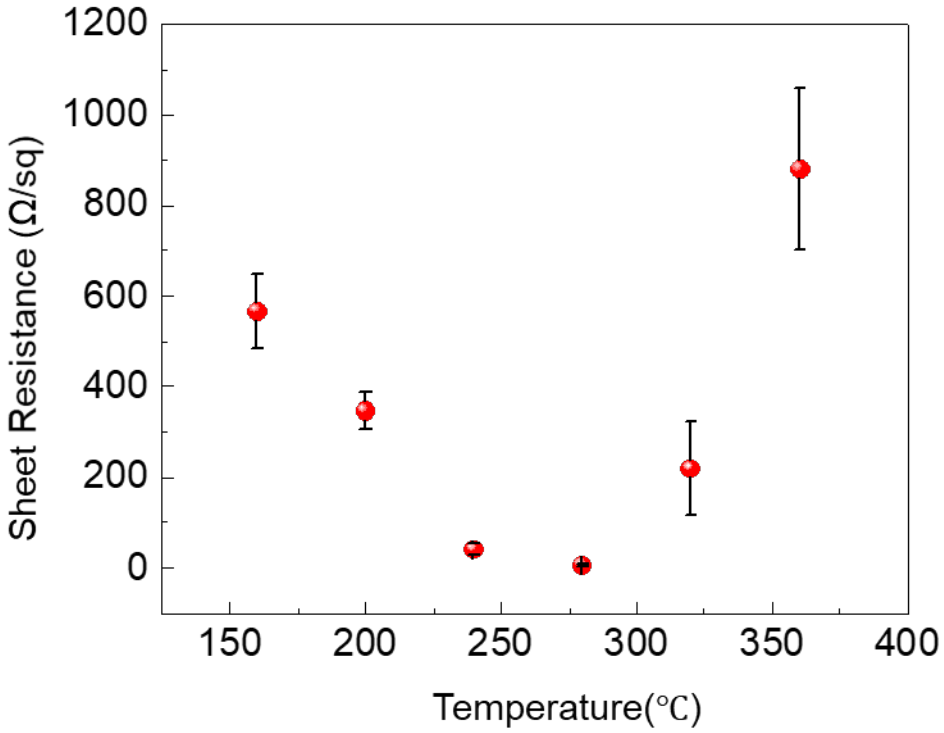

Figure 3.7. The sheet resistance of the Cu@rGO core-shell nanowire based transparent conductive film after annealed in forming gas (10%H_2+90%Ar) at different temperature (160 ℃, 200 ℃, 240 ℃, 280 ℃, 320 ℃, 360 ℃) for 4 h. 280 ℃ is the optimized annealing temperature, if the temperature is lower, it cannot effectively melt the nanowire to form intimate contact at the wire-wire junction. An increase in sheet resistance observed, when the annealing temperature is lower than 200 ℃, the nanowire film is almost insolated due to the presence of oxides on the surface of the nanowire. The temperature cannot be too higher. Overheating will severely melt nanowire and damage the nanowire percolation, which will result in degrading in film conductivity. Note: the nanowires used here are Cu@rGO core-shell nanowire (~6 nm) and all the films have a transparency of 80%.

Reference

1. Environmental and economic assessment of ITO-free electrodes for organic solar cells. *Sol. Energy Mater. Sol. Cells* **2012,** *97*, 14.

2. Laminating solution-processed silver nanowire mesh electrodes onto solid-state dye-sensitized solar cells. *Org. Electron.* **2011,** *12*, 875.

3. Efficient organic solar cells with solution-processed silver nanowire electrodes. *Adv. Mater.* **2011,** *23*, 4371.

4. Highly transparent low resistance ZnO/Ag nanowire/ZnO composite electrode for thin film solar cells. *ACS nano* **2013,** *7*, 1081.

5. Insights on the working principles of flexible and efficient ITO-free organic solar cells based on solution processed Ag nanowire electrodes. *Sol. Energy Mater. Sol. Cells* **2012,** *102*, 148.

6. Lee, J.; Lee, P.; Lee, H.; Lee, D.; Lee, S. S.; Ko, S. H., Very long Ag nanowire synthesis and its application in a highly transparent, conductive and flexible metal electrode touch panel. *Nanoscale* **2012,** *4* (20), 6408-14.

7. Hecht, D. S.; Heintz, A. M.; Lee, R.; Hu, L.; Moore, B.; Cucksey, C.; Risser, S., High conductivity transparent carbon nanotube films deposited from superacid. *Nanotechnology* **2011,** *22* (7), 075201.

8. Roll-to-roll production of 30-inch graphene films for transparent electrodes. *Nature Nanotechnol.* **2010,** *5*, 574.

9. Hecht, D. S.; Thomas, D.; Hu, L.; Ladous, C.; Lam, T.; Park, Y.; Irvin, G.; Drzaic, P., Carbon-nanotube film on plastic as transparent electrode for resistive touch screens. *Journal of the Society for Information Display* **2009,** *17* (11), 941-946.

10. Color in the corners: ITO-free white OLEDs with angular color stability. *Adv. Mater.* **2013,** *25*, 4006.

11. Guo, C. F.; Ren, Z., Flexible transparent conductors based on metal nanowire networks. *Materials Today* **2015,** *18* (3), 143-154.

12. Kang, H.; Kang, I.; Han, J.; Kim, J. B.; Lee, D. Y.; Cho, S. M.; Cho, J. H., Flexible and Mechanically Robust Organic Light-Emitting Diodes Based on Photopatternable Silver Nanowire Electrodes. *The Journal of Physical Chemistry C* **2016,** *120* (38), 22012-22018.

13. Tak, Y.-H.; Kim, K.-B.; Park, H.-G.; Lee, K.-H.; Lee, J.-R., Criteria for ITO (indium–tin-oxide) thin film as the bottom electrode of an organic light emitting diode. *Thin Solid Films* **2002,** *411* (1), 12-16.

14. Zhu, Y.; Ma, X.; Kim, S.; Byrley, P.; Liu, M.; Yan, R. In *Epitaxial, ultra-thin gold coating as a barrier to prevent oxidation of silver nanowires*, ABSTRACTS OF PAPERS OF THE AMERICAN CHEMICAL SOCIETY, AMER CHEMICAL SOC 1155 16TH ST, NW, WASHINGTON, DC 20036 USA: 2017.

15. Ye, S.; Rathmell, A. R.; Chen, Z.; Stewart, I. E.; Wiley, B. J., Metal nanowire networks: the next generation of transparent conductors. *Adv Mater* **2014,** *26* (39), 6670-87.

16. Niu, Z.; Cui, F.; Yu, Y.; Becknell, N.; Sun, Y.; Khanarian, G.; Kim, D.; Dou, L.; Dehestani, A.; Schierle-Arndt, K.; Yang, P., Ultrathin Epitaxial Cu@Au Core–Shell Nanowires for Stable Transparent Conductors. *Journal of the American Chemical Society* **2017,** *139* (21), 7348-7354.

17. Cui, F.; Yu, Y.; Dou, L.; Sun, J.; Yang, Q.; Schildknecht, C.; Schierle-Arndt, K.; Yang, P., Synthesis of Ultrathin Copper Nanowires Using Tris(trimethylsilyl)silane for High-Performance and Low-Haze Transparent Conductors. *Nano Lett* **2015,** *15* (11), 7610-5.

18. Passivation coating on electrospun copper nanofibers for stable transparent electrodes. *ACS nano* **2012,** *6*, 5150.

19. Ag-nanowire films coated with ZnO nanoparticles as a transparent electrode for solar cells. *Appl. Phys. Lett.* **2011,** *99*.

20. Ye, S.; Stewart, I. E.; Chen, Z.; Li, B.; Rathmell, A. R.; Wiley, B. J., How Copper Nanowires Grow and How To Control Their Properties. *Accounts of Chemical Research* **2016,** *49* (3), 442-451.

21. Stewart, I. E.; Ye, S.; Chen, Z.; Flowers, P. F.; Wiley, B. J., Synthesis of Cu–Ag, Cu–Au, and Cu–Pt Core–Shell Nanowires and Their Use in Transparent Conducting Films. *Chemistry of Materials* **2015,** *27* (22), 7788-7794.

22. Synthesis of oxidation-resistant cupronickel nanowires for transparent conducting nanowire networks. *Nano Lett.* **2012,** *12*, 3193.

23. Yang, M.; Hood, Z. D.; Yang, X.; Chi, M.; Xia, Y., Facile synthesis of Ag@Au core–sheath nanowires with greatly improved stability against oxidation. *Chemical Communications* **2017,** *53* (12), 1965-1968.

24. Choi, S.; Han, S. I.; Jung, D.; Hwang, H. J.; Lim, C.; Bae, S.; Park, O. K.; Tschabrunn, C. M.; Lee, M.; Bae, S. Y.; Yu, J. W.; Ryu, J. H.; Lee, S. W.; Park, K.; Kang, P. M.; Lee, W. B.; Nezafat, R.; Hyeon, T.; Kim, D. H., Highly conductive, stretchable and biocompatible Ag-Au core-sheath nanowire composite for wearable and implantable bioelectronics. *Nat Nanotechnol* **2018,** *13* (11), 1048-1056.

25. Ahn, Y.; Jeong, Y.; Lee, D.; Lee, Y., Copper Nanowire–Graphene Core–Shell Nanostructure for Highly Stable Transparent Conducting Electrodes. *ACS nano* **2015,** *9* (3), 3125-3133.

26. Yoon, H.; Shin, D. S.; Kim, T. G.; Kim, D.; Park, J., Facile Synthesis of Graphene on Cu Nanowires via Low-Temperature Thermal CVD for the Transparent Conductive Electrode. *ACS Sustainable Chemistry & Engineering* **2018,** *6* (11), 13888-13896.

27. Dou, L.; Cui, F.; Yu, Y.; Khanarian, G.; Eaton, S. W.; Yang, Q.; Resasco, J.; Schildknecht, C.; Schierle-Arndt, K.; Yang, P., Solution-Processed Copper/Reduced-Graphene-Oxide Core/Shell Nanowire Transparent Conductors. *ACS nano* **2016,** *10* (2), 2600-2606.

Chapter 4. A facile pH-tuned aqueous synthesis of high aspect-ratio copper nanowires for light-weight and free-standing silicon anode with high specific capacity and areal capacity

4.1 Introduction

Lithium-ion batteries (LiBs) dominate most current commercial fields such as portable electronics, critical devices, power cells and large-scale energy storage devices.[1-3] However, traditional graphite-based anodes, which have a specific capacity of ~372 mAg^{-1} (LiC_6),[4] have fallen behind the increasing demand for high-energy density energy storage systems. Novel generation of anodes has been actively pursued in recent decades. Silicon anodes have been considered as the most promising anode material to replace commercial graphite, primarily due to: (1) its highest theory specific capacity ($Li_{22}Si_5$, ~4200 $mAhg^{-1}$), (2) the natural abundance of silicon element on earth, and (3) its relatively low discharge potential (~0.5v V.S. Li/Li^+).[5-7] However, the inevitably of volumetric change (at least 300%) of silicon during lithiation/delithiation process results in a pulverization of silicon particles (SiNPs), the disintegration in the conductive networks, the loosed interfacial contact and unstable solid-electrolyte-interphase (SEI) layers formed on SiNPs, all of which could deteriorate the capacity retention performance.[8-9] Thereby, the contradiction between the dramatic volume change and maintaining the mechanical, conductive networks and favorable interfacial contact has been the top priority to be addressed for silicon anodes.

More recently, many researches have attempted to develop novel current collector for silicon-based anodes in order to solve the problem of this aforementioned issue. Traditional approach is to deposit silicon slurry onto commercial copper foil (~11 μm of thickness) to form anode electrode.[10-11] However, there were always several limitations in using copper foil as current collector: (1) the copper foil accounts for a big ratio of electrode weight when silicon active materials were loaded with only a small quantity conventionally; (2) severely aggregation of SiNPs on Cu foil appears to be a ubiquitous phenomenon during charge/discharge process, which results in low capacity stability and rapidly capacity fade. Carbon materials such as carbon nanotubes (CNTs) or fibers are widely used to replace commercial copper foil as a current collector.[12] For example, Prof. Cui and his co-workers confirmed a silicon-carbon composites anode, which SiNPs are deposited on CNTs based current collector directly.[13] With good conductivity and tensile strength, this strategy retains good cycling stability and decrease the whole anode weight to some extent. Practically, this recipe still has several defects: (1) CNTs are produced by chemical vapor deposition process, leading to high fabrication cost. (2) Relatively high contact resistance found in this nanotube network which could result in a low electrical conductivity, which is mainly due to inadequate conductive networks built in such porous structures.

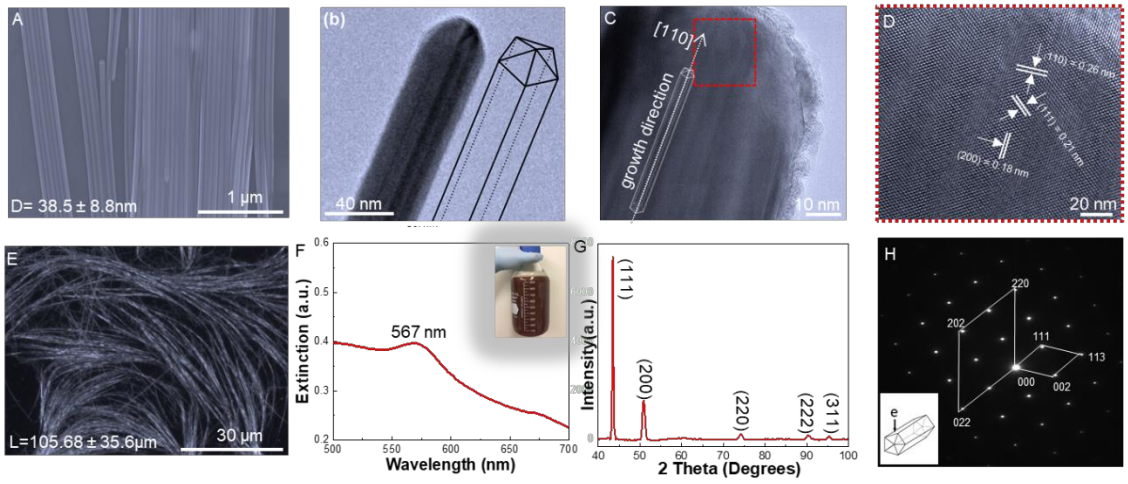

Figure 4.1. Structural and morphological characterization of Cu nanowires that prepared using the standard procedure. (A) SEM images of as-grown Cu nanowires; (B) TEM images of faceted Cu nanowires as illustrated in the inset. (C) HRTEM image of as-grown copper nanowire. (D) the magnified view of red box in (A) on the atomic structure. (E) Low magnification of microscope image of copper nanowire. (F) UV-Vis spectra of copper nanowire samples with 567 nm of maximum absorption peak, the inset is the camera image of scalable synthesized Cu nanowires (1 L). (G) X-ray diffraction pattern of copper nanowires to confirm its face centered cubic (FCC) structure. (H) SAED pattern of Cu nanowire to re-confirm its pure single crystalize structure.

Prevailing the construction of 3D metal nanowire (MNW) networks as an efficient current collector has very obvious advantages in solving the problems mentioned before, such as conductivity, mechanical strength.[13-16] This is because highly conductive nanowire networks with reasonable voids could be built simultaneously and the interfacial contacts between NWs and SiNPs could be significantly enhanced as well. Based on these figure merits, 3D MNW network can thus effectively improve the transfer kinetics performance of electrons for silicon anodes. And more than that, this novel 3D structure can greatly reduce the total weight of anode when compared with the traditional silicon anodes. High aspect-ratio copper nanowire (HARCuNW) network is chosen as the ideal replacement

among all metal nanowires with following reasons: (1) Cu has the second-best intrinsic conductivity and only 6% less conductive than Ag while 30% more conductive than Au; (2) Cu is known as 1000 times much more abundant than Ag or 22000 times more abundant than Au; (3) CuNW could be synthesized with low-cost, scalable, aqueous solution phase technique. (4), the higher the aspect ratio is, the much more conductive the CuNW nanowire network is.[17-19]

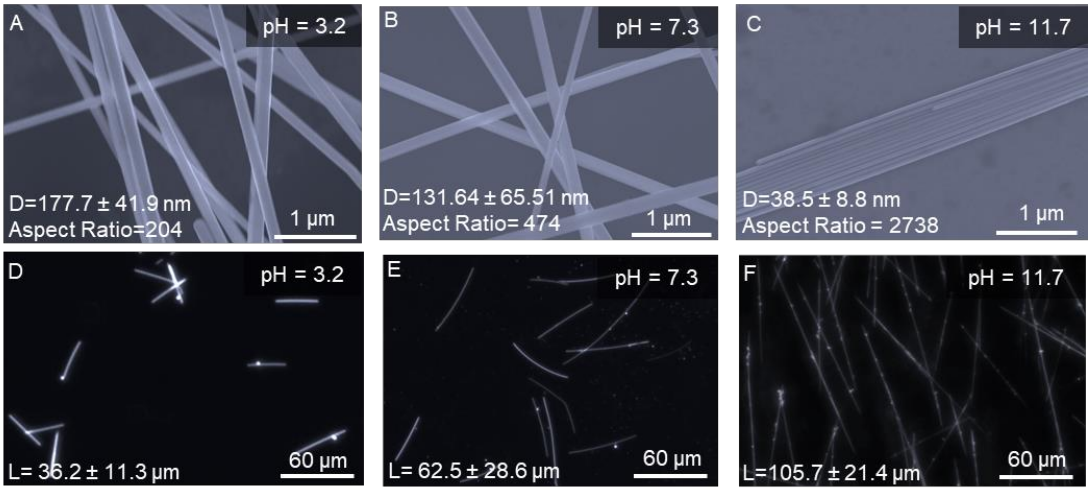

Figure 4.2. The role of pH in copper nanowire shape control. SEM images of copper products with pH =3.2(a), 7.3(b), 11.7(c) in the reaction system to show the diameter distribution: 177.7 ± 41.9 nm, 131.64 ± 65.51 nm, 38.5 ± 8.8 nm. (d-f) Optical images of copper samples with corresponding pH during the reaction to show the length distribution separately: 36.2 ± 11.3 μm, 62.5 ± 28.6 μm, 105.7 ± 21.4 μm. Increased pH could enhance the reducing power of ascorbic acid that can control the nucleation seeding and growth of nanowire.

So far, great efforts have been to prepare HARCuNWs. Cui et al. prepared CuNWs with 997 of aspect ratio (~17 μm long; ~20 nm wide) with the oleylamine-mediated approach, However, this synthesis is time-consuming (~10 h) and costly, because of high operation temperature (~165 ℃) and using highly expensive organic chemical

(tris(trimethylsily)silane).[17] Ye et al. increased the aspect ratio up to 2280 (80 μm long and 35 nm wide) by modifying the ethylenediamine-mediated synthesis. However, the yield of CuNWs is restively low in the final resulted sample and the reducing agent (N_2H_4) used in this recipe was highly toxic that is not environmentally friendly.[19] As a result, there is an ongoing drive to find an economical, green chemistry, scalable route to prepare HARCuNWs with high yield.

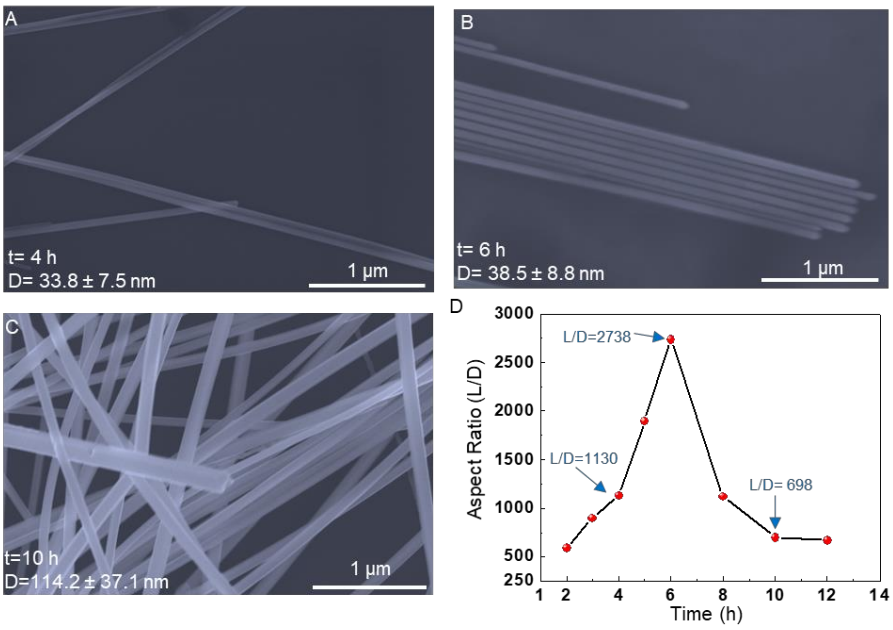

Figure 4.3. SEM images of Cu nanowires formed at 4 h (a), 6 h (b) and 10 h (c) during reaction with the standard condition (pH=11.7). Aspect ratio of Cu nanowires as a function of reaction time was shown in d, which shows that the copper precursor is converted into thin nanowires before 6 h and then the rest of the copper precursor adds to the sides of the nanowires resulting in a dramatic decrease in the aspect ratio of nanowires.

Herein, we report a facile pH tuned aqueous phase synthetic approach to prepare HARCuNWs with average diameter of 38.5 nm and mean length of 105.7 μm, and then a 3D free-standing HARCuNW based silicon anode is successfully fabricated via self-

evaporation method, which display a high initial capacity (~3911 mAh g^{-1}) with good cyclic retention (~1300 mAh g^{-1}) and a comparable commercial-level areal capacity of about 2.5 mAh cm^{-2} after 100 cycles under 0.2C of current rate. Based on the knowledge we have, this is the first time to report CuNWs with 2745 of aspect ratio synthesized with facile pH-tuned strategy and free-standing 3D HARCuNW based silicon anode with high specific capacity and areal capacity retention.

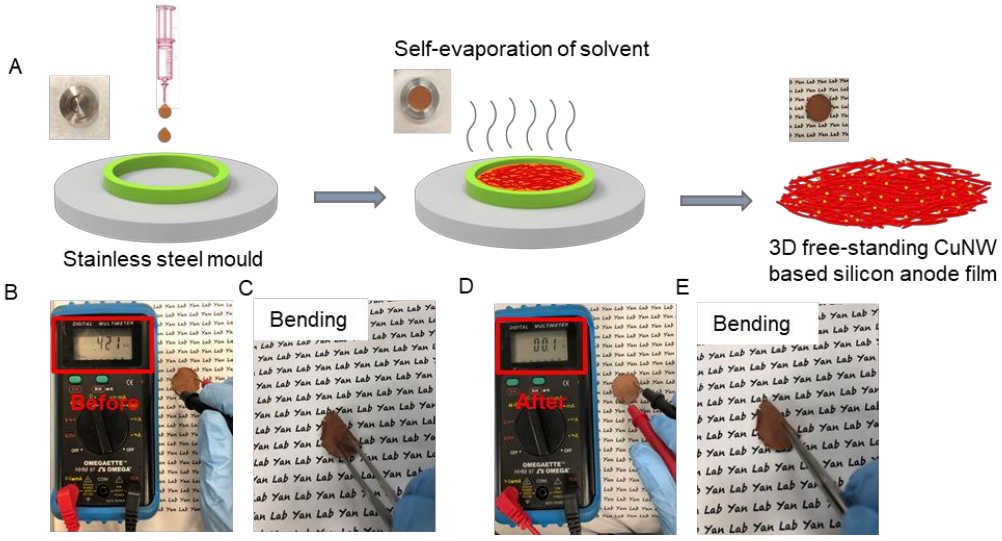

Figure 4.4. Schematic illustration of the free-standing 3D copper nanowire network-based silicon anode. (A) Images showing the fabrication recipe of the free-standing anode film through the solvent evaporation assisted assembly technique; Photograph of the flexible anode film (C) to display a robust mechanical ability and the multimeter (B) suggests a very high resistance (421 Ω) of the anode film before annealing. Photograph of this flexible anode film after annealing (E) and the multimeter(D) shows that the resistance of the anode film is only ~0.01 Ω. Note that all the as-prepared anode films in this experiment are annealing at 280 °C under H_2/Ar (5%/95%) atmosphere for 4 h.

4.2 Results and Discussion

Figure 4.1A displays SEM images of the as-prepared HARCuNWs with an average diameter of ~38.5 nm, as calculated from 100 nanowires randomly selected from the SEM images. The length of the nanowires was about 105.7 μm (Figure 4.1E, 4.2F). The magnified TEM image (Figure 4.1B) discloses that the nanowire exhibited a five-fold twinned pentagonal structure which is commonly accepted by metal nanowires materials. The X-ray diffraction (XRD) spectrum shown in Figure 1g confirms that HARCuNWs have a face-centered cubic (FCC) nanostructure, and the 2 theta peaks at 43.3°, 50.5°, 74.1°, 89.9°, and 90.5° correspond to the {111} , {200}, {220}, {311}, and {222} planes of the FCC copper. No other peaks were observed, which indicates the pure phase nature of the final HARCuNW samples. And this can be reconfirmed with HRTEM and SAED pattern as shown in Figure 4.2C, D, H. When the electron beam is directed parallel to the side parts, as shown in Figure 4.2H, the diffraction pattern corresponds to the overlap of two FCC pattern with [110] and [111] zone axes. The growth direction is determined to proceed along {110} direction. And based on the SAED analysis, the resulted nanowire samples are proved to be single-crystalline that is consistent with previous conclusion. Figure 4.2F further shows the UV-Vis extinction spectra of the HARCuNWs dispersed in toluene, from which an absorption peak locating at 567 nm is observed. This unique peak may originate from the surface plasmon resonance band of the HARCuNWs situating in the region of the Interbrand transitions (below 590 nm) because of the small diameter of HARCuNW

samples. Figure 4.1F inset shows the camera image of the scalable synthesized copper nanowire solution (as much as 1000mL).

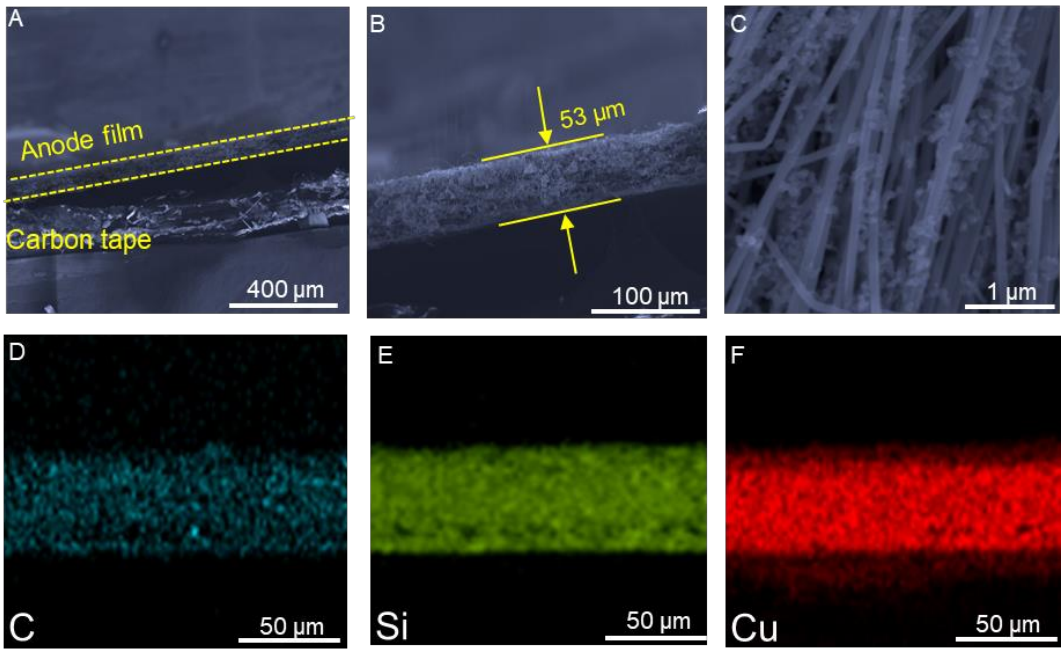

Figure 4.5. SEM characterization of as-prepared free-standing copper nanowire-based silicon anode. (a) Large scale SEM images of the cross section of this free-standing anode film to show its uniform thickness and image (b) shows that the average thickness is about 53 μm. (c) Magnified SEM images of free-standing anode film to reconfirm the CSi nanoparticles are well dispersed in the 3D copper nanowire network which is used as electron channel to fast electron transfer to the active nanoparticles. (d-f) Elemental distribution information of the selected cross-section area of as-prepared film.

To uncover the role of pH during the growth of HARCuNWs. The structure morphology of the HARCuNWs synthesized under different pH (pH=3.2, 7.3, 11.7) was probed via SEM images and the corresponding optical images. Figure 4.2A-F exhibited that when pH is tuned to 3.2, 7.3, 11.7, the corresponding average nanowire diameter is 177.7 nm, 131.64 nm, 38.5 nm while the mean length is 36.2 μm, 62.5 μm and 105.7 μm separately. This

might be explained by the fact that the reducing power of ascorbic acid (AA) can be greatly enhanced by increasing the pH of reaction system.[20-21] And the enhanced reducing power of AA could control the growth of nanowires which is attributed to the truth that the enhanced reducing power induces fast nucleation of Cu nanoseeds with a smaller size and this minimized time for isotropic seed growth reduces variation in the Cu nanoseed diameter and subsequent the reducing power of AA was decreased during the reaction because of the consumption of AA during the reaction. Subsequently, this mild reducing power favors the slow initiation of anisotropic growth for the formation of HARCuNWs with smaller diameters.[22] The nanoseed favors multiply twinned nanoparticles (MTP) bounded by the more closely packed (111) facet planes, the anisotropic elongation is controlled by Oleylamine (OLA) and a reasonable concentration of OLA facilitates the asymmetric growth (Figure4.8), this can be explained by the truth that OLA preferentially interacts with {100} facet planes over {111} facet planes. Loosely packed {100} facet planes tend to provide more space for the attachment of OLA while the more closely packed {111} facet planes serve as low surface energy sites for the deposition of Cu atoms, directing multiply twinned nanoparticles to grow into nanowires.[23] However, free H^+ ions coming from aqueous solution of low pH could consume OLA with amine group which weaken its protection for the side part of HARCuNWs. Besides, high pH has another advantage: $Cu(OH)_2$ could be formed at the initial stage according to the solubility product constant of $Cu(OH)_2$ ($K_{sp}=4.8\times10^{-20}$ at 25℃) and therefore keep Cu^{2+} ions at a relative stable concentration during the nanowire growth stage. Thus, it could provide extra free copper ions for nanowire growth, which helps elongate the length of CuNWs.

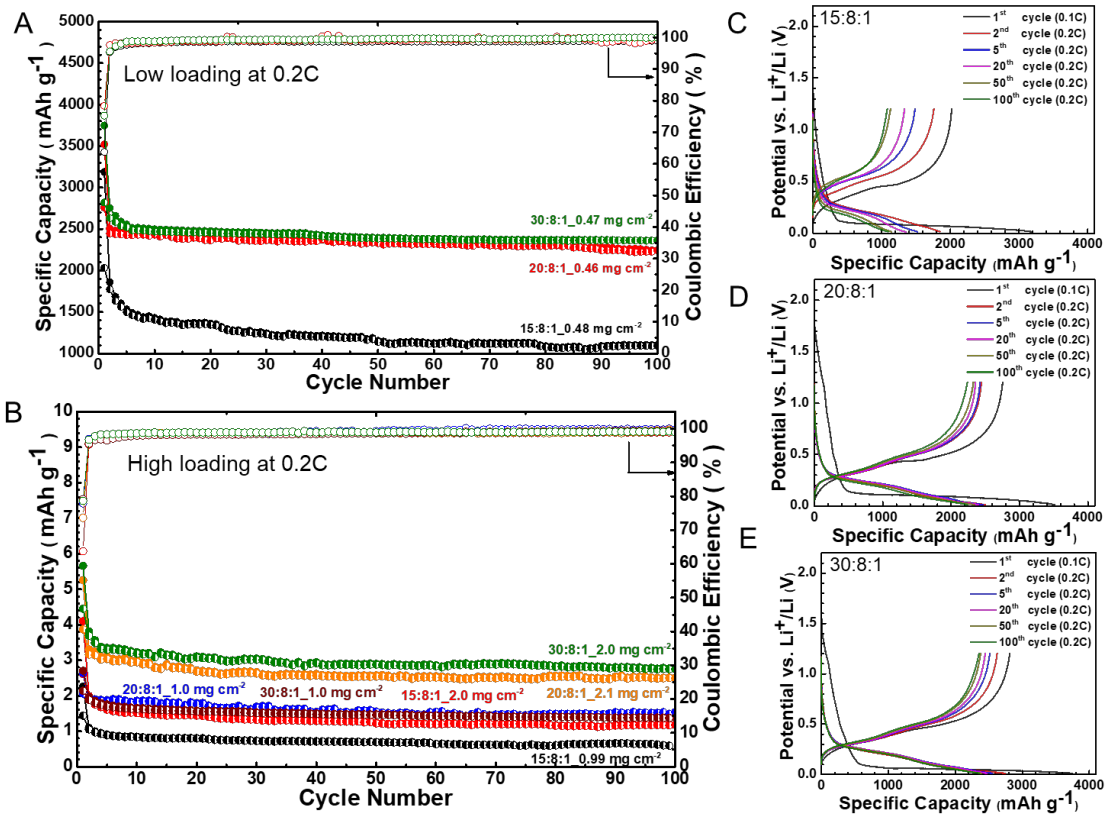

Figure 4.6. Electrochemical characterization of the free-standing samples. (a) the lifespan of the as-prepared free-standing samples of different weight ratio (CuNW: CSiNP: CMC= 15:8:1, 20:8:1, 30:8:1) at a charging rate of 0.2C with an Relatively small Areal mass loading of about 0.47 mg/cm^2. (b) the life span of the samples of different weight ratio (15:8:1, 20:8:1, 30:8:1) at a current rate of 0.2C with a high areal mass loading of about 1mg/cm^2 and 2 mg/cm^2. (c-e) Charge/discharge curve of as-prepared samples with different weight ratio (15:8:1, 20:8:1, 30:8:1) at 0.2C of current rate under 1st cycle, 2nd cycle, 5th cycle, 20th cycle, 50th cycle, 100th cycle.

In a typical synthesis, 100 µL of 1M NaOH solution was added into vial with 17.9 mL of DI water; then 1 mL of $CuCl_2$ aqueous solution was put into viral to form light green solution; 180 µL of OLA was then added and sonicated to prepare a deep-blue emulsion, later 1mL of ascorbic acid was injected to the mixtures and finally the solution was kept in oven at 100 ℃ for 5 h, as the HARCuNWs increase in length and yield, the solution

becomes homogeneously dark red. This structural evolution of the nanowires was also probed. The SEM image shown in Figure 4.3A recorded the reaction lasted for 4 h exhibited the presence of thin HARCuNWs with low yield (~33.8 nm of diameter), and for 6 h (Figure 4.3B), the yield of HARCuNWs significantly increased while the diameter was slightly increased (~38.5 nm of diameter), which shows that the copper precursor is converted into small nano-seeds and then grown as thin nanowires. For 10 h (Figure 4.3C), the results display a dramatic increase in the nanowire diameter (Figure 4.3D) because of the Ostwald Ripening effect and that the rest of free copper atoms were added to the sides of the nanowires.

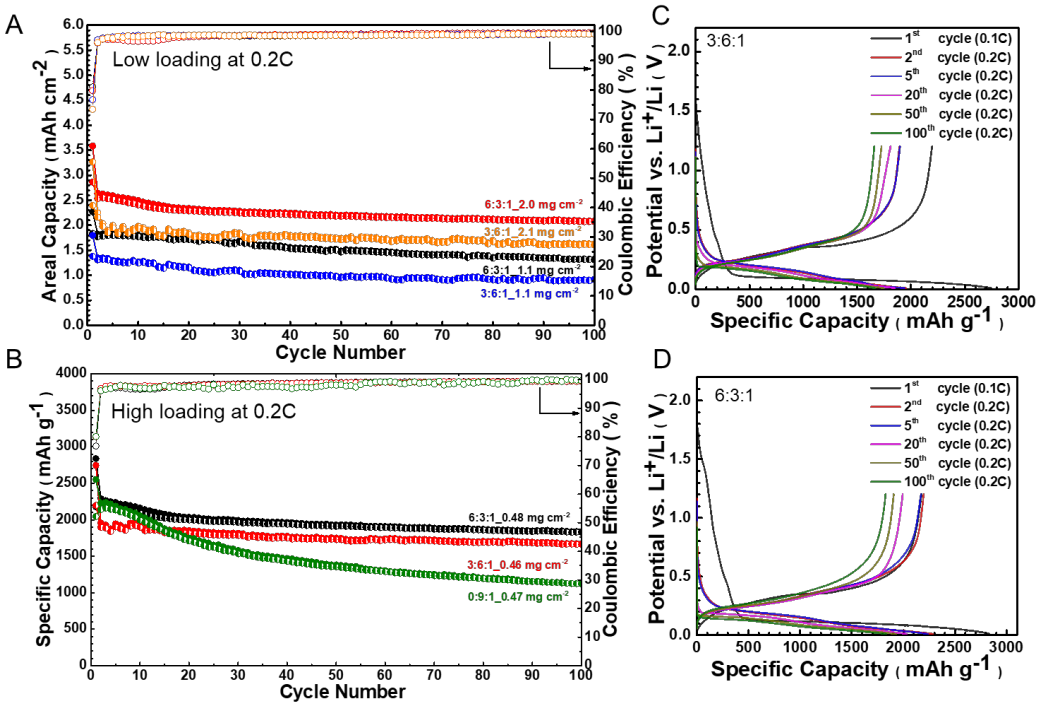

Figure 4.7. Electrochemical characterization of the as-prepared samples coated on commercial copper foil. (a) the lifespan of the samples of different weight ratio (CuNW: CSiNP: CMC= 6:3:1, 3:6:1, 0:9:1) at a charging rate of 0.2C with a relatively small Areal mass loading of about 0.47 mg/cm^2. (b) the life span of the samples of different weight ratio (6:3:1, 3:6:1) at a charging rate of 0.2C with a high areal mass loading of about 1 mg/cm^2 and 2 mg/cm^2. (c-d) Charge/discharge curve of as-prepared samples with different weight ratio (6:3:1, 3:6:1) at 0.2C of charging rate under 1st cycle, 2nd cycle, 5th cycle, 20th cycle, 50th cycle, 100th cycle.

Following synthesis, we next fabricated a free-standing HARCuNW network based current collector to accommodate the CSiNPs inside the porous nanostructure to adapt the large volume change during lithiation/delithiation process. And SiNPs can be dispersed in the pores of 3D HARCuNW network to avoid severely aggregation of CSiNPs. In a typical fabrication (Figure 4.4A), the HARCuNW/CSiNP/CMC mixtures were added to ethanol solution and then kept stirring for overnight to form a homogeneously dispersion. Later the

HARCuNW/CSiNP/CMC ethanol dispersion was slowly poured into a stainless-steel mold and then let the ethanol solvents evaporate under ambient conditions. The self-evaporation of solvents brought the assembly of HARCuNWs forming a free-standing light-weight film. The obtained anode film was then annealed under the forming gas (10% H_2/90% Ar) at 240 ℃ for 4 h. during this annealing process, the oxides on surface of HARCuNWs could be reduced to pure copper and the junctions of HARCuNWs were also welded together, which greatly improved the conductivity of the anode film and this can be confirmed in Figure 4.4B. Surprisingly, this film can also show good mechanical stability during bending process (Figure 4.4C,E). The SEM measurement was carried out for characterizing the microstructure of the composite silicon anode (Figure 4.5), it can be clearly found that the SiNPs are well dispersed in the network of HARCuNWs (Figure 4.5B-F). And the contact between the SiNPs and HARCuNWs are robust because of annealing process. Figure 4.5A, B shows a uniform thickness of as-prepared HARCuNW based silicon anode (~53 μm). Overall, all these measurements demonstrate that this novel free-standing HARCuNW/CSiNP/CMC composite silicon anode is successfully built with self-evaporation, benefiting capacity performance in LIB test.

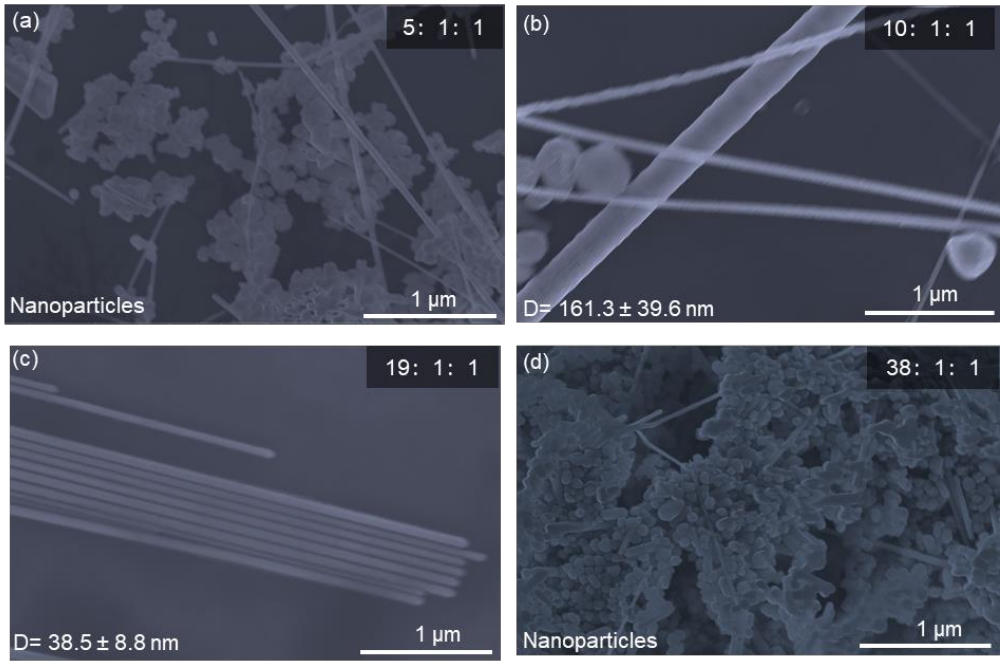

Figure 4.8. The role of oleylamine in copper nanowire shape control. SEM images of copper nanowire samples with increased amount of oleylamine within the reaction system, from (a) to (d), the concentration ratio of oleylamine, ascorbic acid, $CuCl_2$ is 5:1:1,10:1:1, 19:1:1, 38:1:1. Due to the lower surface density compared to the (111) facet, the (100) facet of the nanowire shows a higher chemical reactivity which leads to the attachment of oleylamine and in turn the passivation of the (100) facet. Low concentration of oleylamine cannot provide enough protection on (100) surface, so nanowire growth is now regulated ideally whereas most of them are Cu nanoparticles or irregular by-products. A high concentration of oleylamine could lead to a steady heavy coverage of oleylamine on both (100) side parts and (111) end parts, thereby a isotropic growth for all the different faces and mainly nanoparticles would be obtained.

The electrochemical performance was then measured in the battery testing system (Figure 4.6 and 4.7). In order to find the optimum fabrication parameters for this composite anode, different weight ratio for HARCuNW, CSiNP and CMC (HARCuNW: CSiNP: CMC) was explored in control experiments, as illustrated in Figure 4.6A. It shows the cycle capacity retention of these free-standing silicon composite anodes at a current rate of 0.2C (~0.37 mA cm^{-2}), the HARCuNW/CSiNP/CMC composite anode (20:8:1) achieved 3911 mAh g^{-}

[1] of first cycle lithiation capacity and 78% of initial coulombic efficiency (ICE). Compared with the composite anode (20:8:1), the one with 30:8:1 achieved 3747 mAh g^{-1} of initial specific capacity as well as 75% of ICE. As comparison, by decreasing the usage of HARCuNWs, the ratio was then reduced to 15:8:1. However, this ratio (15:8:1) could only achieve 3188 mAh g^{-1} of specific capacity as well as 64% of ICE. With relatively high usage of HARCuNWs, both the ratio of 20:8:1 and 30:8:1 demonstrate that the excellent cycle stability and the capacity retention is still 89.5% and 85.9% even after 100 cycles respectively compared with the capacity of 2nd cycle while 15:8:1 only reaches 59.4% of capacity retention after 100 cycles. To our surprise, by increasing the loading of CSiNPs with same ratio shown in Figure 4.6B, the composite anode could provide a higher areal capacity without sacrificing specific capacity. At the beginning, with an increasing areal loading of 1 mg cm^{-2} and 2 mg cm^{-2}, HARCuNW/CSiNP/CMC composite anode (30:8:1) can reach 2.7 mAh cm^{-2} and 5.6 mAh cm^{-2} of areal capacity at 0.1C separately. In order to make it more practical, a higher current rate of 0.2 C (0.74 mA cm^{-2} and 1.5 mA cm^{-2} separately) was applied from the 2nd to 100th cycle, the areal capacity can still keep up to 1.4 mAh cm^{-2} and 2.7 mAh cm^{-2} after 100 cycle respectively.

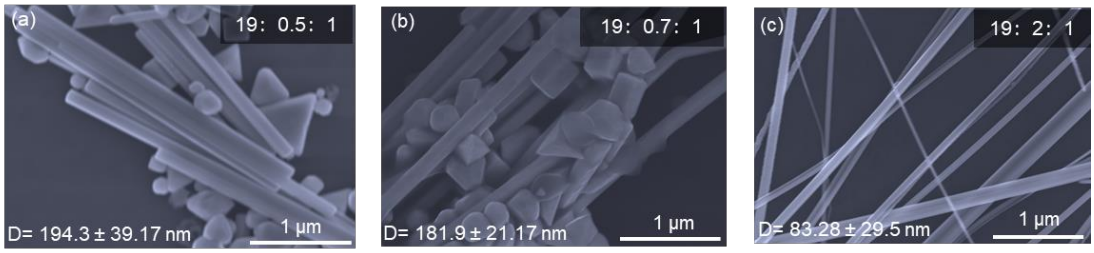

Figure 4.10. Control experiments conducted to study the effect of Ascorbic acid on Cu nanowire growth. SEM images of copper nanowires when the concentration ratio of oleylamine, ascorbic acid and $CuCl_2$ (a) 19:0.5:1; (b)19:0.7:1; (c) 19:2:1. The diameter information can be found in each image. During the nucleation, the more reducing agent, the more nuclei it will produce, the smaller seeds it will obtain as well. However, too high concentration of reducing agent could lead to a too fast reduction, too high amount of free Cu^0 could be formed which contribute to the wire growth is not regulated ideally.

With the HARCuNW/CSiNP/CMC composite anode (20:8:1), when the CSiNPs loading was increased to 1 and 2 mg cm^{-2}, the final 1.5 mAh cm^{-2} and 2.5 mAh cm^{-2} of areal capacity was kept even after 100 cycle at a current rate of 0.2C. And meanwhile, the capacity retention was also reached up to 79.1% and 76.0% respectively after 100 cycles for each loading amount. This could be attributed to the rational voids prepared by 3D HARCuNW network which could accommodate more CSiNPs efficiently. In order to confirm this hypothesis, the control experiment was conducted with less HARCuNWs usage, both cycle stability, specific (or areal) capacity and ICE was severely faded shown in Figure 4.6B, this is because less HARCuNWs could not provide enough contact with CSiNPs and the electron transfer was then retarded. The lithiation/delithiation curves shown in Figure 4.6C-E also reconfirm high HARCuNW could retain a high capacity of comps. For all samples with different ratio, the 1st lithiation curve shows an SEI formation slope, which lead to a low initial coulombic efficiency. The primary lithiation capacity was

below 0.3V, which demonstrate that the electrochemical reaction of silicon allying contributes to the main capacity. At a high current density of 0.5C (0.925 mA cm^{-2}) with a 0.5 mg cm^{-2} of loading amount, a specific capacity of 1625 mAh g^{-1} at 0.5 C is remained while 2422 mAh g^{-1} is kept at 0.2C, and the capacity retention of 87.9% at 0.5 C and 85.9% at 0.2C could be achieved. With a high areal mass loading and high current density (3.7 mA cm^{-2}), HARCuNW/CSiNP/CMC composite anode (30:8:1) still can reach an area capacity of 2.2 mAh cm^{-2}. This high rate performance indicates that a high conductive 3D HARCuNW framework was effectively constructed which could reduce the polarization and aggregated CSiNPs in electronic environment.

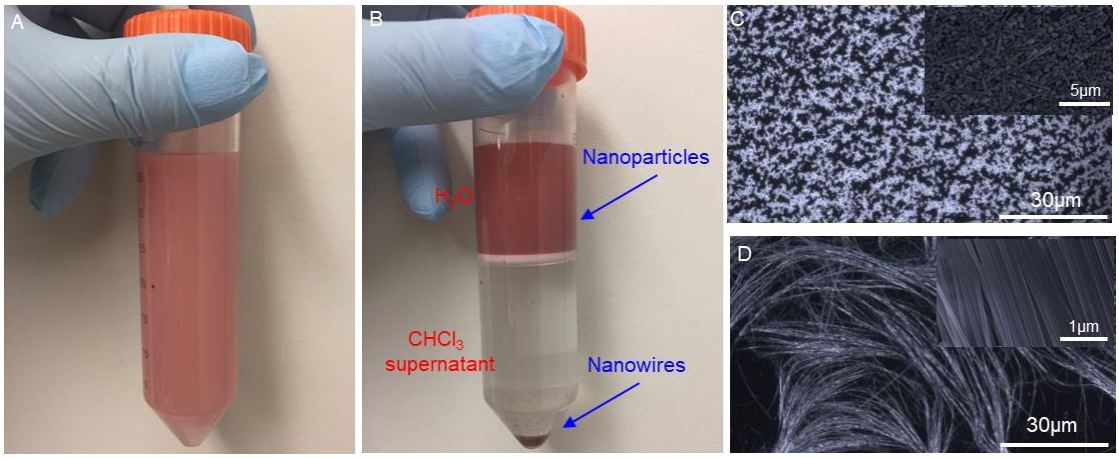

Figure 4.11. Purification of Cu nanowires. (A, B) camera images illustrating of the purification steps and the final products. first, the supernatant in the original solution was decanted to remove excess of oleylamine and then was re-suspended in water. Subsequently, chloroform was added to the solution and vortexed for 1 min, after vortex, the water and chloroform phase separated indicating an obvious interface, after settling for 30 mins, the red flakes composed of Cu nanowires were seen to cross the interface and settle down in the bottom.

In order to make more practical for commercial LIB, HARCuNWs was employed to mix with CSiNPs to form a slurry and then coated on the commercial copper foil. With three different weight ratios of 6:3:1, 3:6:1 and 0:9:1 (HARCuNW/CSiNP/CMC) as comparison. Composite anodes with incorporated HARCuNWs reveal excellent cycle stability compared to the ones without HARCuNWs. 85.5% and 80.3% of capacity retention was achieved by the ratio of 6:3:1 and 3:6:1 separately. However, only 50.6% of capacity retention was obtained by the anodes without HARCuNWs (0:9:1) added in. Because the ultra large volume change of CSiNPs during the charge/discharge process could lead to the pulverization and finally the CSiNPs will detach from the commercial copper foil. At the initial stage, with a 1 mg cm^{-2} and 2 mg cm^{-2} of areal loading, the HARCuNW/CSiNP/CMC composite anode (6:3:1) can reach a corresponding 2.3 mAh cm^{-2} and 3.6 mAh cm^{-2} of areal capacity at a current rate of 0.1C. During the cycles from 2^{nd} to 100^{th}, even a high current rate of 0.2 C (0.74 mA cm^{-2} and 1.5 mA cm^{-2} for each different loading amount) was employed, the areal capacity can still hold 1.3 mAh cm^{-2} and 2.1 mAh cm^{-2} after 100 cycles respectively. With the sample of HARCuNW/ CSiNP/ CMC (6:3:1) composite anode, when the loading amount of CSiNPs increases to 1 and 2 mg cm^{-2}, the areal capacity was up to 1.5 mAh cm^{-2} and 2.5 mAh cm^{-2} without obvious performance degrade found even after 100 cycles under such a high current rate (0.2C). To our surprise, under the condition of higher areal mass loading (2 mg cm^{-2}) and higher current density of 0.5C (3.7 mA cm^{-2}), the HARCuNW/ CSiNP /CMC (6:3:1) composite anode can still have an area capacity of 1.7 mAh cm^{-2} and 87% capacity retention was obtained as well. This can be explained by the fact that the highly conductive 3D copper nanowire network could

obviously improve the electron transfer and thus it can accommodate the quick lithiation/delithiation process.

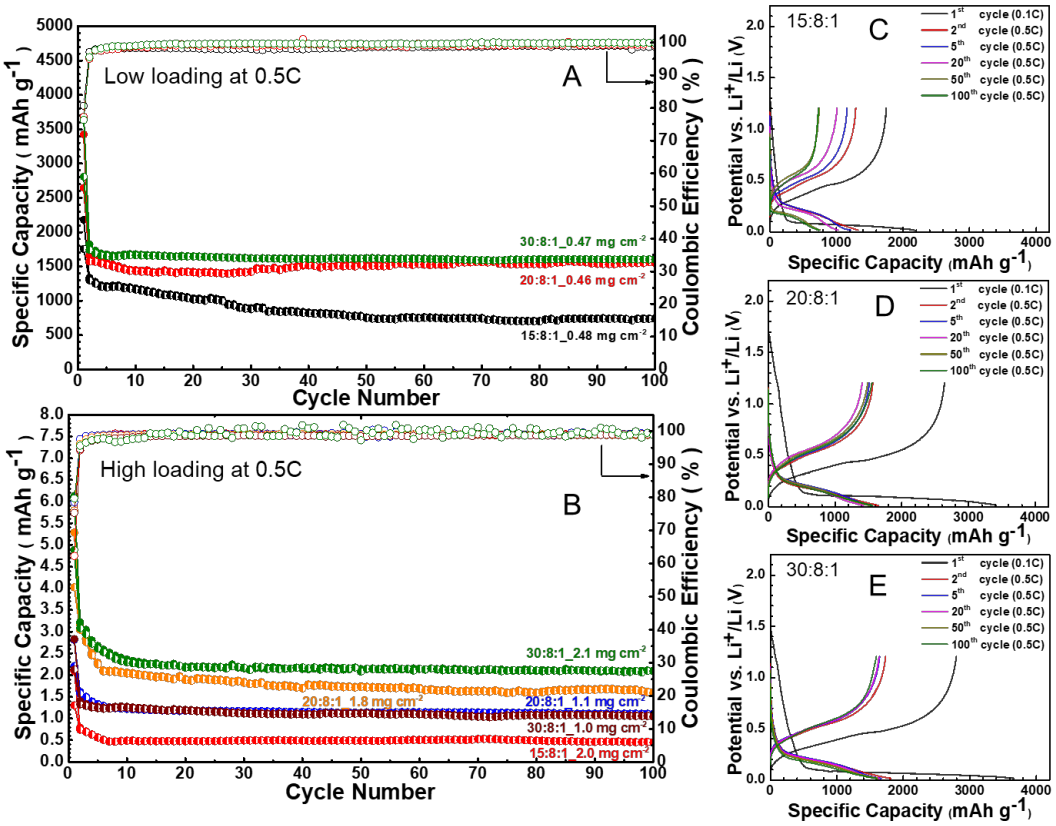

Figure 4.12. Electrochemical characterization of the free-standing samples. (A) the lifespan of the as-prepared free-standing samples of different weight ratio (CuNW: CSiNP: CMC= 15:8:1,20:8:1,30:8:1) at a current rate of 0.5C with an relatively small areal mass loading of about 0.47 mg/cm^2. (B) The life span of the samples of different weight ratio (15:8:1, 20:8:1, 30:8:1) at a current rate of 0.5C with a high areal mass loading of about 1 mg/cm^2 and 2 mg/cm^2. (C-E) Charge/discharge curve of as-prepared samples with different weight ratio (15:8:1, 20:8:1, 30:8:1) at a current rate of 0.5C under 1st cycle, 2nd cycle, 5th cycle, 20th cycle, 50th cycle, 100th cycle.

4.3. Conclusion

In summary, we report a novel synthetic approach by tuning pH to achieve high aspect ratio copper nanowires. This pH tuned method is easily scalable and produces five-fold twinned nanowires with mean diameter of ~38.5 nm and average length of 105.7 μm. And then light-weight free-standing HARCuNW/CSiNP/CMC composite anode (20:8:1) was fabricated with self-evaporation method, which exhibited high specific capacity and areal capacity retention. Furthermore, in order to make it more practical, HARCuNW/CSiNP/CMC slurry (6:3:1) was coated on commercial copper foil and this modified silicon anode shows a dramatically increased cyclic stability compared with that without HARCuNWs. This work advances research into the commercialization of HARCuNWs for LIB.

References

1. Chan, C. K.; Peng, H.; Liu, G.; McIlwrath, K.; Zhang, X. F.; Huggins, R. A.; Cui, Y., High-performance lithium battery anodes using silicon nanowires. *Nat Nanotechnol* **2008,** *3* (1), 31-5.

2. Etacheri, V.; Marom, R.; Elazari, R.; Salitra, G.; Aurbach, D., Challenges in the development of advanced Li-ion batteries: a review. *Energy & Environmental Science* **2011,** *4* (9), 3243.

3. Liu, N.; Wu, H.; McDowell, M. T.; Yao, Y.; Wang, C.; Cui, Y., A yolk-shell design for stabilized and scalable li-ion battery alloy anodes. *Nano Lett* **2012,** *12* (6), 3315-21.

4. Wu, H.; Yu, G.; Pan, L.; Liu, N.; McDowell, M. T.; Bao, Z.; Cui, Y., Stable Li-ion battery anodes by in-situ polymerization of conducting hydrogel to conformally coat silicon nanoparticles. *Nature communications* **2013,** *4*, 1943.

5. Xu, Y.; Zhu, Y.; Han, F.; Luo, C.; Wang, C., 3D Si/C Fiber Paper Electrodes Fabricated Using a Combined Electrospray/Electrospinning Technique for Li-Ion Batteries. *Advanced Energy Materials* **2015,** *5* (1), 1400753.

6. Ge, M.; Rong, J.; Fang, X.; Zhou, C., Porous doped silicon nanowires for lithium ion battery anode with long cycle life. *Nano Lett* **2012,** *12* (5), 2318-23.

7. <Silicon Nanotube Battery Anodes.pdf>.

8. Szczech, J. R.; Jin, S., Nanostructured silicon for high capacity lithium battery anodes. *Energy Environ. Sci.* **2011,** *4* (1), 56-72.

9. Xu, Y.; Yin, G.; Ma, Y.; Zuo, P.; Cheng, X., Nanosized core/shell silicon@carbon anode material for lithium ion batteries with polyvinylidene fluoride as carbon source. *Journal of Materials Chemistry* **2010,** *20* (16), 3216.

10. Yuan, S.; Huang, X. L.; Ma, D. L.; Wang, H. G.; Meng, F. Z.; Zhang, X. B., Engraving copper foil to give large-scale binder-free porous CuO arrays for a high-performance sodium-ion battery anode. *Adv Mater* **2014,** *26* (14), 2273-9, 2284.

11. Li, Q.; Zhu, S.; Lu, Y., 3D Porous Cu Current Collector/Li-Metal Composite Anode for Stable Lithium-Metal Batteries. *Advanced Functional Materials* **2017,** *27* (18), 1606422.

12. Li, W.; Tang, Y.; Kang, W.; Zhang, Z.; Yang, X.; Zhu, Y.; Zhang, W.; Lee, C. S., Core-shell Si/C nanospheres embedded in bubble sheet-like carbon film with enhanced performance as lithium ion battery anodes. *Small* **2015,** *11* (11), 1345-51.

13. Cui, L.-F.; Hu, L.; Choi, J. W.; Cui, Y., Light-Weight Free-Standing Carbon Nanotube-Silicon Films for Anodes of Lithium Ion Batteries. *ACS nano* **2010,** *4* (7), 3671-3678.

14. Lu, L. L.; Ge, J.; Yang, J. N.; Chen, S. M.; Yao, H. B.; Zhou, F.; Yu, S. H., Free-Standing Copper Nanowire Network Current Collector for Improving Lithium Anode Performance. *Nano Lett* **2016,** *16* (7), 4431-7.

15. Ma, X.; Liu, Z.; Chen, H., Facile and scalable electrodeposition of copper current collectors for high-performance Li-metal batteries. *Nano Energy* **2019,** *59*, 500-507.

16. Shang, H.; Zuo, Z.; Yu, L.; Wang, F.; He, F.; Li, Y., Low-Temperature Growth of All-Carbon Graphdiyne on a Silicon Anode for High-Performance Lithium-Ion Batteries. *Adv Mater* **2018,** *30* (27), e1801459.

17. Cui, F.; Yu, Y.; Dou, L.; Sun, J.; Yang, Q.; Schildknecht, C.; Schierle-Arndt, K.; Yang, P., Synthesis of Ultrathin Copper Nanowires Using Tris(trimethylsilyl)silane for High-Performance and Low-Haze Transparent Conductors. *Nano Lett* **2015,** *15* (11), 7610-5.

18. Rathmell, A. R.; Wiley, B. J., The Synthesis and Coating of Long, Thin Copper Nanowires to Make Flexible, Transparent Conducting Films on Plastic Substrates. *Advanced Materials* **2011,** *23* (41), 4798-4803.

19. Ye, S.; Rathmell, A. R.; Stewart, I. E.; Ha, Y. C.; Wilson, A. R.; Chen, Z.; Wiley, B. J., A rapid synthesis of high aspect ratio copper nanowires for high-performance transparent conducting films. *Chem Commun (Camb)* **2014,** *50* (20), 2562-4.

20. Yang, Y.; Liu, J.; Fu, Z. W.; Qin, D., Galvanic replacement-free deposition of Au on Ag for core-shell nanocubes with enhanced chemical stability and SERS activity. *J Am Chem Soc* **2014,** *136* (23), 8153-6.

21. Langille, M. R.; Personick, M. L.; Zhang, J.; Mirkin, C. A., Defining rules for the shape evolution of gold nanoparticles. *J Am Chem Soc* **2012,** *134* (35), 14542-54.

22. Hwang, C.; An, J.; Choi, B. D.; Kim, K.; Jung, S.-W.; Baeg, K.-J.; Kim, M.-G.; Ok, K. M.; Hong, J., Controlled aqueous synthesis of ultra-long copper nanowires for stretchable transparent conducting electrode. *Journal of Materials Chemistry C* **2016,** *4* (7), 1441-1447.

22. Yang, H. J.; He, S. Y.; Tuan, H. Y., Self-seeded growth of five-fold twinned copper nanowires: mechanistic study, characterization, and SERS applications. *Langmuir : the ACS journal of surfaces and colloids* **2014,** *30* (2), 602-10.

Chapter 5. Conclusions

Metal nanowires can be an ideal replacement that meets comparable or even higher ITO-lever performance, if the long-standing problem can be solved: anti-corrosion.

To address this challenge, we propose to develop a novel solution-phase, etch-free, epitaxial deposition technique to grow an ultra-thin (~6 nm), conformal and atomically smooth layer of Au coating on metal nanowire surfaces, which acts as a reliable and economical anti-oxidation barrier to provide long-term device stability, and develop a fabrication method for patterned electrodes. By solving the long-standing stability issue, this project will facilitate the realization of the full commercial potential of metal nanowire transparent conductors. It will inspire novel flexible optoelectronic devices, such as foldable displays, E-textiles, digital clothing, smart-glasses, 3D-shaped touch-sensing surfaces, wearable electronic sensors for safety and healthy living, and flexible organic photovoltaics.

Secondly, we reported a facile solution-processed method to coat GO nanosheets on the surface of high aspect ratio of copper nanowires. The GO layer on CuNW surface could be reduced with thermal annealing process and thus Cu@rGO core-shell nanostructure was achieved. And this work also systematically studied the regular pattern between the film performance (transparency & sheet resistance) and GO layer coating thickness. The Cu@rGO nanowire samples suggest a long-term stability in air and even in high temperature and humidity. High performance transparent electrode films were then

fabricated with these core-shell nanowires that show a comparable ITO level of optical and electric performance. These transparent electrode films display an excellent flexibility in terms of stretching and bending. This work confirms a new and economical route to stabilize metal nanowire, which hold promise for the commercialization of copper nanowires used as optoelectronic devices.

Last but not least, a novel synthetic approach by tuning pH was reported to achieve high aspect ratio copper nanowires. This pH tuned method is easily scalable and produces five-fold twinned nanowires with mean diameter of ~38.5 nm and average length of 105.7 μm. And then light-weight free-standing HARCuNW/CSiNP/CMC composite anode (20:8:1) was fabricated with self-evaporation method, which exhibited high specific capacity and areal capacity retention. Furthermore, in order to make it more practical, HARCuNW/CSiNP/CMC slurry (6:3:1) was coated on commercial copper foil and this modified silicon anode shows a dramatically increased cyclic stability compared with that without HARCuNWs. This work advances research into the commercialization of HARCuNWs for LIB.